5-2009

An Examination of Confined Aquifer Gradient Behavior Under Pumping Conditions

Stefanie Fountain
Clemson University, pecletchick@hotmail.com

AN EXAMINATION OF CONFINED AQUIFER GRADIENT BEHAVIOR UNDER PUMPING CONDITIONS

A Dissertation
Presented to
the Graduate School of
Clemson University

In Partial Fulfillment
of the Requirements for the Degree
Doctorate of Science
Environmental Engineering and Earth Sciences

---

by
Stefanie A. Fountain
May 2009

Accepted by:
Dr. Fred J. Molz, III, Committee Chair
Dr. Raymond Christopher
Dr. Ronald W. Falta
Dr. Lawrence C. Murdoch

ABSTRACT

Accurate and reliable estimates of groundwater flow and contaminant transport models are dependent on an understanding of the aquifer properties used to create the models. The borehole flowmeter has been used with increasing frequency at a variety of sites to produce high resolution vertical hydraulic conductivity ($K(z)$) distributions [Boggs et al. 1990; Rehfeldt et al. 1989b; Molz et al. 1989, Boman et al. 1997; Dinwiddie et al. 1999]. In theory, the validity of measurements obtained using borehole flowmeters is contingent on the hydraulic head gradients near the well at each discrete depth resulting from the pumping-induced flow having reached quasi-steady-state. Previous studies to predict the hydraulic head gradients near a well under pumping conditions have been predicated on various assumptions and have resulted in conflicting estimates of the length of time required for these gradients to reach quasi-steady-state.

This study models hypothetical single-porosity, confined, multi-layer aquifers with a minimum of simplifying assumptions to gain further insight into near-well gradient behavior in aquifers. The challenge, presented through the comparison of models presented herein [Javandel and Witherspoon 1969; Ruud and Kabala 1996, 1997; Hemker 1999a, 1999b; Kabala and El-Sayegh 2002], is to create an independent model capable of accurately and reliably reproducing their bulk results while also addressing the smaller inconsistencies among them. The results of the modeling will be applied to flowmeter analysis so that semi-quantitative estimates of the time required for a system to reach the status where flowmeter readings are valid may be obtained for field testing.

DEDICATION

I would like to dedicate this dissertation and subsequent degree to my husband, family and friends. The journey has been long, but you were there for me through it all. Thank you; I would not have made it without you.

I would also like to thank the Environmental Engineering & Earth Sciences faculty for their kind support, advice, and encouragement over the years.

To my managers and colleagues at Geosyntec Consultants, thank you for being so supportive and understanding as I finished my research and completed this dissertation.

ACKNOWLEDGEMENTS

I wish to thank my advisor, Dr. Fred Molz, III and my committee members: Dr. Raymond Christopher, Dr. Ronald W. Falta, and Dr. Lawrence C. Murdoch for their support throughout this project. This project would not have been possible without the funding and support provided by Dr. Molz. I would like to specifically thank Dr. Falta for providing the model used in this study and for his assistance in learning to use the model. I would also like to thank the Graduate School for their financial support of my research.

TABLE OF CONTENTS

Page

Table of Contents (Continued)

Chapter Page

LIST OF TABLES

List of Tables (Continued)

LIST OF FIGURES

List of Figures (Continued)

List of Figures (Continued)

CHAPTER 1

STATEMENT OF PURPOSE

Accurate and reliable estimates of groundwater flow and contaminant transport models are dependent on an understanding of the aquifer properties used to create the models. More specifically, to reliably predict flows of water and contaminants to a pumping well, the vertical hydraulic conductivity profile, *K(z)*, must be evaluated with sufficient resolution as to represent the layers within the model that contribute flow to the well. The borehole flowmeter has been used with increasing frequency at a variety of sites to produce such high resolution *K(z)* distributions [Boggs et al. 1990; Rehfeldt et al. 1989b; Molz et al. 1989, Boman et al. 1997; Dinwiddie et al. 1999]. Flowmeter tests are conducted by inducing a flow out of the aquifer using a pump and by measuring incremental changes in axial flow with depth within the well. The validity of the method used to interpret these measurements is contingent on the gradients near the well at each discrete depth resulting from the pumping-induced flow having reached quasi-steady-state. At a given radius, r_e, a system is defined as being in quasi-steady-state when the piezometric surface is falling at essentially the same rate for all $r \leq r_e$; a finite-radius system is in true steady-state when the piezometric surface ceases to decline. Recently, a transient flowmeter test has been proposed [Kabala and El-Sayegh 2002]; however, the correct application of theory to evaluate the test results is still based on determining whether the gradients have reached quasi-steady-state or remain in a fully transient regime.

Previous studies to predict the hydraulic head gradients near a well under pumping conditions have been predicated on various assumptions and have resulted in conflicting estimates of the length of time required for these gradients to reach quasi-steady-state. Throughout this report, the terms hydraulic gradients and gradients will be used to mean hydraulic head gradients unless otherwise noted. This study will attempt to model various hypothetical homogeneous and heterogeneous, single-porosity, confined, multi-layer aquifers, with a minimum of simplifying assumptions to resolve the conflicting published results as well as to gain further insight into near-well head gradient behavior.

Through careful construction of numerical solutions to the scenarios outlined above and the comparison to previously published numeric, semi-analytical, and analytical results, further insight is gained into the near-well hydraulic gradient behavior of aquifers under pumping conditions. Based on the new insight, further guidelines of a practical nature are developed for performing successful flowmeter tests.

CHAPTER 2

THE USE OF THE ELECTROMAGNETIC BOREHOLE FLOWMETER FOR MEASURING AND ANALYZING VERTICAL HYDRAULIC CONDUCTIVITY DISTRIBUTIONS

One of the most problematic issues intrinsic to any study dealing with the subsurface characterization of a site is that of determining the vertical variation in hydraulic conductivity (K), associated with the site. Recent studies [Boggs et al. 1990; Rehfeldt et al. 1989b; Molz et al. 1989, Boman et al. 1997; Dinwiddie et al. 1999] have suggested that when certain conditions are met, the borehole flowmeter test provides enough information to determine the relative differences of K between selected measurement intervals.

Device Application and Data Acquisition

Flowmeter data, essentially axial discharge within the wellbore as a function of elevation, may be analyzed to yield K data as a function of depth, $K(z)$ (Figure 2.1). The procedures described in Molz and Young [1993] for conducting the flowmeter test are considered to be representative for electromagnetic borehole flowmeter (EBF) application where water is extracted from the well to induce flow. First, a flowmeter log is run in an attempt to measure any natural (ambient) flow in the well, which, if detected, is recorded and saved for later data analysis. Following the ambient test, a pump is placed in the test well and operated at a constant flow rate, Q_P, causing radially inward flow to the well. Typical practice in the field is to pump for a minimum of 30 minutes prior to taking EBF readings [Flach et al. 2000]. After quasi-steady-state behavior is

obtained, the flowmeter is lowered to near the bottom of the well and a measurement of the axial flow rate at the flowmeter depth is obtained (should be zero at a closed well bottom). The instrument is then raised a distance, Δz, and another reading is taken, and so on (Figure 2.1). The result is a series of data points that represent cumulative vertical discharge, Q, within the well screen as a function of vertical position, z. Immediately above the top of the screen, the meter reading should be equal to Q_P, the steady-state pumping rate. This procedure is typically repeated several times to ascertain that the readings are stable.

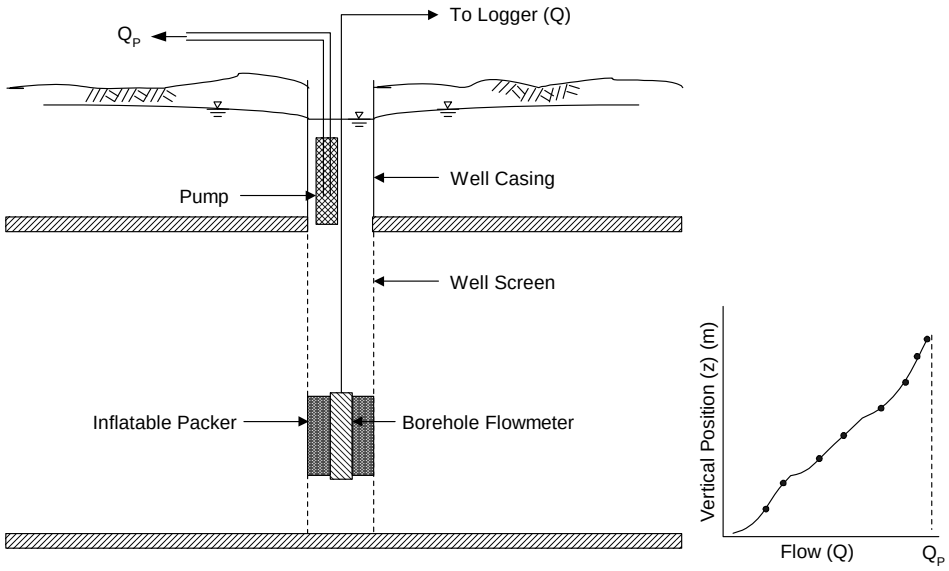

Figure 2.1 Typical apparatus and geometry of an EBF test. Adapted from: Molz and Young [1993].

Analysis of Measurement Data

As described by Molz and Young [1993], there are several related methods for analyzing flowmeter data to obtain $K(z)$. Generally, in analyzing borehole flowmeter

data, it is assumed that the aquifer is composed of a series of *n*-horizontal layers (Figure 2.2).

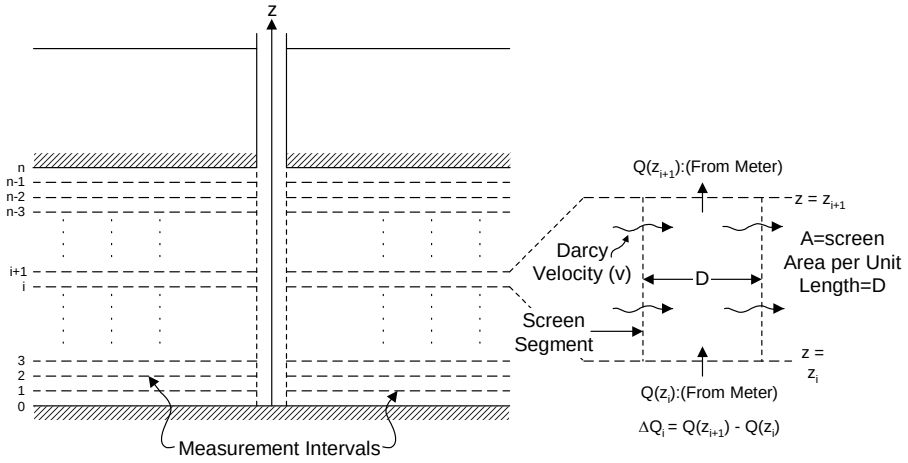

Figure 2.2 Idealized aquifer geometry. Adapted from: [Molz and Young 1993].

The differential flow between adjacent layers at given depth, ΔQ_i, due to pumping is calculated by taking the difference between two successive meter readings. The differential ambient flow, Δq_i, is calculated in the same manner, if detected. An average hydraulic conductivity, $<K>$, for the entire screened section of a well may be calculated by determining the transmissivity (T) for both a standard pumping test and/or a standard recovery test using the Cooper-Jacob method [1946]:

$$T_{PUMPING} =< K > b = \frac{2.303 \times Q_P \times \Delta \log(t)}{4 \times \pi \times \Delta s} \tag{2-1}$$

$$T_{RECOVERY} =< K > b = \frac{2.303 \times Q_P \times \Delta \log\left(\frac{t}{t - t_1}\right)}{4 \times \pi \times \Delta s} \tag{2-2}$$

where T is the transmissivity (m^2/d), t is time (d), t_1 is the duration of pumping (d), s is the drawdown (m), Δs is the change in head over t_1, and b is the aquifer thickness (m).

The flowmeter data are then analyzed using the methods based on a study by Javandel and Witherspoon [1969], which may be manipulated to yield an equation for calculating hydraulic conductivity [Molz et al. 1989]:

$$\frac{K_i}{< K >} = \frac{(\Delta Q_i - \Delta q_i)/\Delta z_i}{Q_P / b} \tag{2-3}$$

where K_i is the hydraulic conductivity of the i^{th} layer (m/d), $<K>$ is the arithmetic average hydraulic conductivity (m/d), and Δz_i is the thickness of i^{th} layer (m).

Device Design and Theoretical Basis

The EBF, developed originally by the Tennessee Valley Authority (TVA), operates according to Faraday's law of induction. The device consists of an electromagnet and two electrodes cast in a durable epoxy, which is cylindrically molded to minimize turbulence effects as water passes by the electromagnet and the electrodes (Figures 2.2 and 2.3). A voltage directly proportional to the translational velocity of the flowing water is then induced across a conductor (the flowing water) moving at right angles through a magnetic field (the electromagnet). The electrodes are used to measure the induced voltage. Electronics attached to the electrodes transmit a voltage proportional to the induced voltage to the device display. The EBF has been shown to be an ideal groundwater velocity measurement device due to its ability to sense and accurately measure low flows. The 1-inch (0.025 m) inner-diameter EBF developed by

the TVA and manufactured by the Quantum Engineering Corporation is sensitive to flows ranging from 40 mL/min to 40 L/min (0.05 m^3/d to 57.6 m^3/d) [Waldrop 1995].

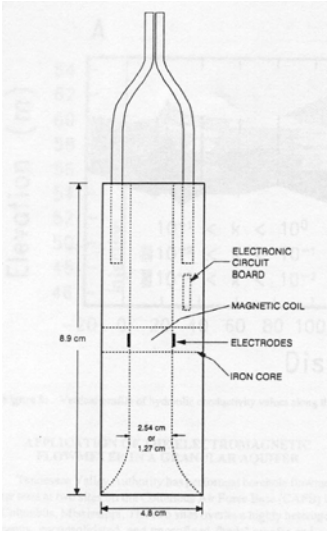

Figure 2.3 Schematic diagram of the EBF [Molz and Young 1993].

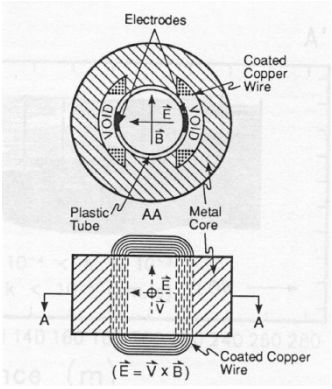

Figure 2.4 Horizontal and vertical cross-sectional views of the EBF sensor [Molz and Young 1993].

Pumping the well until quasi-steady-state behavior is obtained is necessary to ensure meaningful flow measurements. If borehole flowmeter readings are taken before to quasi-steady-state conditions are attained, the flow measurements for a particular depth (ΔQ_i) may be higher or lower, depending on the relative K for the depth of measurement,

than the quasi-steady-state flow for that depth due to cross-flow between layers resulting from vertical hydraulic gradients. This deviation of ΔQ_i during transient conditions in turn results in calculated K values that deviate from their "true" value. The magnitude and behavior of the deviations, however, are not clear at the present time. Whereas the details of applying the EBF and accounting for the possible errors as well as the post-test analysis of the data having been discussed in detail [Molz and Young 1993; Kabala 1994; Ruud and Kabala 1996; Boman et al. 1997; Young 1998; Dinwiddie et al. 1999; Ruud et al. 1999; Arnold and Molz 2000], the final questions left to be answered definitively is how long of a pumping interval is required for a system to attain quasi-steady-state conditions and how close to such conditions must one be to obtain K values that are useful in a practical sense.

To estimate the time required for the flows at the well to reach quasi-steady-state, some *a priori* knowledge of the geological profile of the well is required. This knowledge will typically consist of the boring log recorded at the time of the well installation. Using this information, a model may be constructed to estimate the hydraulic behavior over the depth of the borehole or the length of the well screen. The model may then be used to predict the hydraulic gradient for each layer as a function of time. As these gradients cease to change "appreciably", the flow out of each layer will cease to change "appreciably" and the aquifer is considered to have reached "practical" quasi-steady-state. In most applications, it is more important to accurately identify high-K layers than low-K layers. Thus, information on how such layers behave in the vicinity of quasi-steady-state is important also.

CHAPTER 3

GENERAL THEORY OF VERTICALLY STRATIFIED AQUIFERS

There exists, in general, two ways to characterize vertically stratified aquifers: 1) as systems where there is no connection, or water flow, between the layers (Figure 3.1), or 2) as systems where crossflow between the layers occurs (Figure 3.2). Of these two cases, the allowance for crossflow between layers is more realistic physically; however, it is more complex to evaluate. The actual amount and behavior of crossflow that a system experiences will be a function of time, the vertical to horizontal K ratio, or anisotropy, and the differential horizontal K (or more specifically, differences in the ratio of horizontal K and specific storage, or hydraulic diffusivity) between adjacent layers. The amount of crossflow occurring between layers at any given time prior to quasi-steady-state (please see Chapter 1 for a definition of quasi-steady-state) affects the behavior of the hydraulic gradients for each layer. Once quasi-steady-state is approached in the vicinity of the well, the hydraulic gradients at the well face are essentially equal and constant and crossflow becomes negligible.

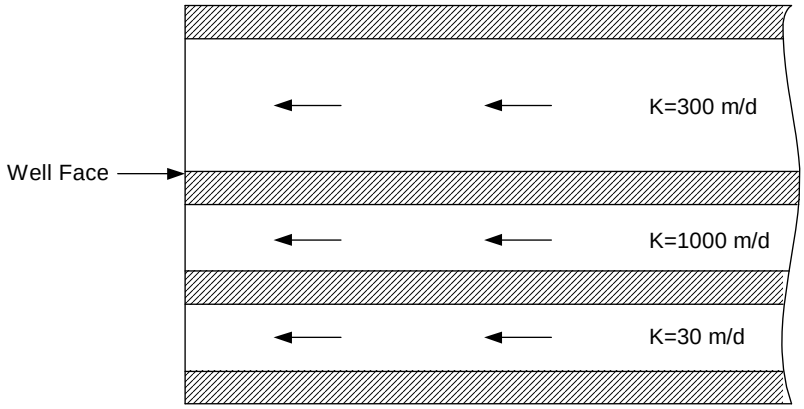

Figure 3.1 Conceptualization of flow to a fully penetrating well in a stratified system without crossflow.

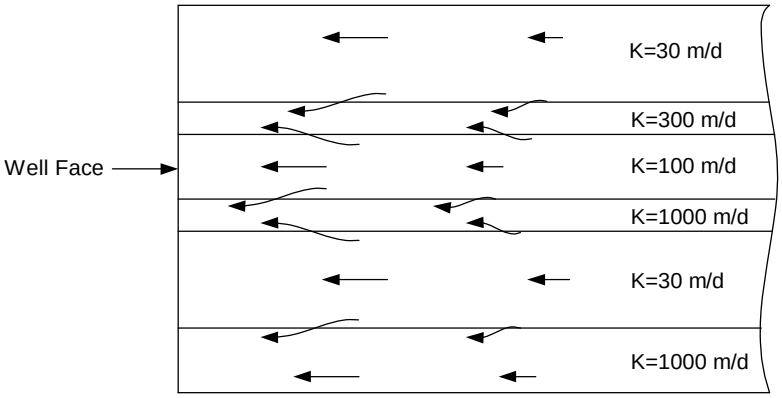

Figure 3.2 Conceptualization of flow to a fully penetrating well in a stratified system with crossflow. Adapted from: [Katz and Tek 1962].

Theoretical Behavior of Stratified Systems

A study by Katz and Tek [1962] led to the following conclusions regarding stratified aquifers: 1) the time during which the use of arithmetic averages of K for a stratified aquifer are inaccurate is small; 2) initially high flow rates often detected during initial system response may account for a large portion of the total water production; and 3) stratified systems with a thickness (b) to well radius (r_w) ratio greater than 10 and with less than a factor of two difference in permeability between layers behave identically to

single layer systems constructed using an arithmetic mean permeability of the layered system. The second finding was confirmed by Russell and Prats [1962], who found that an exponential rate decline in production occurs rapidly. Russell and Prats [1962] showed, that for a two-layer system, the time to reach the exponential decline in production could be approximated by:

$$\frac{(kh)_{TOTAL}\, t}{(\theta h)_{TOTAL}\, c\mu r_{eff}^2} \approx 0.3 \tag{3.1}$$

where k is the permeability, h is the thickness of a given layer, c is the coefficient of compressibility for water, μ is the water viscosity, and *TOTAL* denotes the property total (i.e., $(Kh)_{TOTAL}$ for a two-layer system equals $k_1h_1+k_2k_2$).

Factors Influencing Crossflow

As a vertically stratified aquifer undergoes pumping, the higher-*K* layers will initially account for the majority of the system water yield. As the higher-*K* layers begin to deplete water from storage, a vertical head gradient between the higher-*K* layers and the lower-*K* layers is induced and the water in the lower-*K* layers begins to respond to the change in vertical head gradient by flowing into the higher-*K* layers. This movement of water from one layer to another, or crossflow, will continue until the difference in hydraulic head between layers becomes zero. When crossflow becomes negligible, the system will be near quasi-steady-state. This implies that the hydraulic head gradients at the well face are constant and equal and flow to the well is constant, uniform, and horizontal.

It is possible to place upper and lower bounds on the amount of crossflow a given system may experience by considering the limiting cases. The lower bound for crossflow is the case where the producing layers are isolated from each other by impermeable layers (Figure 3.1). The upper bound for crossflow is the situation where the lower-*K* layers are able to indefinitely supply water to the higher-*K* layers and where flow between the lower and higher-*K* layers is instantaneous (i.e., infinite vertical *K*) [Katz and Tek 1962]. Whereas it may be possible, due to large differences in *K* between layers, to reliably and accurately portray an aquifer as a series of sub-aquifers separated by confining units (Figure 3.1), it is less probable that an aquifer may be represented using an infinite vertical *K*. It should be noted, however, that vertical wells often behave in a manner consistent with an infinite vertical *K* [Elci et al. 2001]. Katz and Tek [1962] proposed that the effect of vertical *K* on crossflow is related to the relative thickness of the system compared to the system extents; i.e., decreasing the thickness of the system will have the same effect as increasing the vertical *K*. In general, as the measured vertical heterogeneity resolution is increased, it becomes less feasible to approximate a system according to either limiting scenario. For this reason, it is important to understand the factors that influence the degree of crossflow in a system at a given place and time.

CHAPTER 4

COMPARISON OF DIFFERENT METHODS FOR MODELING HYDRAULIC GRADIENT OR DRAWDOWN BEHAVIOR IN VERTICALY STRATIFIED CONFINED AQUIFERS

Analytical Models

Numerous researchers have presented analytical models to solve for the flows in multi-layer aquifer systems. Generally, these solutions are highly complex and any advantage they may have due to the exactness of the solution is far outweighed by their impracticality in terms of evaluation and inflexibility with respect to the assumptions and conditions that must be satisfied for the solution(s) to be applicable. Katz and Tek [1962] and Russell and Prats [1962] developed analytical models that provided solutions for bounded two-layer aquifers with crossflow and a constant drawdown at the wellbore. Jacquard [1960] presented an analytical solution for a similar system but with a constant pumping rate. Several other analytical solutions for two-layer systems allow for partially penetrating wells where the well is located in only one of the two layers [Javandel and Witherspoon 1980; Javandel and Witherspoon 1983; Szekely 1995]. The vast majority of remaining analytical models for multi-layer aquifer systems can be more accurately described as multi-aquifer solutions, as they are only applicable for multiple aquifer units separated by aquitards (Figure 3.1). The analytical solutions provided by Neuman and Witherspoon [1969], Hemker [1985], Hunt [1985], Maas [1987], and Hemker and Maas [1987] all fall into this category. In 1989, Sen [1989] presented an analytical solution for the case of a vertically graded aquifer where the vertical hydraulic conductivity

distribution was assumed to vary linearly with elevation and no crossflow between adjacent layers was allowed. Whether for reasons of analyzing increasing numbers of layers, ease of application, or analyzing multiple scenarios with the same formulation, numerical or semi-analytical methods provide considerable advantages over analytical solutions for multi-layer aquifer problems.

Numerical Models

The set of numerical models used in conjunction with borehole flowmeter tests can be broadly classified into two main categories based on the boundary condition assumed at the wellbore: 1) drawdown in the well is calculated based on the stipulation that the flows from each layer are proportional to the transmissivity of the layer with the head in the well held constant; and 2) the flux out of each layer is calculated based on the drawdown in the well for a given time with the overall pumping rate out of the well held constant; the drawdown at the well for the constant pumping rate or uniform well drawdown condition must be iteratively determined or systematically guessed. Alternatively, the drawdown in the well may be solved directly through the use of a finite-element method [Javandel and Witherspoon 1969] or other implicit method. Once the boundary condition at the well has been selected, other secondary assumptions as to the inclusion and nature of wellbore storage, skin effects, well losses, crossflow between adjacent layers, etc. may be incorporated.

Several numerical or semi-analytical models that incorporate one of the two well boundary conditions and some combination of the secondary assumptions are available. For the purposes of this study, the focus will be on four fairly comprehensive models

constructed specifically to analyze multi-layer aquifers which have undergone validation and have been compared to at least one other model of the four: Javandel and Witherspoon [1969], Ruud and Kabala [1996, 1997], Hemker [1999a, 1999b], and Kabala and El-Sayegh [2002].

Javandel and Witherspoon [1969]

One of the earliest comprehensive numerical solutions was set forth by Javandel and Witherspoon [1969] for a two-layer confined aquifer with a single pumping well. The numerical code constructed by Javandel and Witherspoon [1969] is a finite element model formulated to solve transient fluid flow in heterogeneous, two-layer and multi-layer, isotropic and anisotropic aquifers. Both constant rate pumping and constant head boundaries are permitted boundary conditions at the well, no flow boundaries are imposed on the top and bottom of the aquifer, and a constant head boundary is assumed to exist far from the production well. Crossflow between the different layers is allowed. The results from the Javandel and Witherspoon [1969] study revealed four key findings. First, at early times the gradient behaviors in layers with different K are significantly different due to preferential flow in the higher-K layer(s). This difference diminishes with time as the flows in the layers equilibrate and the drawdown in each layer approaches the Theis solution: the smaller the difference in K values between the layers, the shorter the time frame for convergence to the Theis solution, due to decreasing amounts of crossflow between layers. Second, after the first few minutes of pumping, the differences between the near-well drawdown in the layers and the Theis solution are negligible. Javandel and Witherspoon [1969] note, however, this may not be true away

from the wellbore or in thick, multi-layer aquifers. Third, deviations from the Theis solution in a given layer are less for those layers with higher-*K* values. Finally, once the system has attained a quasi-steady-state condition, implying that flow is constant and horizontal out of each layer, the flux from each layer into the well is proportional to the *K* of the layer.

Ruud and Kabala [1996]

In 1996, Ruud and Kabala proposed a numerical model for simulating the near-well hydraulic behavior of layered confined aquifers under pumping conditions. The model was constructed to determine the non-uniform wellbore flux distribution for a fully penetrating well. The model is a fully implicit finite difference approximation subject to no flow boundaries at the top and bottom of the aquifer, no drawdown at the effective radius boundary, and the pumping condition (also referred to as the well constraint boundary) at the wellbore. The results of Ruud and Kabala's modeling efforts suggest that, contrary to the results of Javandel and Witherspoon [1969], the flux along the wellbore for some layers may be persistently transient or non-uniform. For the parameter values studied, the Javandel and Witherspoon [1969] analysis showed that flows toward a well in layered aquifers quickly become horizontal. In certain cases, therefore, the Ruud and Kabala [1996] model findings deviate from the Javandel and Witherspoon [1969] model findings. The situations in which the conclusions differ are those aquifers having low hydraulic conductivity and high storativity (i.e., low hydraulic diffusivity), which was not considered in detail by Javandel and Witherspoon [1969]. They also pointed out correctly that the hydraulic diffusivity ratio between adjacent layers, rather than the

magnitude of the corresponding K ratio, is the appropriate parameter for analyzing multi-layer aquifers and flowmeter tests.

Hemker [1999a, 1999b]

Hemker's [1999a, 1999b] model for analyzing flow behavior to a well in layered aquifers is a hybrid analytical-numerical model where the radial component is solved analytically and the vertical component is solved numerically. The model was originally constructed to study changes in specific storage (S_s) under pumping conditions. The mathematical formulation for the model is essentially the same as that used by Ruud and Kabala [1997] with obvious changes made to allow for the analytical-numerical solution scheme. The constant head model [1999a], which assumes that the flow into the well from each layer is proportional to the layer transmissivity, allows for ready comparison to the majority of other analytical and numerical models available for modeling layered systems; however, even in homogeneous systems this assumption of a constant head in the well or uniform wellbore flux is not generally correct. Hemker [1999b] suggested using a uniform drawdown at the well boundary (i.e., the flow into the well from each layer is not necessarily proportional to the layer transmissivity prior to steady-state) as a more realistic boundary condition. This type of boundary condition greatly complicates the solution of the model due to the need for iteration in solving the fluxes from each layer such that they satisfy the boundary condition. Hemker [199b] acknowledges that the drawdown in the well could alternatively be solved directly using the principle of superposition [Javandel and Witherspoon 1969] or other simultaneous solution techniques. Hemker's results [1999b] largely focus on scenarios with partially-

penetrating wells in confined aquifers, with scenarios focusing on fully-penetrating wells in confined aquifers discussed to a lesser extent. With respect to fully-penetrating wells in confined aquifers, Hemker [1999b] found that at early times, the two well boundary conditions (constant head versus uniform drawdown) resulted in drawdowns at the well that differed by as much as 27% and that this difference gradually decreases with time. Hemker [1999b] also reported that the system exhibited vertical gradients in the layers until 0.1 days (2.4 hours).

Kabala and El-Sayegh [2002]

Kabala and El-Sayegh [2002] have assembled a fairly comprehensive review of the transient flowmeter test models including no crossflow models, numerical crossflow models, semi-analytical crossflow models with no skin, semi-analytical crossflow models with infinitesimal skin, and semi-analytical crossflow models with thick skin, in addition to their own model which is a semi-analytical model that accounts for uniformly thick skin, wellbore storage, and crossflow. Like the Javandel and Witherspoon [1969] model, the Kabala and El-Sayegh [2002] model is constructed using the constant head boundary. The Kabala and El-Sayegh [2002] model also uses an approximation of transient crossflow characterized by the differential quotient of layer-averaged drawdowns in adjacent layers. The Kabala and El-Sayegh [2002] model was compared to the Ruud and Kabala [1996, 1997] model, which relaxes the uniform wellbore flux and pseudo-steady-state crossflow assumptions. Kabala and El-Sayegh [2002] concluded that their model compared favorably with the Ruud and Kabala [1996, 1997] model for the scenarios tested. In addition, Kabala and El-Sayegh [2002] concluded that their model was capable

of interpreting multiple pumping rate transient flowmeter tests so long as the proper Laplace transform inversion algorithm is used, such as the De Hoog et al. inversion [De Hoog et al. 1982].

Summary of Selected Models

Of the four models discussed, only the Javandel and Witherspoon [1969] and Ruud and Kabala [1996, 1997] models deal specifically and rigorously with the assessment of individual layer hydraulic gradient behavior. The Javandel and Witherspoon [1969] model resulted in short times to hydraulic gradient quasi-steady-state and postulated that from a practical standpoint, deviations from the Theis solution were negligible after a dimensionless time of 1,000 (see Chapter 5 for the definition of dimensionless time), which was generally on the order of several minutes. Ruud and Kabala [1996, 1997] found that for some systems, or some layers within certain systems, reaching quasi-steady-state could require a significantly long time. For example, the layer flows for a two-layer system with K-values of 4.0E-05 m/s and 4.0E-07 m/s and with S_s-values of 1.0E-05 and 1.0E-03 m^{-1} had not reached quasi-steady-state at three hours or a dimensionless time of nearly 29,000 (calculated in the same manner as Javandel and Witherspoon [1969]. The Hemker [1999b] model examined layer-specific behavior as a function of cumulative flow and behavior radially distant from the well, but made little mention of the transient behavior of individual layer hydraulic head gradients. The single scenario consisting of a fully-penetrating well in a confined, heterogeneous aquifer reported by Hemker [1999b] was reported to attain quasi-steady-state in 2.4 hours. The Kabala and El-Sayegh [2002] model was constructed specifically to analyze

multiple pumping rate transient flowmeter tests, which does not require quasi-steady-state conditions. Kabala and El-Sayegh [2002] do note however, that whereas their model results compares well to the Ruud and Kabala [1996, 1997] model results, errors for the Kabala and El-Sayegh [2002] model increase as the hydraulic diffusivity contrast increases.

The challenge presented through the comparison of these four models is to create an independent model capable of:

1. accurately and reliably reproducing their bulk results;
2. addressing the smaller inconsistencies between them; and
3. providing meaningful and conclusive data regarding the hydraulic gradient behavior for layered systems.

This report will discuss the influences of key parameters on the hydraulic gradient response including:

- layer hydraulic conductivity;
- layer specific storage;
- layer thickness;
- layer arrangement; and
- overall system thickness.

In addition, the following inconsistencies in the literature conclusions will be addressed and resolved, especially the conflicting statements of the time required to attain quasi-steady-state from Javandel and Witherspoon [1969] and Ruud and Kabala [1997].

Finally, the potential implications of the common practice of pumping for 30 minutes prior to taking EBF readings with respect to the values of *K* obtained is discussed.

CHAPTER 5

HYDRAULIC GRADIENT BEHAVIOR IN SINGLE-DOMAIN, MULTI-LAYER CONFINED AQUIFERS WITH HOMOGENEOUS AND ISOTROPIC OR ANISOTROPIC LAYERS

Physical Model

The problem of a multi-layer, confined aquifer with radial flow to a well screened along the entire thickness of the aquifer (b) under a steady pumping influence (Q_P) may be conceptualized as a series of j horizontal, homogeneous layers (Figure 5.1). Each layer may have a distinct hydraulic conductivity (K_{rj}), specific storage (S_{sj}), and associated discharge, Q_j. The resultant flows (assuming horizontal flow) from each layer are then summed to obtain the overall pumping rate, Q_P.

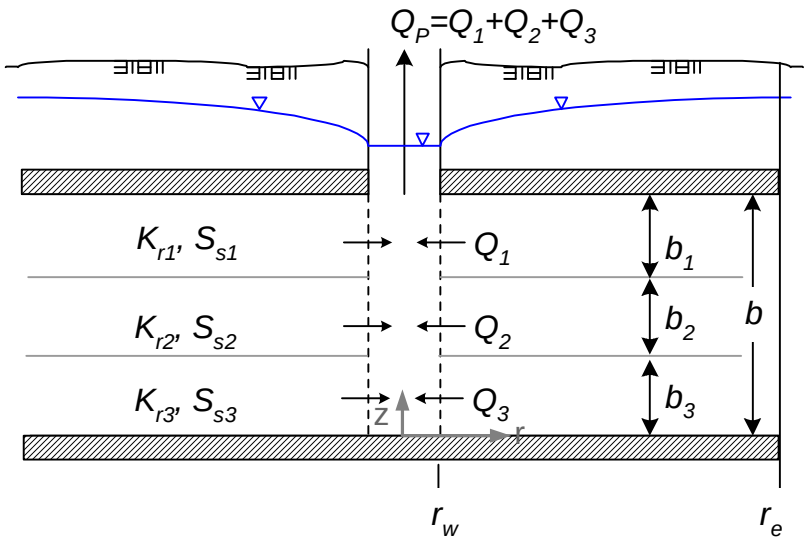

Figure 5.1 Schematic representation of a three-layer, fully confined, finite radius aquifer with flow to a fully penetrating well.

The governing equation used to describe flow in similar single layer, non-homogeneous systems having radial symmetry is [Hantush 1964]:

$$S_s \frac{\partial s}{\partial t} = \frac{K_r}{r}\frac{\partial s}{\partial r} + \frac{\partial}{\partial r}\left(K_r \frac{\partial s}{\partial r}\right) + \frac{\partial}{\partial z}\left(K_z \frac{\partial s}{\partial z}\right) \tag{5-1}$$

where s is the drawdown at any given location (m), K_r is the hydraulic conductivity in the radial direction (m/d), K_z is the hydraulic conductivity in the vertical direction (m/d), S_s is the specific storage (m^{-1}), r denotes the radial direction, z denotes the vertical direction, and t is time (d). For the purposes of this study, the following initial and boundary conditions apply:

$$\begin{aligned} &s(r,z,0) = 0 \\ &s(\infty,z,t) = 0 \\ &\frac{\partial s(r,0,t)}{\partial z} = \frac{\partial s(r,b,t)}{\partial z} = 0 \end{aligned} \tag{5-2}$$

in combination with the constant pumping rate at the well boundary condition:

$$Q_P = -2\pi r_w \int_0^b K(r_w,z)\frac{\partial s(r_w,z,t)}{\partial r}\,dz \tag{5-3}$$

Eqn. 5-2 is applied to each layer of the system simultaneously (skin effects, head losses in the well, flow turbulence through the well screen, and pore-elastic effects at the well were not considered). Rearranging Eqn. 5-1 and employing the anisotropy relationship ($K_z=\alpha K_r$) and the definition of hydraulic diffusivity:

$$D_L = \frac{K_{rL}}{S_{sL}} \tag{5-4}$$

where L is the layer designation, yields:

$$\frac{1}{D_L}\frac{\partial s_L}{\partial t} = \frac{1}{r}\frac{\partial s_L}{\partial r} + \frac{\partial^2 s_L}{\partial r^2} + \alpha\frac{\partial^2 s_L}{\partial z^2} \tag{5-5}$$

Similarly, the boundary conditions are extended to the multi-layer problem:

$$\begin{aligned} &s_L(r,z,0) = 0 \\ &s_L(r_e,z,t) = 0 \\ &\frac{\partial s_L(r,0,t)}{\partial z} = \frac{\partial s_L(r,b,t)}{\partial z} = 0 \end{aligned} \tag{5-6}$$

with the constant pumping rate at the well boundary condition:

$$Q_P = -2\pi r_w \sum_{L=1}^{n} K_{rL} b_L \frac{\partial s_L(r_w,z,t)}{\partial r} \tag{5-7}$$

Steady-State Derivation

The steady-state relationship for a single-layer, confined aquifer with a finite effective radius may be obtained from Eqn. 5-1, combined with the pumping condition at the well (Eqn. 5-7) and the other boundary conditions (Eqn. 5-6).

$$0 = \frac{K_r}{r}\frac{\partial s}{\partial r} + K_r\frac{\partial^2 s}{\partial r^2} + K_z\frac{\partial^2 s}{\partial z^2} \tag{5-8}$$

At steady-state, we can further assume that all flow is horizontal, such that the vertical term goes to zero. As K_r is considered to be uniform, we may drop that coefficient and we are left with the following:

$$0 = \frac{1}{r}\frac{ds}{dr} + \frac{d^2 s}{dr^2} \tag{5-9}$$

Employing the pumping boundary condition (Eqn. 5-7) with the second condition from Eqn. 5-6 results in the following:

$$s(r_w) = \frac{Q_P}{2\pi b K_r} \ln\left(\frac{r_e}{r_w}\right) \tag{5-10}$$

where r_e is the effective radius.

Adapting this single-layer solution to the multi-layer problem, employing the same basic boundary conditions and assumptions, we obtain:

$$s_L(r_w) = \frac{Q_{PL}}{2\pi b_L K_{rL}} \ln\left(\frac{r_e}{r_w}\right) \tag{5-11}$$

According to Eqn. 5-7, the sum of the flows from all layers for the system must be equal to the total pumping rate, Q_P. Using a three-layer case to rigorously examine the steady-state case, we obtain (from Eqn. 5-7):

$$Q_P = -2\pi r_w \left(K_1 b_1 \frac{\partial s_1}{\partial r} + K_2 b_2 \frac{\partial s_2}{\partial r} + K_3 b_3 \frac{\partial s_3}{\partial r} \right) = Q_1 + Q_2 + Q_3 \tag{5-12}$$

Furthermore, at quasi-steady-state, the gradients in each layer are constant and equal to one another and at r_w, the layer drawdowns must be equal to the overall drawdown, $s(r_w)$, such that:

$$s(r_w) = \frac{Q_1}{2\pi K_1 b_1} \ln\left(\frac{r}{r_w}\right) = \frac{Q_2}{2\pi K_2 b_2} \ln\left(\frac{r}{r_w}\right) = \frac{Q_3}{2\pi K_3 b_3} \ln\left(\frac{r}{r_w}\right) \tag{5-13}$$

From Eqns. 5-12 and 5-13, the following must hold true at steady-state:

$$\frac{Q_P}{\left(K_1 b_1 + K_2 b_2 + K_3 b_3\right)} = \frac{Q_1}{K_1 b_1} = \frac{Q_2}{K_2 b_2} = \frac{Q_3}{K_3 b_3} \tag{5-14}$$

From Eqn. 5-14, we obtain:

$$Q_1 = \frac{K_1 b_1}{\left(K_1 b_1 + K_2 b_2 + K_3 b_3\right)} Q_P \tag{5-15}$$

$$Q_2 = \frac{K_2 b_2}{\left(K_1 b_1 + K_2 b_2 + K_3 b_3\right)} Q_P \tag{5-16}$$

$$Q_3 = \frac{K_3 b_3}{\left(K_1 b_1 + K_2 b_2 + K_3 b_3\right)} Q_P \tag{5-17}$$

This implies that at steady-state, the rate of change in drawdown (i.e., the hydraulic gradient) is constant and equal throughout the domain and is additionally proportional to the transmissivity of the layer. This steady-state analysis for the three-layer case may be extended to systems with any finite number of layers:

$$s(r) = \frac{Q_P}{2\pi \sum_{j=1}^{n} K_j b_j} \ln\left(\frac{r_e}{r_w}\right) \tag{5-18}$$

Eqn. 5-18 may be alternatively written as:

$$s(r) = \frac{Q_P}{2\pi b \overline{K}} \ln\left(\frac{r_e}{r_w}\right) \tag{5-19}$$

where $b=\Sigma b_j$ and:

$$\overline{K} = \frac{\sum_{j=1}^{n} K_j b_j}{\sum_{j=1}^{n} b_j} \tag{5-20}$$

Numerical Model

TMVOC [Pruess and Battistelli 2002], a specialized module of the TOUGH2 simulator [Pruess et al. 1999], was employed throughout this study to simulate different aquifer scenarios. TMVOC was developed primarily to analyze non-aqueous phase liquid (NAPL) fate and transport for both unsaturated and saturated subsurface conditions. By selecting for certain modules and by properly parameterizing select variables, it is possible to employ TMVOC to analyze the single-phase (i.e., water), confined aquifer flow to a well under a constant pumping rate. TMVOC was selected for this study based on its ability to solve radial domain scenarios as well as its being an integral finite difference model (IFDM) which allows for the direct solution of drawdown in a well for a multi-layer aquifer system subject to pumping. A robust body of literature about and using the TOUGH2 and TMVOC simulators exists, including verification and validation of the models [Moridis and Pruess 1995; Pruess et al. 1996]. As the TMVOC simulator has been previously verified and validated by the developers and other researchers, these steps are not repeated herein; however, testing of the simulator for special cases was performed by comparing the model results to several analytical solutions to ensure proper use of the simulator in this application.

Model Space and Time Discretization

The mass and energy balance equations solved by the TOUGH2 family of codes may be expressed as [Finsterle et al. 2006; Pruess and Battistelli 2002]:

$$\frac{d}{dt}\int_{V_n} M^{\kappa} dV_n = \int_{\Gamma_n} F^{\kappa} \bullet n d\Gamma_n + \int_{V_n} q^{\kappa} dV_n \tag{5-22}$$

where the integration is performed over the subdomain V_n, which is bounded by the surface Γ_n; M represents mass, with κ representing the mass component (i.e., water); F represents mass flux; q represents sinks or sources; and n is the unit normal vector on surface element $d\Gamma_n$, pointing inward into V_n. The mass accumulation term for water is [Finsterle et al. 2006]:

$$M^{\kappa} = \phi \sum_{\beta} S_{\beta} \rho_{\beta} x_{\beta}^{\kappa} \tag{5-23}$$

where β is the phase, ϕ is porosity, S_β is the saturation of phase β, ρ_β is the density of phase β, and x_β^{κ} is the mass fraction of component κ in phase β (in the TMVOC version of the TOUGH code, this is a molar fraction). The advective mass flux is summed over phases [Finsterle et al. 2006]:

$$F^{\kappa}\Big|_{adv} = \sum_{\beta} x_{\beta}^{\kappa} F_{\beta} \tag{5-24}$$

Applying Darcy's law yields [Pruess and Battistelli 2002]:

$$F_{\beta} = \rho_{\beta} u_{\beta} = -k \frac{k_{r\beta} \rho_{\beta}}{\mu_{\beta}} \left(\nabla P_{\beta} - \rho_{\beta} g \right) \tag{5-25}$$

where u_β is the Darcy velocity in phase β, k is absolute permeability, $k_{r\beta}$ is relative permeability of phase β (since this study involves the single phase flow of water, $k_{r\beta}$ is equal to 1), μ_β is viscosity, and

$$P_\beta = P + P_{c\beta} \tag{5-26}$$

where P_β is the pressure in phase β, P is the reference pressure, and $P_{c\beta}$ is the capillary pressure (zero for single phase). Eqn. 5-22 can be discretized in time and space using the IFDM method, using appropriate volume averages, to obtain [Pruess and Battistelli 2002]:

$$\int_{V_n} M^\kappa dV_n = V_n M_n \tag{5-27}$$

$$\int_{\Gamma_n} F^\kappa \bullet n d\Gamma_n = \sum_m A_{nm} F_{nm} \tag{5-28}$$

Where F_{nm} is the average value of the normal component of F over the surface A_{nm} between volume elements V_n and V_m. For the Darcy flux term [Pruess and Battistelli 2002]:

$$F_{\beta,nm} = -k_{nm}\left[\frac{k_{r\beta}\rho_\beta}{\mu_\beta}\right]_{nm}\left[\frac{P_{\beta,n} - P_{\beta,m}}{D_{nm}} - \rho_{\beta,nm} g_{nm}\right] \tag{5-29}$$

where nm denotes the interface between blocks n and m, D_{nm} is the distance between the nodal points n and m, and g_{nm} is the component of gravitational acceleration from m to n.

Numerical Model Application

Verification of the numeric model was conducted by comparing the numeric model results to: 1) the steady-state solution for a homogeneous, isotropic, fully-confined, fully-penetrating well, finite-radius system [Thiem 1906]; and 2) transient solutions for a homogeneous, isotropic, fully-confined, fully-penetrating well, infinite-radius system [Hantush 1964; Theis 1935; Lee 1998]. It should be noted that the analytical time-domain solutions assume the aquifer to be infinite in horizontal extent; however, these solutions may be compared to the finite numerical case until the far radial boundary begins to influence the system behavior. Once steady-state for the finite-radius system is attained the transient analytical solutions are no longer comparable. To ensure that the assumptions of the analytical infinite domain solutions may be comparable over a significant range of time, a sufficiently large effective radius is employed in the numerical model.

Equivalency of the IFDM to the FDM

The mass and energy balance equations solved by the TOUGH2 family of codes can be related to the parameters typically evaluated in single-phase groundwater flow (e.g., head or drawdown, hydraulic diffusivity (hydraulic conductivity and specific storage), flow, etc.). Substituting Eqns. 5-24 and 5-25 into Eqn. 5-22 results in [Pruess and Battistelli 2002]:

$$\frac{dM_n^\kappa}{dt} = \frac{1}{V_n}\sum_m A_{nm} F_{nm}^\kappa + q^\kappa \tag{5-30}$$

For single-phase groundwater flow [Finsterle et al. 2006],

$$\frac{dM_n^{\kappa}}{dt} = \rho_\beta S_s \frac{dh_n}{dt} \tag{5-31}$$

where S_s is specific storage and h is the hydraulic head in element n. Other terms are defined as:

$$M_w = \phi \rho_w \tag{5-32}$$

$$K_{nm} = k_{nm} \frac{\rho_\beta g}{\mu_\beta} \tag{5-33}$$

$$\nabla h = \frac{\nabla P_\beta}{\rho_\beta g} + \nabla z \tag{5-34}$$

where K_{nm} is the hydraulic conductivity of phase β. Changes in hydraulic head, h, can be related to drawdown, s, as follows:

$$ds = -dh \tag{5-35}$$

Eqns. 5-28 through 5-30 can be substituted into Eqns. 5-26 and 5-27 to obtain:

$$\frac{1}{D}\frac{ds}{dt} = \frac{1}{V_n}\sum_m \frac{A_{nm}}{D_{nm}}\left(-\nabla s\right) + q \tag{5-36}$$

Eqn. 5-36 demonstrates that as with Eqn. 5-5, the IDFM system of equations can be simplified such that the hydraulic diffusivity, D, and the sum of Δz, or the aquifer thickness (b) are the sole variables that differ between simulations (assuming that the radial domain is held constant across all model scenarios).

Numerical Model Set-up

Universal Parameters

Universal parameters are those which were determined prior to beginning modeling and which are held constant across all simulations. These parameters include:

- Temperature – 20 degrees Celsius; the temperature of the system was selected such that the viscosity of water is 1 centipoise (cp).
- Water compressibility (β) – 4.4E-10 Pa^{-1}.
- Water density (ρ) – 998.2 kg/m^3, the density of water at 20 degrees Celsius.
- Porosity (ϕ) of the well elements – 0.99. In real-world applications, the porosity inside the well would be considered to be 1.0; 0.99 was employed to avoid instability in the model.
- Well parameters:
    - Permeability (k) of the well elements – Sinks and sources (water in this study) are handled through the GENER module in TMVOC, where a production (<0) or generation rate (>0) is defined and applied to the elements specified. The extraction rate (production rate) is specified within in the GENER module to be a constant mass rate throughout each simulation. The elements where the production or generation rate is applied must also be defined in the ROCKS module. To simulate an open well with negligible losses, the permeability of the elements making up the interior of the well

should be assigned a k greater than any applied within the aquifer elements. For this study, the k was initially set to 1.0E-07 m^2 and was incrementally increased until the differences between successive model run drawdowns were no longer changing. The extraction rate (production rate) is then applied to the bottom-most well element to simulate water extraction.

- Well Radius (r_w) – set to 0.05 m (or 4 in, a typical flowmeter test well diameter).
- Effective Radius (r_e) – set to 20,000 m to avoid boundary effects during the time-frame of interest (i.e., early time or time prior to steady-state).

Variable Definitions

There are several variables must be defined for each simulation or calculated based on defined parameters:

- Porosity (ϕ) – porosity is set for each material defined in ROCKS using typical values for the materials being considered in each simulation. For instance, ϕ is set to 0.35 for medium sands.
- Pore compressibility (COM) – The pore compressibility must be defined for each material defined in the ROCKS module and is a function of the layer specific Storage (S_s):

$$COM = \frac{S_s}{\rho g \varphi} - \beta \tag{5-37}$$

where g is the acceleration of gravity (9.81 m/s^2). Storage may be defined as the following:

$$\frac{\partial M}{\partial t} = \frac{\partial M}{\partial h}\frac{\partial h}{\partial t} \tag{5-38}$$

where dM/dH is the storage coefficient. Using Eqns. 5-32 and 5-38, the following is obtained:

$$\frac{\partial M}{\partial h} = \frac{\partial(\phi\rho)}{\partial h} \tag{5-39}$$

Using the product rule on the right-hand term yields:

$$\frac{\partial(\phi\rho)}{\partial h} = \rho\frac{\partial\phi}{\partial h} + \phi\frac{\partial\rho}{\partial h} \tag{5-40}$$

where the first portion of the right-hand term represents aquifer compression and the second portion represents water compression. The density of a slightly compressible liquid, such as water, may be defined as:

$$\rho = \rho_o \exp\{\beta_l(P - P_o)\} \tag{5-41}$$

where r=r_o at P=P_o and β_l is the compressibility of water (4.4E-10 Pa^{-1}). Again, using the chain rule:

$$\frac{\partial\rho}{\partial h} = \frac{\partial\rho}{\partial P}\frac{\partial P}{\partial h} \tag{5-42}$$

where:

$$P = \rho g h + \rho g z \tag{5-43}$$

such that:

$$\frac{\partial P}{\partial h} = \rho g \tag{5-44}$$

Then, using Eqn. 5-41, the following is obtained:

$$\frac{\partial \rho}{\partial P} = \beta_l \rho_o \exp\{\beta_l (P - P_o)\} = \beta_l \rho \tag{5-45}$$

which may be rearranged to obtain:

$$\beta_l = \frac{1}{\rho}\frac{\partial \rho}{\partial P} \tag{5-46}$$

The combination of Eqns. 5-41 though 5-46 yields:

$$\phi \frac{\partial \rho}{\partial h} = \varphi \rho g \frac{\partial \rho}{\partial P} = \rho(\phi \rho g)\beta_l \tag{5-47}$$

Now, for aquifer compression,

$$\frac{\partial \phi}{\partial h} = \frac{\partial \phi}{\partial P}\frac{\partial P}{\partial h} = \rho g \frac{\partial \phi}{\partial P} \tag{5-48}$$

From soil mechanics, the compressibility of soil may be defined as:

$$C_b = \frac{-1}{V_T}\frac{\partial V_T}{\partial \sigma'} \tag{5-49}$$

Where C_b is compressibility, V_T is total volume, and σ' is effective stress. If it is assumed that the change in total volume is the sum of the change in void volume (V_V) and the change in solids volume (V_S) and additionally

that the change in V_S is much less than the change in V_V such that dV_T is approximately equal to dV_V. Furthermore, $V_V=\phi V_T$. This results in:

$$C_b = \frac{-1}{V_T}\frac{\partial(\phi V_V)}{\partial P} \tag{5-50}$$

As mass (M) is defined on a unit volume basis, V_T=1 and the following may be obtained:

$$C_b = \frac{\partial \phi}{\partial P} \tag{5-51}$$

Thus:

$$\frac{\partial \phi}{\partial h} = \rho g C_b \tag{5-52}$$

Combining Eqns. 5-47 and 5-52 with Eqn. 5-40 results in:

$$\frac{\partial M}{\partial h} = \rho\frac{\partial \phi}{\partial h} + \phi\frac{\partial \rho}{\partial h} = \rho(\rho g)(C_b + \phi\beta_l) \tag{5-53}$$

Thus, the storage term becomes:

$$\frac{1}{\rho}\frac{\partial M}{\partial h} = \rho g(C_b + \phi\beta_l) = S_s \tag{5-54}$$

However, in TOUGH2, pore compressibility (COM) is defined as:

$$COM = \left(\frac{1}{\varphi}\frac{d\varphi}{dP}\right)_{Temperature} \tag{5-55}$$

Resulting in a definition of S_s of:

$$S_s = \rho g \varphi (COM + \beta) \tag{5-56}$$

- Permeability (k) – Permeability is calculated using the selected hydraulic conductivities (K) for each material defined in the ROCKS module:

$$k = \frac{K\mu}{\rho g} \tag{5-57}$$

- Production rate (Q_p) – the production rate is selected to be within the range of measurement of the EBF.

Implementation Boundary Conditions

From Eqn. 5-6, the scenarios modeled in this study are subject to no flow boundaries at the top and bottom of the aquifer (i.e., a fully-confined, non-leaky aquifer). This type of boundary condition is the default boundary condition in TMVOC; therefore no modification to the input file is made for these boundaries.

The simulations in this study are also subject to zero drawdown at the outer radius. To implement this boundary condition in TMVOC, the elements adjacent to the far boundary are assigned very large volumes. For this study, these elements were assigned volumes on the order of 10^{60} m^2.

The final boundary condition employed throughout this study is a constant pumping rate over the duration of the simulation (Eqn. 5-7). This is implemented in TMVOC through the use of the GENER module, where the variable GX is set to the desired Q_p in kg/s for the simulation. TMVOC defines production as QX<0 and injection as QX>0. The production rate is applied at the bottom well element adjacent to the well face.

Definitions of Initial Conditions

All simulations were initialized according to Eqn. 5-6, whereby the initial drawdown throughout the aquifer is equal to 0. Because TMVOC actually solves for the pressure in each element at each time, the upper-most layer of the grid is set to a reference pressure (P_0). For the purposes of this study, this reference pressure is defined as atmospheric pressure at sea level, or 101,305.97 Pascals (Pa). The initial pressure in each successively lower grid layer (j) is set to:

$$P_j = P_0 + \rho g\left(z_j - z_0\right) \tag{5-58}$$

where z_j is defined as the elevation at the center point of each element row.

Grid Generation

The radial discretization of the numerical model described here is used throughout this study. The well radius (r_w) is fixed at 0.05 m (a typical well radius employed in field installation for flowmeter testing) while the outer radius (r_e) is fixed at 20,000 m to avoid boundary effects during the time frame of interest (time from pumping commencement to the time when quasi-steady-state is achieved). The domain between r_w and r_e was discretized according to:

$$r_{i+1} = r_i + \alpha r_i \tag{5-59}$$

where:

$$\alpha = \left(\frac{r_e}{r_w}\right)^{1/(NI-1)} - 1 \tag{5-60}$$

Additionally, the interior of the well was divided into two elements, where the interface between the two elements is at $r_w/2$. Initially, the radial domain was setup with an r_e of 735 m. However, setting of the r_e at this distance resulted in deviations from the Theis solutions at later times and greater distances from the well. Therefore, the r_e was moved out to 20,000 m; this resulted in a much better match between the model and Theis results at later times and greater distances from the well. A comparison of the results for both simulations over 735 m, shows a relative difference near the well face of approximately 1%. It is difficult to assess the sensitivity of the model in the radial domain by increasing the r_e since this also changes the solution; however, the small changes in grid spacing near the well resulting from the change in r_e did not significantly affect the drawdown at the well. This is an indication that the model space has been adequately discretized and that the model is relatively insensitive to further increases in grid density.

For a selected homogeneous aquifers with thicknesses of 2 m, the vertical domain was divided into four equally thick grid-layers. The results from this simulation were compared to those where the vertical domain was divided into eight equally thick grid-layers. The difference in steady-state drawdowns between the two simulations was less than 0.3% at the well. This small difference, which is negligible compared to the magnitudes of the drawdowns, indicates that the grid is relatively insensitive to changes in discretization.

Sources of Error

There are several sources of error associated with the use of TMVOC as the numerical simulator to the physical system defined in this Chapter. The first is related to

the convergence criteria defined in the input file. The principle criterion is defined in the PARAM module of the input file, where RE1 is the convergence criterion for relative error. The default value for this parameter was initially used and then incremented until the differences in the model output were negligible. Throughout this study, this is set to 10^{-5}. The mass balance error is constrained by RE1; the model will not converge if the mass balance error divided by the component mass in each element is greater than RE1.

Another potential source of error is related to the discretization of the simulation domain. The effect of the grid spacing on the results was evaluated through increasing refinement of the mesh until the differences between model run outputs was negligible. In general, the model is not very sensitive to changes in grid spacing as discussed above.

A third source of error is the truncation of the pressures in the output files (although the pressures are stored with 14 digits in the memory while the model is running). In many of the simulations, the change in pressure at each node at early times is small and truncation of the pressures may result in the incorrect calculation of the change in pressure between elements or time steps. The magnitude of this error source was checked by comparing the output file results to the FOFT module output which employs an additional significant digit over the main output file results. The average relative percent difference (RPD) between the two sets of results was 0.18%. This level of difference is considered small and not significant.

Evaluation of the numerical model error may be done using several metrics, including the mean error (ME), the mean absolute error (MAE), the root mean squared error (RMSE), and the average RPD. When these error metrics are small compared to the

actual drawdowns (less than 1% at the well) the errors in the model are a small part of the overall model response [Anderson and Woessner 1991].

Model Verification

In verifying the numerical model, a homogeneous aquifer with a thickness (b) of 2 m, a well radius (r_w) of 0.05 m, an effective radius (r_e) of 18,400 m, a hydraulic conductivity (K) of 100 m/d, a specific storage (S_s) of 3.5E-04 m^{-1}, and a pumping rate (Q_p) of 34.6 m^3/d was employed. The K was selected to be typical of a medium sand; a porosity of 0.35 was employed in the input file.

Steady-State

The steady-state analytical drawdown solution for a homogeneous, finite radius system is defined as [Thiem 1906]:

$$s(r) = \frac{Q_P}{2\pi b K_r} \ln\left(\frac{r_e}{r}\right) \tag{5-61}$$

As shown in Figure 5.2, the model drawdown across the aquifer approaches the Thiem solution for the test scenario as time increases. The average RPD between the steady-state model drawdown throughout the aquifer and the drawdown as calculated using the Thiem solution is 0.88%, indicating that the two solutions are in agreement with one another. The ME between the drawdown datasets is 1.6E-03 m, the MAE is 1.6E-03 m, and the RMSE between the datasets is 2.0E-03 m. These errors are small compared to the actual drawdowns (from 0.44% to 0.56% at the well) indicating that errors in the model are a small part of the overall model response. It should be noted that to run the simulation to steady-state, that the well k was modified from 1.E-4 m^2 to 1.E-6 m^2; this

was necessary to avoid late-time instabilities in the model solution (i.e., the model would not converge according to the criteria specified in the input file: either convergence in one cycle or convergence with no iteration in two successive cycles).

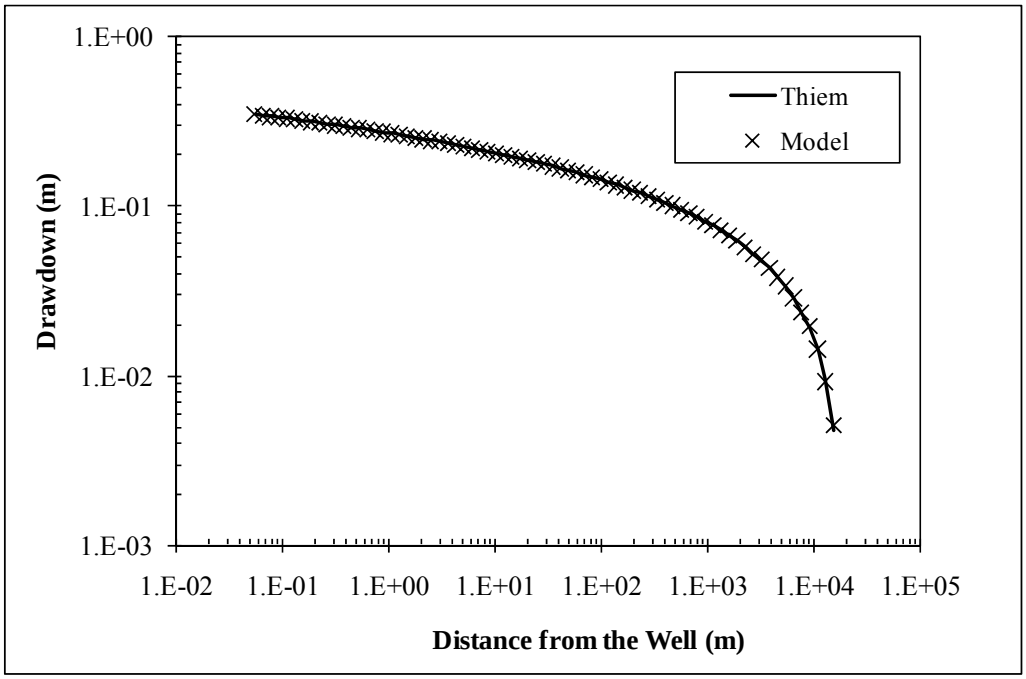

Figure 5.2 Comparison between the model results and the Thiem solution for a homogeneous, confined aquifer with b=2 m, r_w=0.05 m, r_e=18,400 m, Q_p=34.6 m^3/d, K=100 m/d, and S_s=3.5E-04 m^{-1}.

Transient

The transient analytical drawdown solution for a homogeneous, infinite-radius system is defined as [Hantush 1964]:

$$s(r,t) = \frac{Q}{4\pi Kb} s(\tau, \rho) \tag{5-62}$$

where

$$s(\tau,\rho)=\frac{4}{\pi}\int_0^{\infty}\frac{\left[1-EXP\left(-\tau u^2\right)\right]\left[J_1(u)Y_0(\rho u)-Y_1(u)J_0(\rho u)\right]}{u^2\left[J_1^2(u)+Y_1^2(u)\right]}du \tag{5-63}$$

and

$$\tau=\frac{Kt}{S_s r_w^2};\rho=\frac{r}{r_w} \tag{5-64}$$

The Hantush solution (Eqns. 5-62 through 5-64) is based on the following assumptions [Batu 1998]:

- The aquifer is homogeneous and isotropic;
- The aquifer is horizontal with a constant thickness (*b*);
- The aquifer is not leaky;
- The aquifer is infinite in horizontal extent;
- The well fully penetrates the aquifer; and
- The pumping rate of the well is constant.

The Hantush solution is applicable for all values of time and radial distances from the well. A special case of the Hantush solution is defined for determining the drawdown at the well-face (r_w) [Lee 1998]:

$$s(r_w,t)=\frac{Q}{4\pi Kb}\frac{8}{\pi^2 r_w^2}\int_0^{\infty}\frac{1-EXP\left(-x^2\kappa t\right)}{\left(J_1^2(xr_w)+Y_1^2(xr_w)\right)x^3}dx \tag{5-65}$$

The Hantush equation may also be simplified provided that:

$$t>\frac{30r_w^2S_s}{K} \tag{5-66}$$

to the Theis solution:

$$s(r,t) = \frac{Q}{4\pi bK} W(u) \tag{5-67}$$

where $W(u)=E_1(u)$, the exponential integral, which is defined as:

$$W(u) = -0.5772 - \ln u - \sum_{n=1}^{\infty} (-1)^n \frac{u^n}{n \cdot n!} \tag{5-68}$$

The Theis solution has an additional assumption to those of the Hantush solution: the diameter of the well is infinitesimally small compared to the horizontal extent; i.e., wellbore storage is negligible. Prior to the time defined by Eqn. 5-66, the Theis solution is not applicable [Hantush 1964].

Comparison of the three analytical solutions (Eqns. 5-62, 5-65, and 5-67) for drawdown at the well over time (Figure 5.3) show good agreement, especially as time increases (for this comparison, the formulation specific to r_w was employed). As discussed, the Theis solution is not applicable at very small times. This is reflected in comparing the drawdown at t=1.2E-08 days as determined using the Theis equation to the Hantush results (RPD=23.1%) and numerical model results (RPD=22.9%). The average RPD between the numerical model results and the Hantush results is 0.5%. At early time (t=1.2E-06 d), the ME between the drawdown datasets is -8.7E-04 m, the MAE is 8.7E-04 m, and the RMSE between the datasets 1.5E-03 m. These errors are small compared to the actual drawdowns (from -0.88% to 1.5% at the well) indicating that errors in the model are a small part of the overall model response. At late time (t=6.9 d), the ME between the drawdown datasets is 1.1E-03 m, the MAE is 1.3E-03 m, and the RMSE

between the datasets 4.8E-03 m. These errors are small compared to the actual drawdowns (from 0.34% to 1.4% at the well) indicating that errors in the model are a small part of the overall model response.

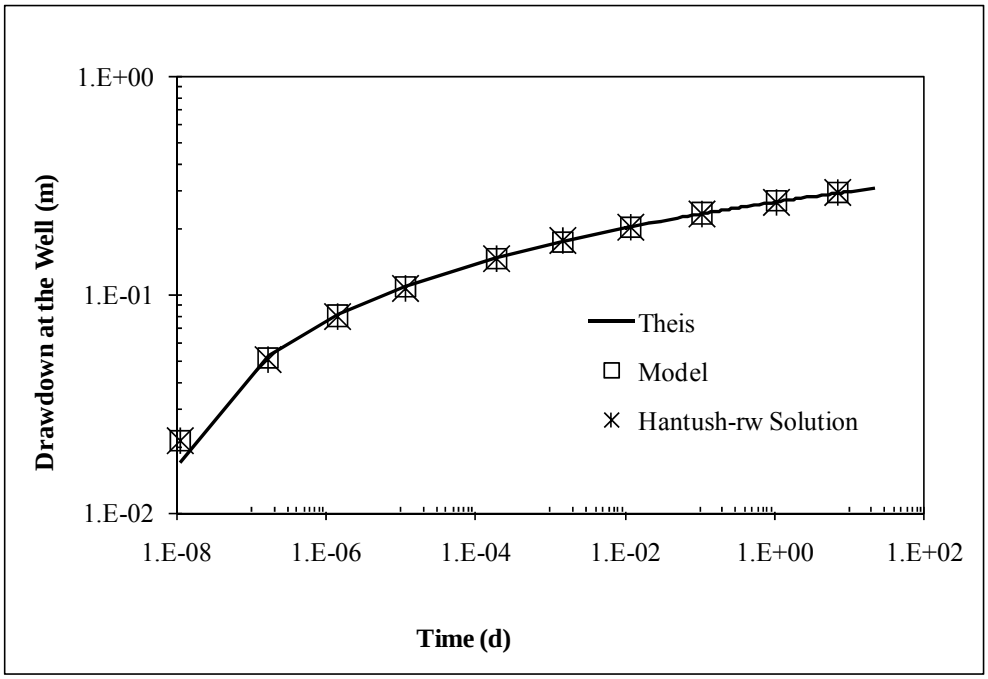

Figure 5.3 Comparison between the numerical model results, Hantush solution, and Theis solution for a homogeneous, confined aquifer with b=2 m, r_w=0.05 m, r_e=735 m, Q_p=34.6 m^3/d, K=100 m/d, and S_s=3.5E-04 m^{-1}.

Solution of Eqn. 5-63 was performed using the software Mathematica [Wolfram Research 1999]. In cases where ρ=1 (i.e., r=r_w), the solution is relatively straight-forward as the function defined in Eqn. 5-33 is smooth (Figure 5.4). For the cases where ρ>1 (i.e., r>r_w), solution of the integrand in Eqn. 5-63 is complicated by the oscillatory nature of the function (Figure 5.5).

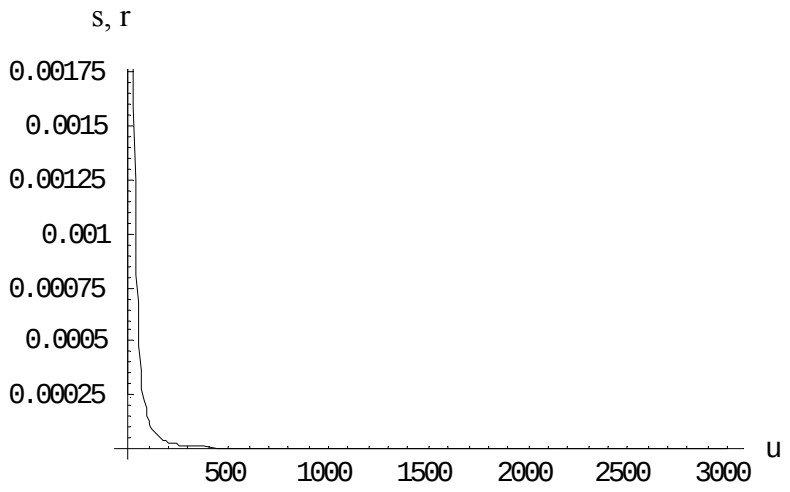

Figure 5.4 Function $s(\tau,\rho)$ where τ=1 and ρ=1.

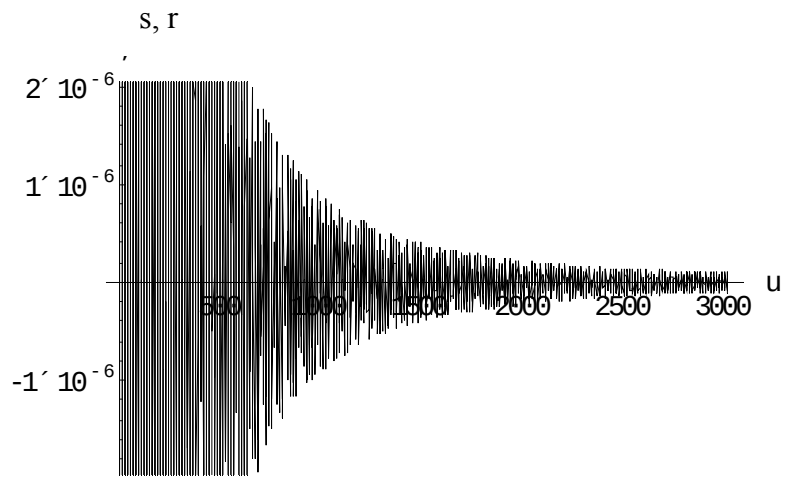

Figure 5.5 Function $s(\tau,\rho)$ where τ=1 and ρ=2.

Comparison of the numerical model drawdown results across the aquifer for selected times to the Hantush solution (general formulation) for those times as well as to the Theis solution for the same times yields a similar pattern of agreement between the different datasets (i.e., the datasets converge at later times and show small differences at earlier times) (Figure 5.3). Despite the inability to accurately solve the general Hantush

formulation for all $r>r_w$, it is clear from evaluating the numerical model results compared to the Hantush results and the Theis results that the numerical model is behaving consistently with these models (Figure 5.6).

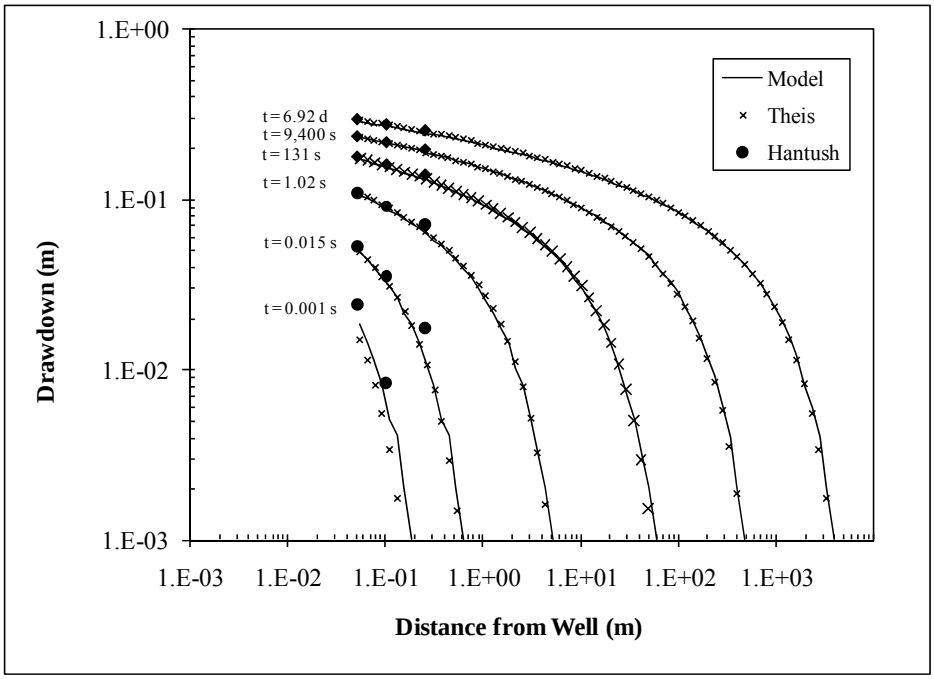

Figure 5.6 Comparison between the numerical model results, Hantush solution, and Theis solution for a homogeneous, confined aquifer with b=2 m, r_w=0.05 m, r_e=735 m, Q_p=34.6 m^3/d, K=100 m/d, and S_s=3.5E-04 m^{-1}.

As was observed in the comparisons between the drawdown at the well solutions, the deviation between the numerical model drawdown throughout the aquifer and the analytical solutions is greatest at early times. It is important to note that while the values of the numerical model drawdowns differ from the analytical solutions at these early times, the shape of the drawdown curves for each solution series are consistent with one another, further confirming that the model is behaving appropriately.

Hydraulic Diffusivity

As defined in Eqn. 5-4, hydraulic diffusivity (D) is a function of K and S_s. To obtain the values of D for each layer, individual layer K-values were selected while the S_s was generally determined as a function of K. In terms of real-world applications, it is often unrealistic to assume that all aquifers and aquifer layers have the same S_s. Using data compiled from readily available resources [Anderson and Woessner 1992; Maidment 1993], a relationship of S_s based on K was developed. This relationship was derived based on visual inspection of the data set, which indicated that the data can be separated into three K ranges. It is important to note this distinction as S_s is actually a function of the matrix geometry and compressibility, not K. However, as both S_s and K are functions of the matrix geometry, and geometry is related to compressibility, it is reasonable to assume that the two parameters correlate. A simple regression was performed on the three regions of the data to obtain an equation correlating S_s to K. This relationship (Figure 5.7) is not intended to be definitive of all systems, but is used instead to give approximate and reasonable estimates of S_s for the various scenarios modeled.

As stated in Chapter 2, in most applications, it is more important to accurately identify high-K layers than low-K layers. For this reason, the scenarios in this study focus primarily on K values of 1.0E-02 m/d and greater (sands and gravel). From Figure 5-7, this region is represented by a constant S_s relationship of 3.5E-04 1/m. As such, the majority of scenarios considered herein employ S_s=3.5E-04 1/m, with modifications as needed to illustrate certain behaviors later in this Chapter.

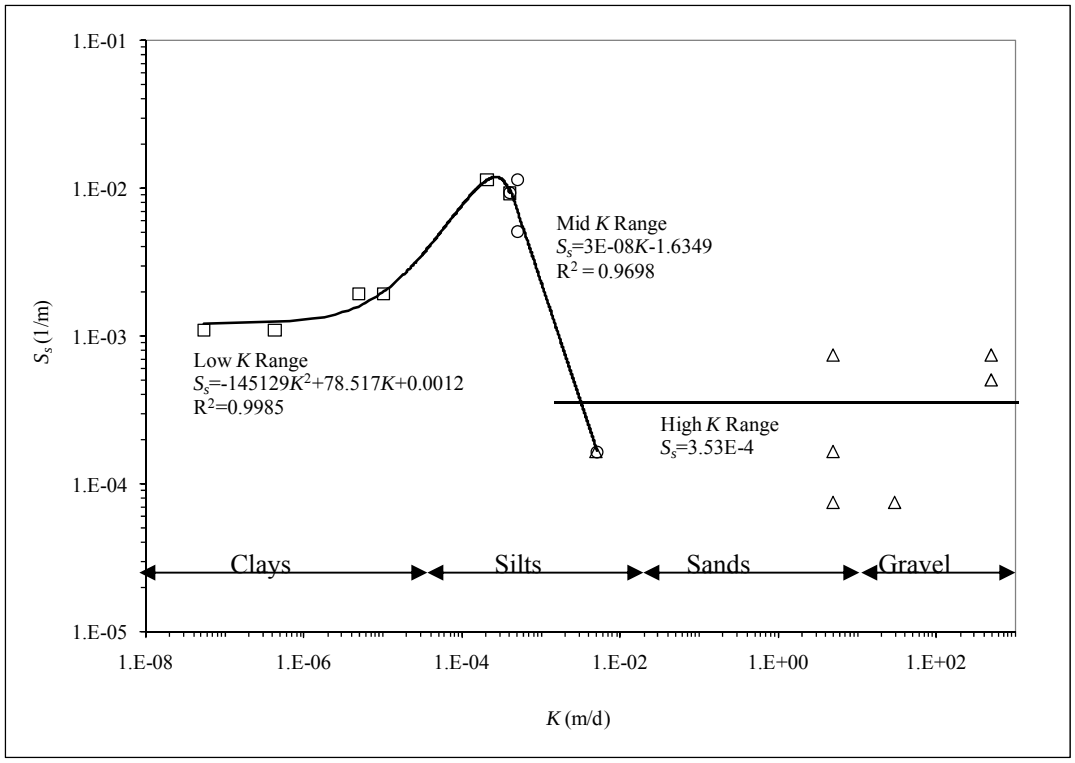

Figure 5.7 Correlation between K and S_s.

Numerical Definition of Quasi-Steady-State

For the purposes of this analysis, quasi-steady-state will be considered to have been attained when the maximum relative percent difference between the gradients at the well is approximately five percent (5%). This criterion was selected based on inspection of several sets of preliminary results and an examination of the gradient behaviors over time. The value of five percent was selected as the time when the gradients, when plotted, ceased to change "appreciably", with only small changes over large periods of time observed (as discussed in Chapter 2). The maximum relative percent difference (error) (RPD) is defined as:

$$RPD = \frac{Minimum\ Gradient - Maximum\ Gradient}{\left(Minimum\ Gradient + Maximum\ Gradient\right)/2} \times 100 \qquad (5\text{-}21)$$

Summary of Scenarios

Throughout the course of the single-domain analyses, 96 different arrangements of K and S_s were employed (Table 5.1). The remaining system variables are as described in the text; each combination of K and S_s may be used with different system parameter values as needed to illustrate different phenomena.

Table 5.1 Summary of Scenarios.

Scenario	b (m)	a	K_1 (m/d)	K_2 (m/d)	K_3 (m/d)	S_{s1} (1/m)	S_{s2} (1/m)	S_{s3} (1/m)	Q_p (L/min)	Δz (m)
Q1	0.9	1	1	0.01	0.2	3.5E-04	3.5E-04	3.5E-04	0.300	0.30
Q2	0.9	1	100	0.01	0.2	3.5E-04	3.5E-04	3.5E-04	0.208	0.30
Q3a	0.9	1	0.01	0.0001	0.002	3.5E-04	3.5E-04	3.5E-04	0.00300	0.30
Q3b	1.8	1	0.01	0.0001	0.002	3.5E-04	3.5E-04	3.5E-04	0.00600	0.30
Q3c	3.6	1	0.01	0.0001	0.002	3.5E-04	3.5E-04	3.5E-04	0.01200	0.30
Q3d	7.2	1	0.01	0.0001	0.002	3.5E-04	3.5E-04	3.5E-04	0.0240	0.30
Q3e	14.4	1	0.01	0.0001	0.002	3.5E-04	3.5E-04	3.5E-04	0.0480	0.60
Q3f	28.8	1	0.01	0.0001	0.002	3.5E-04	3.5E-04	3.5E-04	0.0960	1.20
Q4a	0.9	1	1	0.01	0.2	3.5E-04	3.5E-04	3.5E-04	0.300	0.30
Q4b	1.8	1	1	0.01	0.2	3.5E-04	3.5E-04	3.5E-04	0.600	0.30
Q4c	3.6	1	1	0.01	0.2	3.5E-04	3.5E-04	3.5E-04	1.20	0.30
Q4d	7.2	1	1	0.01	0.2	3.5E-04	3.5E-04	3.5E-04	2.40	0.30
Q4e	14.4	1	1	0.01	0.2	3.5E-04	3.5E-04	3.5E-04	4.80	0.60
Q4f	28.8	1	1	0.01	0.2	3.5E-04	3.5E-04	3.5E-04	9.60	1.20
Q5a	0.9	1	100	1	20	3.5E-04	3.5E-04	3.5E-04	30.0	0.30
Q5b	1.8	1	100	1	20	3.5E-04	3.5E-04	3.5E-04	60.0	0.30
Q5c	3.6	1	100	1	20	3.5E-04	3.5E-04	3.5E-04	120	0.30
Q5d	7.2	1	100	1	20	3.5E-04	3.5E-04	3.5E-04	240	0.30
Q5e	14.4	1	100	1	20	3.5E-04	3.5E-04	3.5E-04	480	0.60
Q5f	28.8	1	100	1	20	3.5E-04	3.5E-04	3.5E-04	960	1.20
Q6a	0.9	1	10,000	100	2,000	3.5E-04	3.5E-04	3.5E-04	2,999	0.30
Q6b	1.8	1	10,000	100	2,000	3.5E-04	3.5E-04	3.5E-04	5,999	0.30
Q6c	3.6	1	10,000	100	2,000	3.5E-04	3.5E-04	3.5E-04	11,997	0.30
Q6d	7.2	1	10,000	100	2,000	3.5E-04	3.5E-04	3.5E-04	23,994	0.30

Table 5.1 Summary of Scenarios, continued.

Scenario	b (m)	a	K_1 (m/d)	K_2 (m/d)	K_3 (m/d)	S_{s1} (1/m)	S_{s2} (1/m)	S_{s3} (1/m)	Q_p (L/min)	Δz (m)
Q6e	14.4	1	10,000	100	2,000	3.5E-04	3.5E-04	3.5E-04	47,989	0.60
Q6f	28.8	1	10,000	100	2,000	3.5E-04	3.5E-04	3.5E-04	95,977	1.20
Q7a	0.9	1	1	0.2	0.01	3.5E-04	3.5E-04	3.5E-04	0.300	0.30
Q7b	0.9	1	0.2	1	0.01	3.5E-04	3.5E-04	3.5E-04	0.300	0.30
Q7c	28.8	1	1	0.2	0.01	3.5E-04	3.5E-04	3.5E-04	9.60	1.20
Q7d	28.8	1	0.2	1	0.01	3.5E-04	3.5E-04	3.5E-04	9.60	1.20
1	0.9	1	1	0.01	0.2	3.5E-04	3.5E-04	3.5E-04	0.1	0.3
2	0.9	1	1	0.01	0.2	6.0E-05	6.0E-05	6.0E-05	0.1	0.3
3	0.9	1	1	0.01	0.2	1.0E-03	1.0E-03	1.0E-03	0.1	0.3
4	0.9	1	1	0.01	0.2	3.5E-04	3.5E-04	3.5E-04	0.6	0.3
5	0.9	1	100	1	20	3.5E-04	3.5E-04	3.5E-04	5	0.3
6	0.9	1	10,000	100	2,000	3.5E-04	3.5E-04	3.5E-04	5	0.3
7	1.8	1	1	0.01	0.2	3.5E-04	3.5E-04	3.5E-04	0.3	0.3
7a	1.8	1	1	0.01	0.2	3.5E-04	3.5E-04	3.5E-04	0.3	0.3
8	1.8	1	1	0.01	0.2	6.0E-05	6.0E-05	6.0E-05	0.3	0.3
9	1.8	1	1	0.01	0.2	1.0E-03	1.0E-03	1.0E-03	0.3	0.3
10	1.8	1	1	0.01	0.2	3.5E-04	3.5E-04	3.5E-04	5	0.3
11	1.8	1	100	1	20	3.5E-04	3.5E-04	3.5E-04	0.5	0.3
12	1.8	1	100	1	20	3.5E-04	3.5E-04	3.5E-04	5	0.3
13	1.8	1	100	1	20	3.5E-04	3.5E-04	3.5E-04	40	0.3
14	1.8	1	10,000	100	2,000	3.5E-04	3.5E-04	3.5E-04	5	0.3
15	3.6	1	1	0.01	0.2	3.5E-04	3.5E-04	3.5E-04	0.5	0.3
16	3.6	1	1	0.01	0.2	6.0E-05	6.0E-05	6.0E-05	0.5	0.3

Table 5.1 Summary of Scenarios, continued.

Scenario	b (m)	a	K_1 (m/d)	K_2 (m/d)	K_3 (m/d)	S_{s1} (1/m)	S_{s2} (1/m)	S_{s3} (1/m)	Q_p (L/min)	Δz (m)
17	3.6	1	1	0.01	0.2	1.0E-03	1.0E-03	1.0E-03	0.5	0.3
18	3.6	1	1	0.01	0.2	3.5E-04	3.5E-04	3.5E-04	5	0.3
18a	3.6	1	1	0.01	0.2	3.5E-04	3.5E-04	3.5E-04	5	0.3
19	3.6	1	1	0.01	0.2	3.5E-04	3.5E-04	3.5E-04	10	0.3
20	3.6	1	100	1	20	3.5E-04	3.5E-04	3.5E-04	5	0.3
21	3.6	1	10,000	100	2,000	3.5E-04	3.5E-04	3.5E-04	5	0.3
22a	7.2	1	1	0.01	0.2	3.5E-04	3.5E-04	3.5E-04	1	0.3
23a	7.2	1	1	0.01	0.2	6.0E-05	6.0E-05	6.0E-05	1	0.3
24a	7.2	1	1	0.01	0.2	1.0E-03	1.0E-03	1.0E-03	1	0.3
22b	7.2	1	10	0.1	2	3.3E-03	3.3E-03	3.3E-03	1	0.3
23b	7.2	1	10	0.1	2	6.0E-04	6.0E-04	6.0E-04	1	0.3
24b	7.2	1	10	0.1	2	1.0E-02	1.0E-02	1.0E-02	1	0.3
25	7.2	1	1	0.01	0.2	3.5E-04	3.5E-04	3.5E-04	5	0.3
25a	7.2	1	1	0.01	0.2	3.5E-04	3.5E-04	3.5E-04	5	0.3
25b	7.2	1	1	0.01	0.2	3.5E-04	3.5E-04	3.5E-04	5	0.3
25c	7.2	1	1	0.01	0.2	3.5E-04	3.5E-04	3.5E-04	5	0.3
26	7.2	1	1	0.01	0.2	3.5E-04	3.5E-04	3.5E-04	10	0.3
27	7.2	1	100	1	20	3.5E-04	3.5E-04	3.5E-04	5	0.3
28	7.2	1	10,000	100	2,000	3.5E-04	3.5E-04	3.5E-04	5	0.3
29	14.4	1	1	0.01	0.2	3.5E-04	3.5E-04	3.5E-04	5	0.6
30	14.4	1	1	0.01	0.2	6.0E-05	6.0E-05	6.0E-05	5	0.6
31	14.4	1	1	0.01	0.2	1.0E-03	1.0E-03	1.0E-03	5	0.6
32	14.4	1	100	1	20	3.5E-04	3.5E-04	3.5E-04	5	0.6
33	14.4	1	10,000	100	2,000	3.5E-04	3.5E-04	3.5E-04	5	0.6

Table 5.1 Summary of Scenarios, continued.

Scenario	b (m)	a	K_1 (m/d)	K_2 (m/d)	K_3 (m/d)	S_{s1} (1/m)	S_{s2} (1/m)	S_{s3} (1/m)	Q_p (L/min)	Δz (m)
34	28.8	1	1	0.01	0.2	6.0E-05	6.0E-05	6.0E-05	5	1.2
35	28.8	1	1	0.01	0.2	1.00E-03	1.00E-03	1.00E-03	5	1.2
36	28.8	1	1	0.01	0.2	3.5E-04	3.5E-04	3.5E-04	5	1.2
37	28.8	1	1	0.01	0.2	3.5E-04	3.5E-04	3.5E-04	40	1.2
38	28.8	1	100	1	20	3.5E-04	3.5E-04	3.5E-04	5	1.2
39	28.8	1	100	1	20	3.5E-04	3.5E-04	3.5E-04	40	1.2
40	28.8	1	10,000	100	2,000	3.5E-04	3.5E-04	3.5E-04	5	1.2
41	28.8	1	10,000	100	2,000	3.5E-04	3.5E-04	3.5E-04	40	1.2
42a	7.2	1	1	1	1	3.33E-04	3.33E-02	1.67E-03	1	0.3
43a	7.2	1	1	1	1	6.0E-05	6.00E-03	3.00E-04	1	0.3
44a	7.2	1	1	1	1	1.00E-03	1.00E-01	5.00E-03	1	0.3
42b	7.2	1	10	10	10	3.33E-03	3.33E-01	1.67E-02	1	0.3
43b	7.2	1	10	10	10	6.00E-04	6.00E-02	3.00E-03	1	0.3
44b	7.2	1	10	10	10	1.0E-02	1.00E+00	5.00E-02	1	0.3
45	7.2	1	1	0.01	0.2	1.00E-03	1.00E-05	2.00E-04	1	0.3
46	7.2	1	1	0.01	0.2	2.00E-04	2.00E-06	4.00E-05	1	0.3
47	7.2	1	1	0.01	0.2	2.00E-03	2.00E-05	4.00E-04	1	0.3
48	7.2	1.5	100	1	20	3.5E-04	3.5E-04	3.5E-04	5	0.3
49	7.2	1.25	100	1	20	3.5E-04	3.5E-04	3.5E-04	5	0.3
50	7.2	0.5	100	1	20	3.5E-04	3.5E-04	3.5E-04	5	0.3
51	7.2	0.25	100	1	20	3.5E-04	3.5E-04	3.5E-04	5	0.3
52	7.2	0.1	100	1	20	3.5E-04	3.5E-04	3.5E-04	5	0.3

As can be seen in Table 5.1, the simulations employed in this study are focused on the higher-*K* regions of the correlation relationship. This is appropriate as the flowmeter is typically used to determine the dominant regions of flow within an aquifer; layers with *K* less than 1.0E-04 m/d would be considered to be no-flow layers in a practical sense (i.e., clays or consolidated materials), thereby creating multi-aquifer systems rather than multi-layer systems. A robust body of research exists to describe multi-aquifer systems and therefore they are not dealt with in this study. Additionally, with the exception of boundary effects, flow in multi-layer aquifers is generally assumed to be horizontal with no crossflow occurring between the layers.

Results and Discussion

Once pumping commences and water is removed from the higher-*K* layer(s), water begins to be released from storage in the lower-*K* layer(s) into the higher-*K* layer(s). Eventually, the hydraulic gradients near the well in each layer become equal and constant, indicating that the system has attained quasi-steady-state (Scenario Q1; Figure 5.8). In Figure 5.8, crossflow is indicated by the changing hydraulic head gradients for each layer at early times. Numerically, hydraulic head gradients at the well will be considered to have attained quasi-steady-state when the maximum RPD between any two grid-layer's hydraulic gradients at the well is less than 5%. The hydraulic gradients at the well for the system shown in Figure 5.8 attained quasi-steady-state at 9.3E+02 seconds (1.6E+01 minutes).

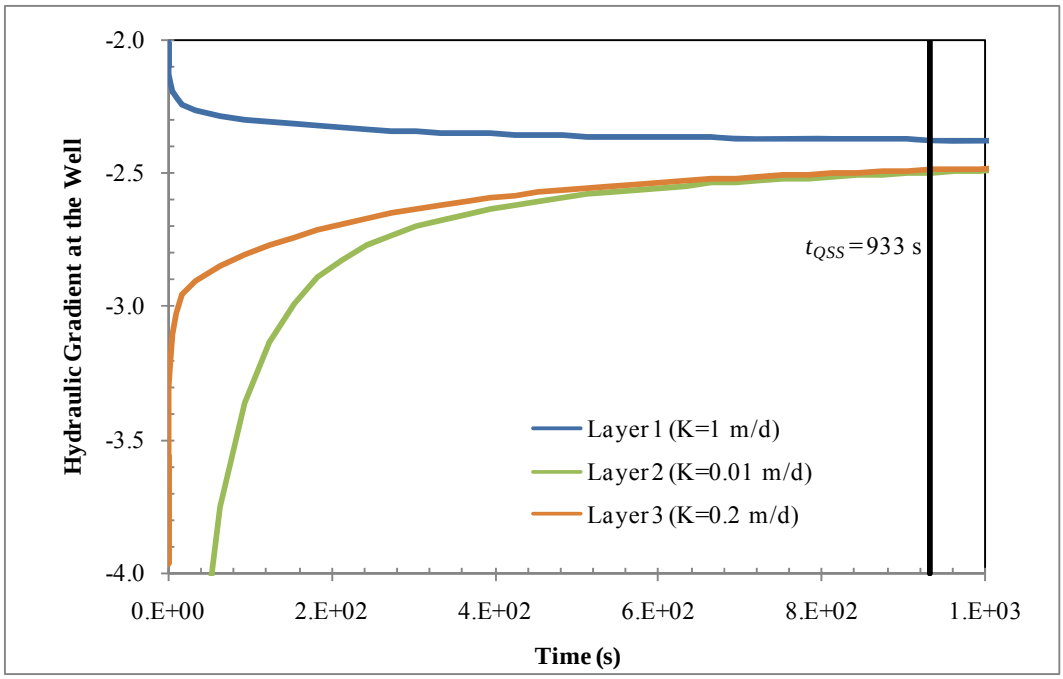

Figure 5.8 Gradients at the well for selected grid-layers as a function of time for Scenario Q1.

Having reached quasi-steady-state does not imply that the entire system has reached steady-state. For the system depicted in Figure 5.8, quasi-steady-state of the gradients at the well was attained at t=9.3E+02 seconds (1.6E+01 minutes), while steady-state drawdown at the well was attained after t=8.6E+02 days (obtained from the model output; the model terminates at the system steady-state). This difference between the time to reach quasi-steady-state and steady-state implies that crossflow is an early-time phenomenon that occurs close to the well.

As can be seen from results presented in Figure 5.9, the use of an arithmetic average K (used in the analytical model) to describe the overall system behavior is valid during the early time of this study (i.e., the analytical model and the numerical model results are approximate to each other).

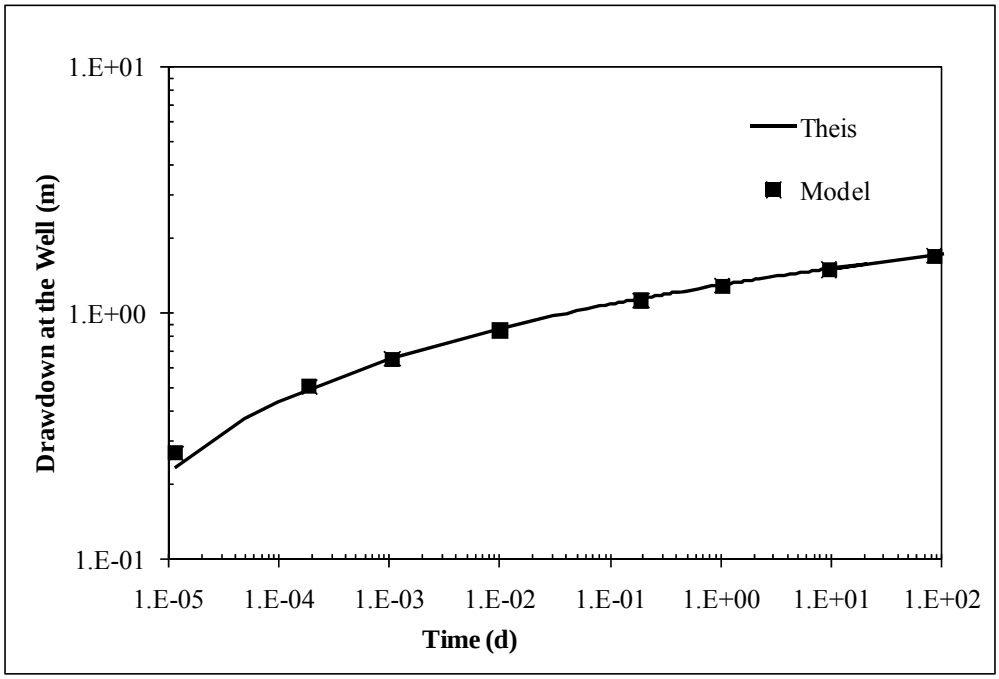

Figure 5.9 Drawdown at the well as a function of time for Scenario Q1. Analytical solution – solid squares; model solution: solid line.

These results also confirm the results published by Katz and Tek [1962], who found that the arithmetic average of the layer *K* values may be used to accurately predict multi-layer system behaviors at early times.

To evaluate the dominance of the horizontal flow from higher-*K* (higher-*D*) layers compared to the influence of crossflow, the high-*K* layer from Scenario Q1 was further increased by a factor of 100 (Scenario 2Q), with all other parameters maintained the same as in Scenario Q1. By examining the early-time hydraulic gradients for Scenario Q2 (Figure 5.10), it can be seen that the hydraulic gradients at the well in the higher-*K* layer remain essentially constant, implying that crossflow into this layer is negligible compared to the horizontal flow from this layer. In contrast, the hydraulic gradients in the lower-*K*

layers are initially changing rapidly, indicating a deviation from the Theis solution, which may be attributed in part to crossflow. As time progresses, the rate of change of the gradients in the lower-*K* layers decrease as the gradients become constant and approximately equal to the gradients in the higher-*K* layer. As expected, the hydraulic gradients in the mid-value *K*-layer approach those of the high-*K* layer more rapidly than the low-*K* layer.

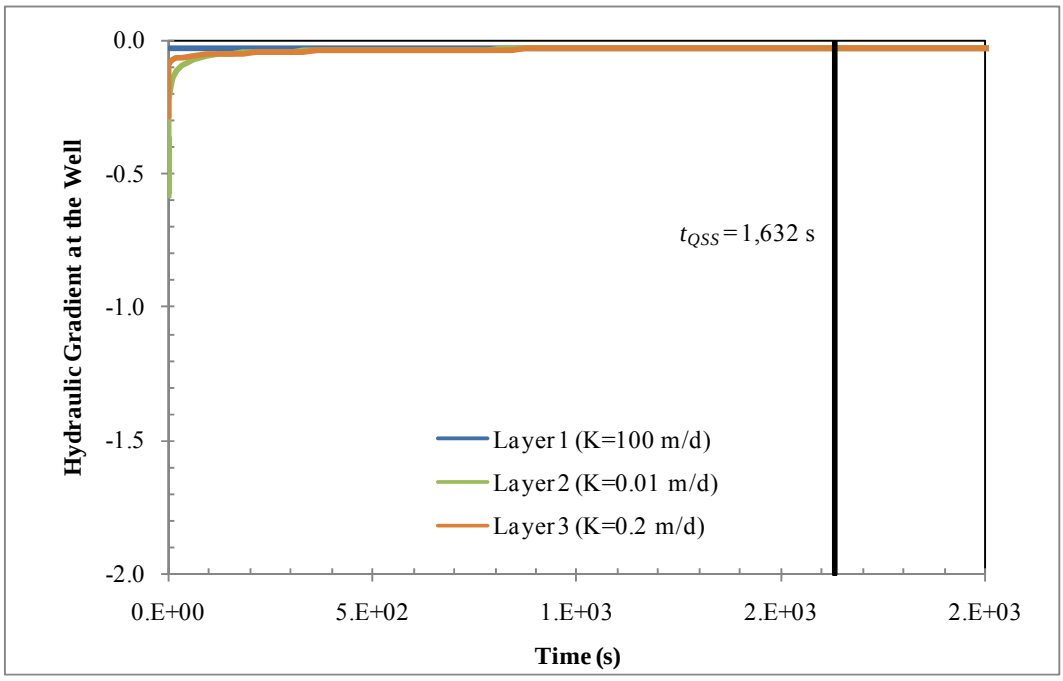

Figure 5.10 Hydraulic gradients at the well as a function of time for Scenario Q2.

The results from Figures 5.8 and 5.10 illustrate the Javandel and Witherspoon [1969] finding that larger-*K* layers deviate less from the Theis curve at early time (evidenced by nearly constant hydraulic gradients over time) than do lower-*K* layers. The large changes in hydraulic head gradients in the lower-*K* layer are a direct result of the preferential horizontal flow in the higher-*K* layer and the gradient between the larger-*K*

and lower-*K* layers generating a vertical flow component. The magnitude of the crossflow out of the lower-*K* layer and into the higher-*K* layer is much less than the magnitude of the horizontal flow from the larger-*K* layer, resulting in hydraulic gradients in the larger-*K* layer that remain essentially constant. In contrast, the amount of water leaving the lower-*K* layer due to cross-flow is proportionally a much larger component of the overall behavior of the lower-*K* layer, resulting in hydraulic gradients that change appreciably initially.

In comparing the behaviors of Scenario Q1 (Figure 5.8) and Scenario Q2 (Figure 5.10), the lower-*K* layer in Scenario Q2 has a larger overall influence on the time required for the system to attain quasi-steady-state (2.7E+01 minutes for Scenario Q2 and 1.5E+01 minutes for Scenario Q1) due to the larger influence of crossflow in the lower-*K* layers in Scenario Q2 than is observed from the lower-*K* layer in Scenario Q1. This phenomenon is most clearly illustrated by observing the flows out of each layer (Figures 5.11 and 5.12 for Scenario Q1 and Scenario Q2, respectively). In these figures, the flow out of the high-*K* layer is essentially constant for both scenarios. However, the flows out of the lower-*K* layers are characterized by a period of fluctuation followed by steady flow. The fluctuation is the result of vertical crossflow. This period of fluctuation is longer and with larger fluctuations for Scenario Q2, due to the crossflow being proportionally larger in these layers.

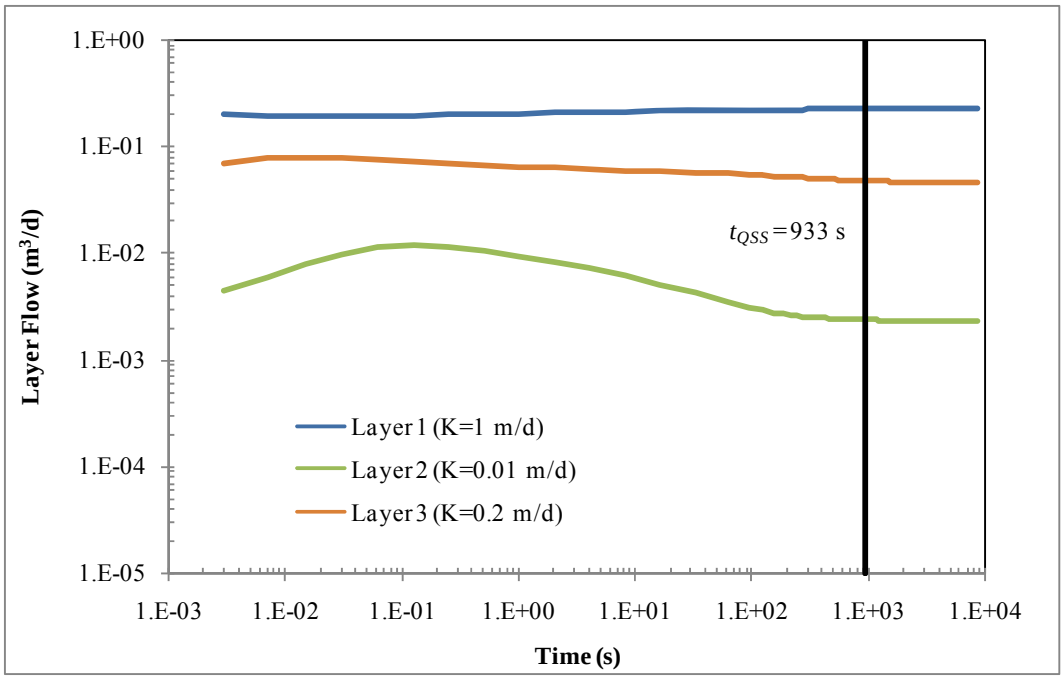

Figure 5.11 Flow into the well from each layer for Scenario Q1.

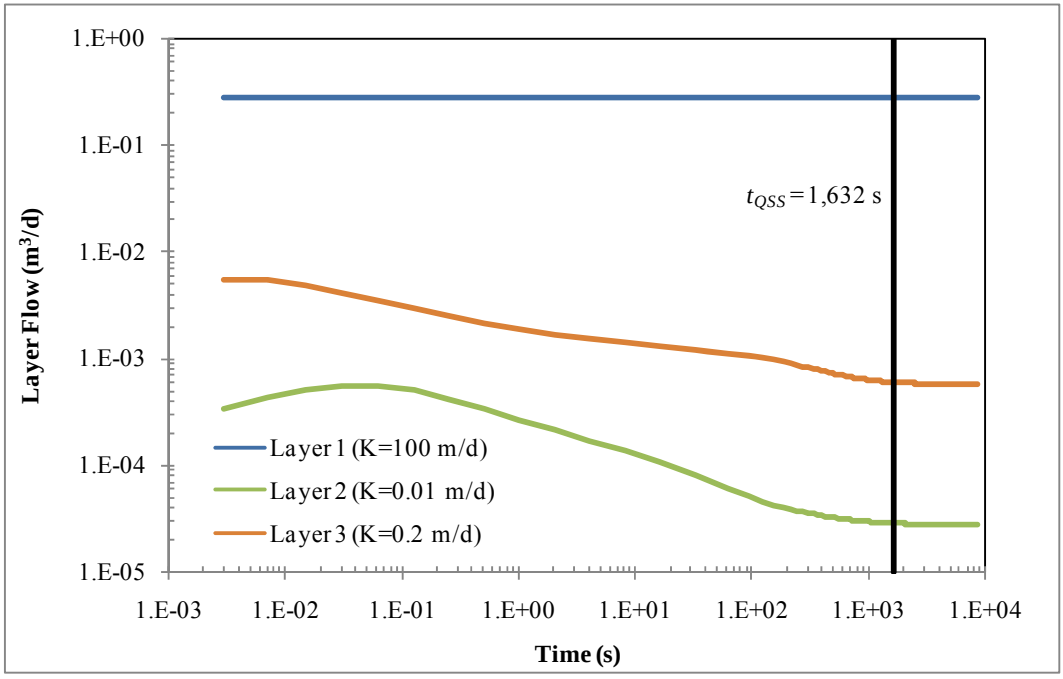

Figure 5.12 Flow into the well from each layer for Scenario Q2.

This early transient behavior of the hydraulic gradients (influenced by crossflow) is the cause of the system's drawdown deviating from the Theis solution. The Theis solution becomes approximate once the system attains quasi-steady-state and all flow is horizontal and proportional to the layer transmissivity. This is again consistent with the results found by Javandel and Witherspoon [1969]. Examination of Figures 5.8 and 5.10 illustrates the non-uniform behavior of the hydraulic gradients at early times. This behavior becomes more prominent in lower-*K* layers as the hydraulic diffusivity between the layers increases, for the reasons described above. The initially larger gradients in the lower-*K* layers also explain why the flows from the lower-*K* layers are initially higher than their steady-state values.

In determining the transient response behavior of the entire aquifer, it is useful to examine the maximum RPD between the layer hydraulic gradients as a function of time (Figure 5.13). By examining this relationship, it is apparent that the rate of change in the difference between gradients decreases with time. This type of relationship holds true for each of the systems examined during this study.

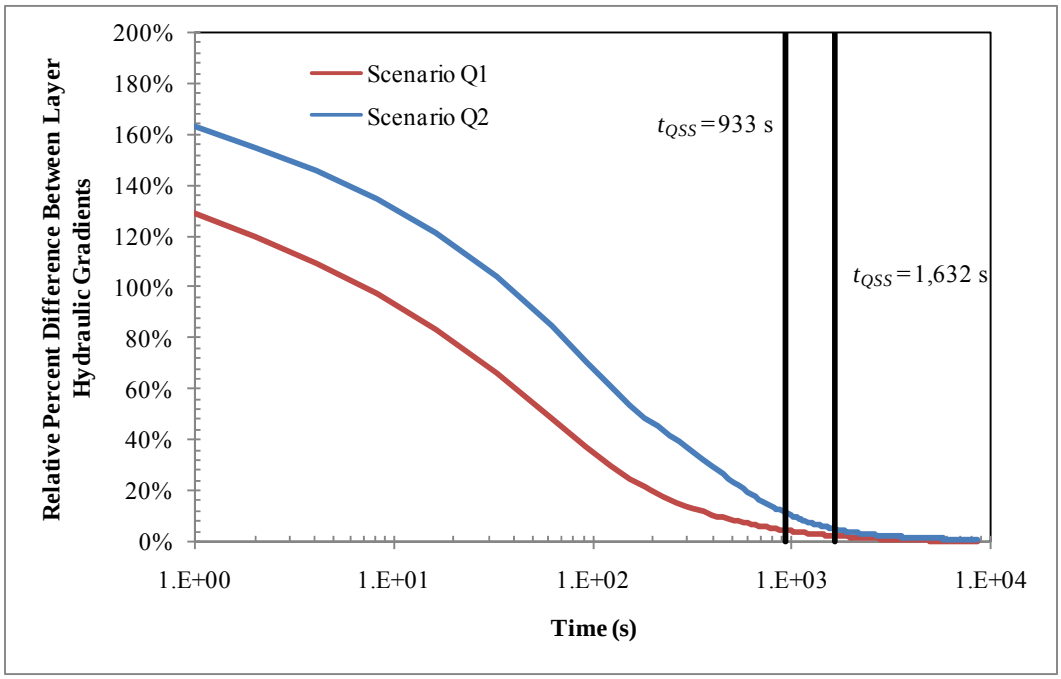

Figure 5.13 Maximum RPD in layer hydraulic gradients at the well as a function of time for Scenario Q1 and Scenario Q2.

Yet another way to look at the transient effects of pumping on an aquifer is to compare the calculated K for each layer compared to the input layer K's. This is accomplished using Eqn. 2-3, modified such that the ambient flow is removed from the equation, since no ambient flow occurs in this study:

$$K_i = < K > \frac{\Delta Q_i / \Delta z_i}{Q_P / b} \tag{5-69}$$

Using equation 5.69, the individual layer K values were calculated using the model output, flow from each layer at the well face. These calculated layer K values were then normalized by the input layer K values to assess the relative effect of taking flowmeter measurements before quasi-steady-state (Figure 5.14).

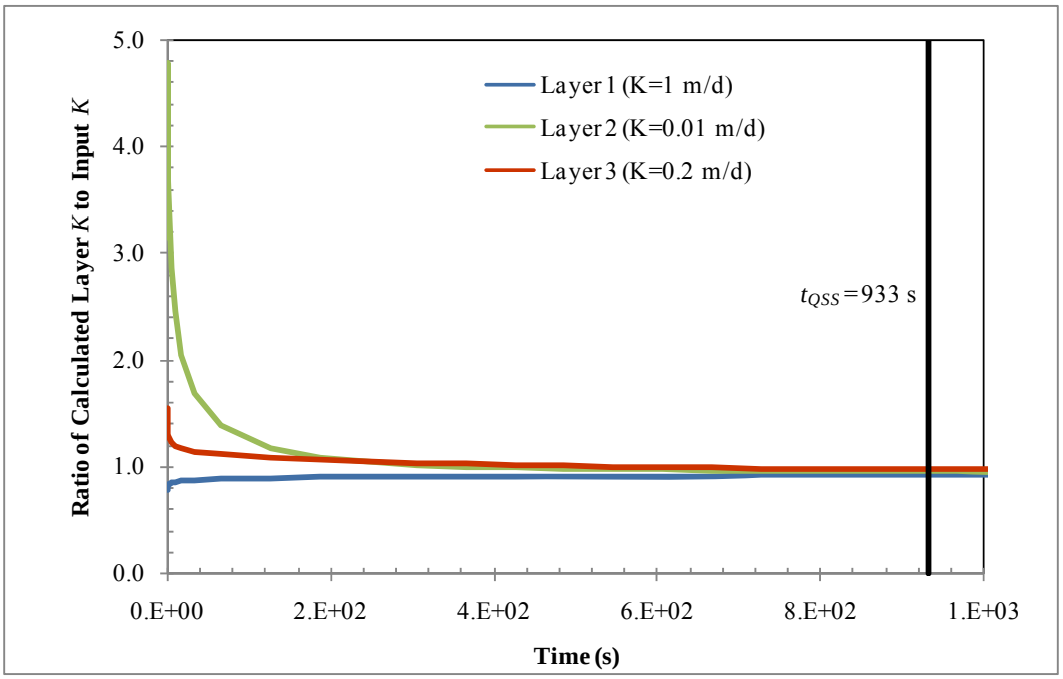

Figure 5.14 Ratio between calculated and model input layer *K* values for Scenario Q1.

As can be seen in Figure 5.14, the calculated layer *K* values initially differ from the input layer *K* values, but rapidly approach the input values as shown by the values approaching 1. The early differences are largest in the lowest-*K* layer (Layer 2). The ratios also show that the lower-*K* layers initially yield inflated calculated *K*'s (i.e., *K*-values larger than the model input values), while the high-*K* layer is underestimated. This finding is again tied to the crossflow phenomenon. The importance of the differences between the calculated and model input layer-*K* values will be examined in greater detail in later in this chapter.

Aquifer Thickness Effects

A series of aquifer systems were modeled to determine the effect of overall aquifer thickness (*b*) on the time required for the hydraulic gradients to attain quasi-

steady-state (Scenarios 3 through 6). The thickness of these Scenarios was varied from 0.9 m to 28.8 m (Figure 5.15). For comparison purposes, it is useful to determine the flow rate for each scenario such that a dimensionless flow rate (Q_{PD}) was held constant for the scenarios:

$$Q_{PD} = \frac{Q}{b}\left\langle \frac{S_S}{K} \right\rangle \tag{5-70}$$

This results in a flow rate for each scenario that is scaled according to the thickness of the aquifer as well as the average hydraulic diffusivity of the aquifer. This also results in the maximum drawdown at the well being constant for each simulation. It should be noted that holding the drawdown constant for all test conditions is not a practical approach for field testing; in addition, this dimensionless flow rate will not correspond to an actual flow rate that would be practical to use in the field. Rather, the use of the dimensionless pumping rate is intended to minimize the number of variables between simulations such that simulation results are easily compared.

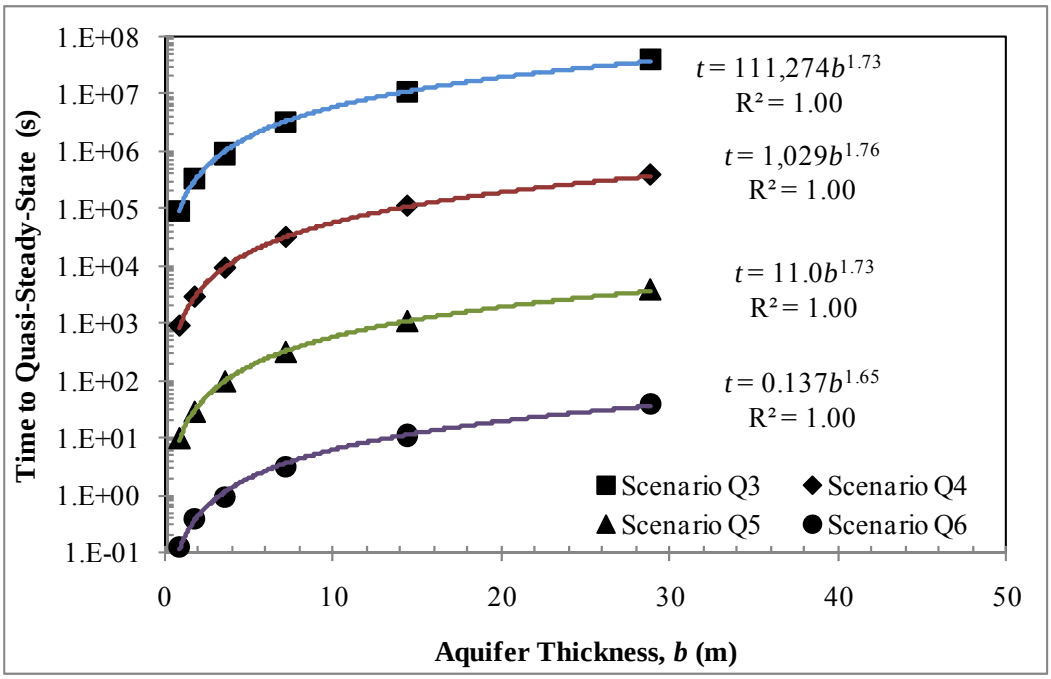

Figure 5.15 Time to quasi-steady-state for Scenarios Q3-Q6 (with varying aquifer thicknesses, *b*).

The times to quasi-steady-state for each of the four scenarios results shown in Figure 5.15 indicate that the time to attain quasi-steady-state is a function of the ratio of the hydraulic diffusivities (*D*) between the layers as well as the overall aquifer thickness (*b*). For each of the four scenarios, as *b* is increased, the time to quasi-steady-state increases according to a power relationship.

The average power of the four relationships is 1.72, indicating that the increase in the time required to attain quasi-steady-state is small at smaller thicknesses and becomes larger between successive increases in aquifer thickness. Having a power relationship implies that there is no theoretical bound on the time required to attain quasi-steady-state as the aquifer thickness approaches infinity. In reality, however, there may be many mechanisms that will influence the time to quasi-steady-state.

This same exercise was performed using the same scenario parameters but with flow rates typical of EBF testing (0.1 to 5 L/min, see Table 5.1). These simulations (Figure 5.16) yield similar results and consistent conclusions to those observed in Figure 5.15. The Scenario Series are defined as:

Scenario Series	Scenarios
A	1, 7, 15, 22a, 29, 38
B	5, 11, 20, 27, 32, 40
C	6, 14, 21, 28, 33, 42

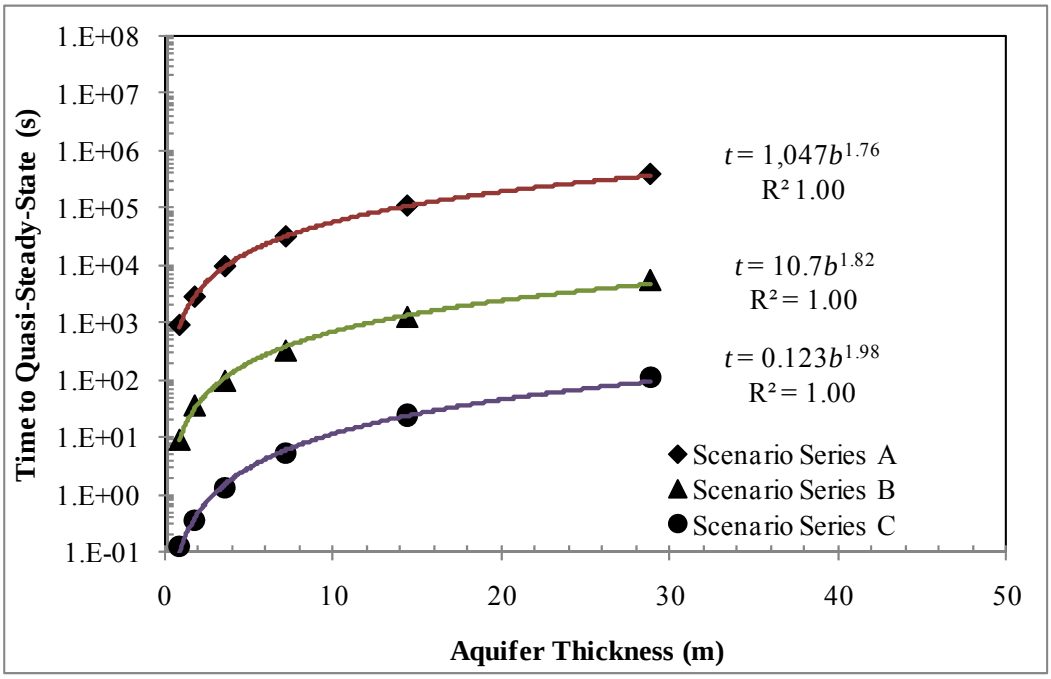

Figure 5.16 Time to quasi-steady-state for Scenario Series A, B, and C (with varying aquifer thicknesses, *b*).

Layer Thickness Effects

Having examined the effect of aquifer thickness on the time required to attain quasi-steady-state, understanding how layer thickness affects the time to quasi-steady-state is the next natural step. To assess the effect of layer thickness, the layers in Scenario 25 were made successively thinner, with keeping the same *K*-value distribution (Table 5.2). The times to quasi-steady-state for Scenarios 25 are also presented in Figure 5.17. These results show that as the layer thickness is decreased, the time to quasi-steady-state decreases in a linear fashion.

Table 5.2 Summary of Layer Thickness Scenarios and Times to Quasi-Steady-State.

Depth (m)	**Scenario Layer-*K* Values**			
	25	**25a**	**25b**	**25c**
7.05	1	1	1	1
6.75	1	1	1	0.01
6.45	1	1	0.01	0.2
6.15	1	1	0.01	1
5.85	1	0.01	0.2	0.01
5.55	1	0.01	0.2	0.2
5.25	1	0.01	1	1
4.95	1	0.01	1	0.01
4.65	0.01	0.2	0.01	0.2
4.35	0.01	0.2	0.01	1
4.05	0.01	0.2	0.2	0.01
3.75	0.01	0.2	0.2	0.2
3.45	0.01	1	1	1
3.15	0.01	1	1	0.01
2.85	0.01	1	0.01	0.2
2.55	0.01	1	0.01	1
2.25	0.2	0.01	0.2	0.01
1.95	0.2	0.01	0.2	0.2
1.65	0.2	0.01	1	1
1.35	0.2	0.01	1	0.01
1.05	0.2	0.2	0.01	0.2
0.75	0.2	0.2	0.01	1
0.45	0.2	0.2	0.2	0.01
0.15	0.2	0.2	0.2	0.2
t_{QSS} **(s)**	32,365	16,478	7,827	3,161

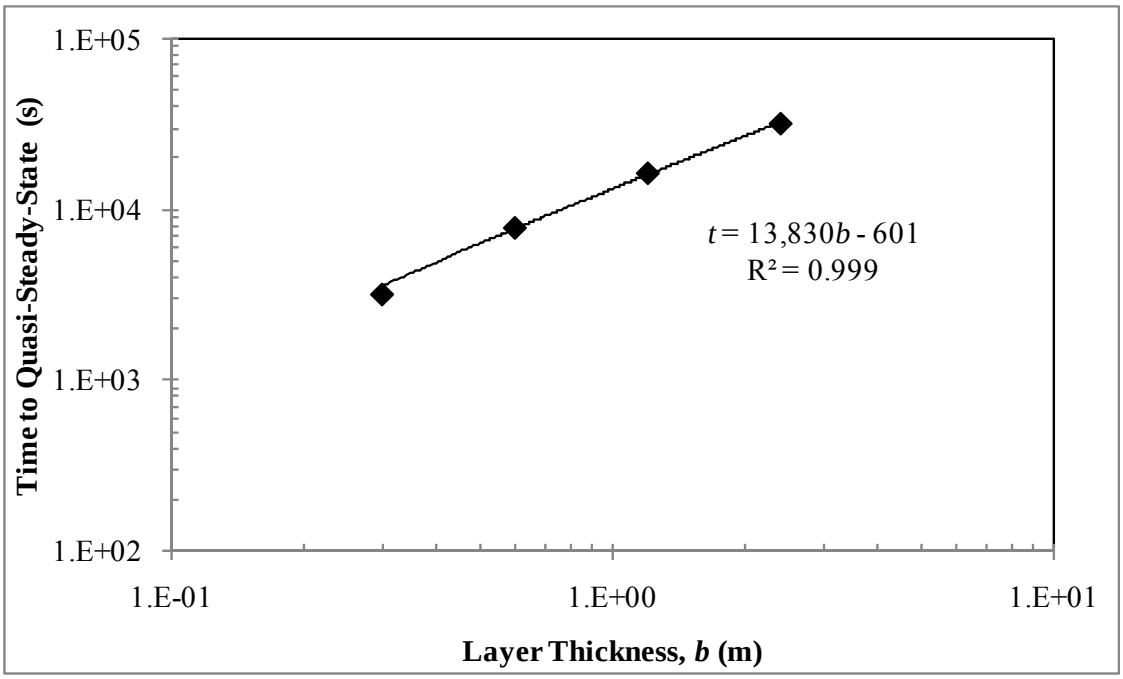

Figure 5.17 Time to quasi-steady-state for Scenario 25 (with varying layer thicknesses).

It is important to note that while the time to quasi-steady-state decreases with decreasing layer thickness, it does not decrease to the same time to quasi-steady-state as systems with similar layer thicknesses, but with only one set of layers (Table 5.3). In Table 5.3, layer-*K* values for selected scenarios are rearranged to yield the same thickness and pattern as Scenario Q1 (a 90 m scenario). The times to quasi-steady-state for the scenarios in Table 5.3 are presented in Figure 5.18. Again, as the layer thickness is decreased, the time to quasi-steady-state decreases; however the times remain greater than that for the minimum scenario (Scenario Q1). This reinforces the conclusions from the aquifer thickness analysis that as the overall aquifer thickness is increased, the time to quasi-steady-state increases.

Table 5.3 Summary of Layer Thickness Scenarios and Times to Quasi-Steady-State.

	Scenario Layer-*K* Values						
Layer	**Q1**	**7**	**7a**	**18**	**18a**	**25**	**25c**
24						1	1
23						1	0.01
22						1	0.2
21						1	1
20						1	0.01
19						1	0.2
18						1	1
17						1	0.01
16						0.01	0.2
15						0.01	1
14						0.01	0.01
13						0.01	0.2
12				1	1	0.01	1
11				1	0.01	0.01	0.01
10				1	0.2	0.01	0.2
9				1	1	0.01	1
8				0.01	0.01	0.2	0.01
7				0.01	0.2	0.2	0.2
6		1	1	0.01	1	0.2	1
5		1	0.01	0.01	0.01	0.2	0.01
4		0.01	0.2	0.2	0.2	0.2	0.2
3	1	0.01	1	0.2	1	0.2	1
2	0.01	0.2	0.01	0.2	0.01	0.2	0.01
1	0.2	0.2	0.2	0.2	0.2	0.2	0.2
t_{QSS} **(s)**	933	2,836	1,473	9,278	2,206	32,365	3,161

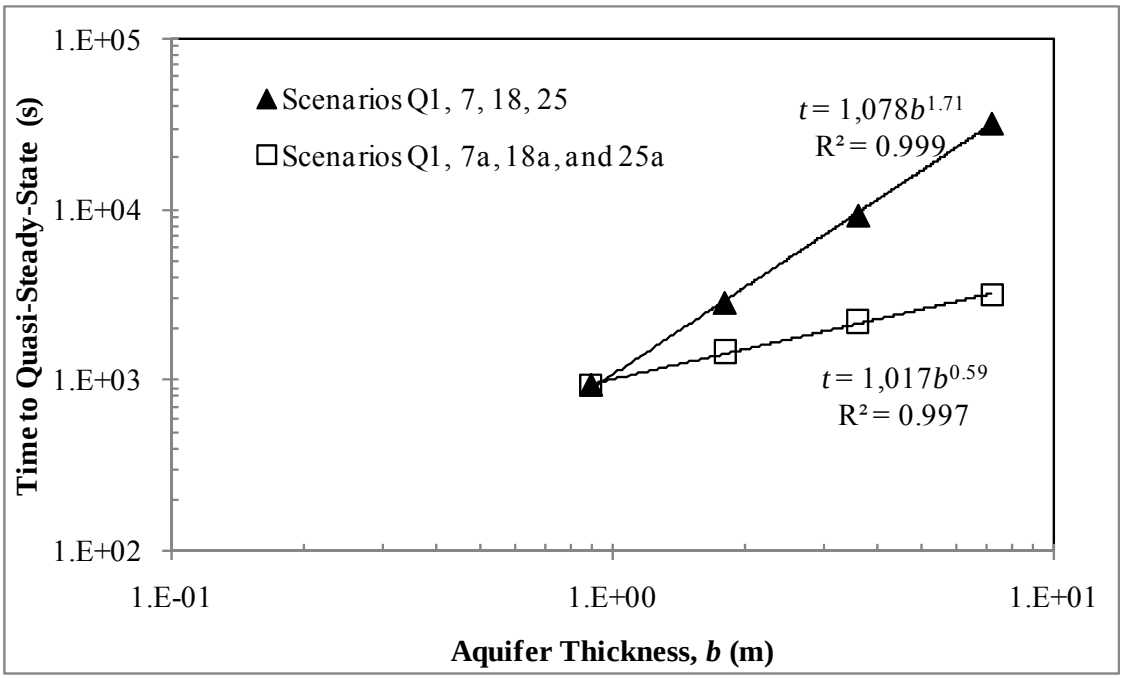

Figure 5.18 Time to quasi-steady-state for Table 5.3 scenarios.

Pumping Rate Effects

To assess the effect of pumping rate, Q_P, on the time required for a system to attain quasi-steady-state, the Q_P in several scenarios was systematically increased (Table 5.4; see Table 5.1 for other parameter definitions). It should be noted that several of the pumping rates employed for the model scenarios are unrealistically high and were evaluated for mathematical purposes only (e.g., Scenarios Q5 and Q6).

In general, increasing the Q_P resulted in small differences in the time required to attain quasi-steady-state. These differences, with the exception of the thickest systems with the smallest layer-K values (Scenarios Q4f, 36, and 37) with the smallest pumping rates, are not significant with respect to real-world application.

Table 5.4 Summary of Layer Arrangement Scenario Times to Quasi-Steady-State.

Scenario	b (m)	K_1 (m/d)	K_2 (m/d)	K_3 (m/d)	Q_p (L/min)	5% RPD t_{QSS} (s)
1	0.9	1	0.01	0.2	0.1	916
Q4a	0.9	1	0.01	0.2	0.3	933
4	0.9	1	0.01	0.2	0.6	916
5	0.9	100	1	20	5	9.09
Q5a	0.9	100	1	20	30	10.0
6	0.9	10,000	100	2,000	5	0.127
Q6a	0.9	10,000	100	2,000	2,999	0.127
7	1.8	1	0.01	0.2	0.3	2,836
Q4b	1.8	1	0.01	0.2	0.6	2,886
10	1.8	1	0.01	0.2	5	2,853
11	1.8	100	1	20	0.5	36.4
12	1.8	100	1	20	5	33.9
13	1.8	100	1	20	40	36.4
Q5b	1.8	100	1	20	60	29.0
14	1.8	10,000	100	2,000	5	0.35
Q6b	1.8	10,000	100	2,000	5,999	0.38
15	3.6	1	0.01	0.2	0.5	9,733
Q4c	3.6	1	0.01	0.2	1	9,716
18	3.6	1	0.01	0.2	5	9,278
19	3.6	1	0.01	0.2	10	9,300
20	3.6	100	1	20	5	98.3
Q5c	3.6	100	1	20	120	98.3
21	3.6	10,000	100	2,000	5	1.31
Q6c	3.6	10,000	100	2,000	11,997	0.96
22a	7.2	1	0.01	0.2	1	32,365
Q4d	7.2	1	0.01	0.2	2	32,219
25	7.2	1	0.01	0.2	5	32,106
26	7.2	1	0.01	0.2	10	32,468
27	7.2	100	1	20	5	334
Q5d	7.2	100	1	20	240	322
28	7.2	10,000	100	2,000	5	5.38
Q6d	7.2	10,000	100	2,000	23,994	3.22
32	14.4	100	1	20	5	1,306
Q5e	14.4	100	1	20	480	1,115
33	14.4	10,000	100	2,000	5	24.3
Q6e	14.4	10,000	100	2,000	47,989	11.4

Table 5.4 Summary of Layer Arrangement Scenario Times to Quasi-Steady-State, continued.

Scenario	b (m)	K_1 (m/d)	K_2 (m/d)	K_3 (m/d)	Q_p (L/min)	5% RPD t_{QSS} (s)
Q4f	28.8	1	0.01	0.2	0.1	522,280
Q4f	28.8	1	0.01	0.2	0.5	435,074
Q4f	28.8	1	0.01	0.2	0.5	416,736
36	28.8	1	0.01	0.2	5	398,507
Q4f	28.8	1	0.01	0.2	10	398,857
37	28.8	1	0.01	0.2	40	397,241
38	28.8	100	1	20	5	5,803
39	28.8	100	1	20	40	4,419
Q5f	28.8	100	1	20	960	3,990
40	28.8	10,000	100	2,000	5	111
41	28.8	10,000	100	2,000	40	88.1
Q6f	28.8	10,000	100	2,000	95,977	39.9

Based on these findings, pumping rate is not considered to be a significant factor in the time needed to attain quasi-steady-state, and therefore, the pumping rate should be selected based on the study limitations (i.e., time, purge water disposal costs/options, etc.).

Layer Arrangement Effects

As discussed previously, the contrast in D between layers is an important factor in the time required for a multi-layer aquifer to attain quasi-steady-state under pumping conditions. Now, the impact that layer placement has on the time required for a system to attain quasi-steady-state will be addressed. The systems used in this analysis are Scenarios Q4a, Q7a, Q7b, and Q4f, Q7c, and Q7d. In each of the three scenarios, the

layers are of equal thickness. Two overall aquifer thicknesses were evaluated for the scenarios: (a) b=0.9 m and (b) b=28.8 m.

As with previous simulations, a Q_{PD}=4.2E-04 was employed. The layer arrangement is a factor in the time required for systems to attain quasi-steady-state. The times to quasi-steady-state (t_{QSS}) for each of the scenarios are provided in Table 5.5; the RPD between the scenario with the minimum time to quasi-steady-state and the other two scenarios for the two thicknesses is also provided. The differences in the times for the thin aquifer (Scenarios Q4a, Q7a, and Q7b), although having RPDs of 6.2% and 3.3% are not significant in terms of real-world application as they differ from the scenario with the shortest time to quasi-steady-state by less than 2 minutes. In thicker systems (Scenarios Q4f, Q7c, and Q7d), similar RPDs were observed (8.4% and 8.5%), but with the time required to reach quasi-steady-state being much larger (by approximately three orders of magnitude) than the thin systems. Unlike with the thin systems, the differences between the three thicker systems is significant in real-world application as there is approximately 10 hours difference between the time to quasi-steady-state required for Scenario Q4f and the other two scenarios.

Table 5.5 Summary of Layer Arrangements and Times to Quasi-Steady-State.

Scenario	***b* (m)**	**t_{QSS} (s)**
Q4a	0.9	9.3E+02
Q7a	0.9	9.9E+02
Q7b	0.9	9.0E+02
Q4f	28.8	4.0E+05
Q7c	28.8	4.3E+05
Q7d	28.8	4.3E+05

The scenarios with largest times to quasi-steady-state are those where the lower-*K* layers are adjacent to one another with the lowest-*K* layer located adjacent to a boundary condition (Scenarios Q7a and Q7c).

Specific Storage Effects

To better understand the differences in hydraulic gradient behaviors at the well-face, a three-layer system was simulated using three different S_s values (Scenarios 1-3 (0.9 m), Scenarios 7-9 (1.8 m), Scenarios 15-17 (3.6 m), Scenarios 22a-24a (7.2 m), Scenarios 29-31 (14.4 m), and Scenarios 34-36 (28.8 m)): 6.0E-05 1/m, 3.5E-04 1/m, and 1.0E-3 1/m. These values were selected based on the relationship shown in Figure 5.7 and represent the maximum, average, and minimum S_s of the sands and gravel portion of the relationship. The S_s was held constant over the thickness of the aquifer. The times to quasi-steady-state for the three sets of simulations are presented in Figure 5.19.

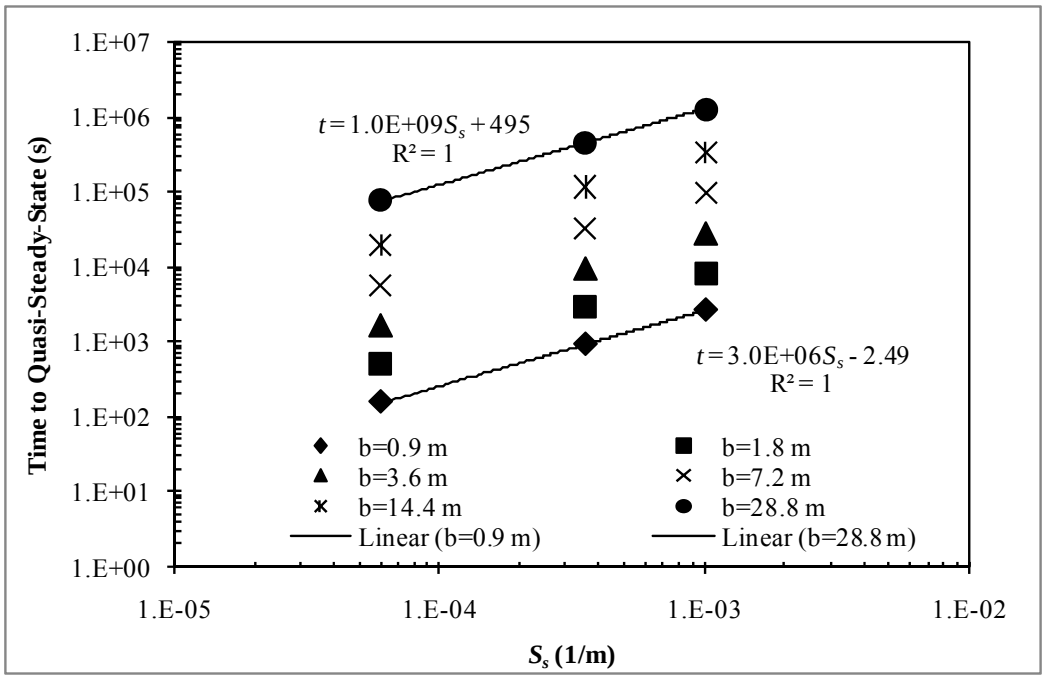

Figure 5.19 Time to quasi-steady-state as a function of S_s for Scenarios 1-3 (0.9 m), Scenarios 7-9 (1.8 m), Scenarios 15-17 (3.6 m), Scenarios 22a-24a (7.2 m), Scenarios 29-31 (14.4 m), and Scenarios 34-36 (28.8 m).

Results of these simulations (Figure 5.19) show that the time to quasi-steady-state as a function of S_s is linear. Comparison of these results indicates that, all other parameters being equal, systems with larger S_s take longer to reach quasi-steady-state than those with smaller S_s. This is due to an increase in available water volume for release from storage and the longer time period over which this release occurs.

To evaluate the conclusion from Ruud and Kabala [1996] that the hydraulic diffusivity (D) is the driving force behind the time required to attain quasi-steady-state, two sets of scenarios were evaluated. Each set of scenarios had the same layer-D values, but different layer-K and S_s values (Table 5.6), such that Scenario 22a is paired with 22b, 23a with 23b, and 24a with 24b. The times to quasi-steady-state for the paired scenarios

are comparable (RPD of less than 1.5% for each of the corresponding scenario sets). This supports findings from Ruud and Kabala [1994, 1996] that it is the ratio of D between layers (rather than the K ratio between layers) that determines the transient behavior of the hydraulic head gradients.

Next, systems were analyzed such that K was homogeneous throughout the system and S_s was varied to yield different layer D values (Table 5.7). To further examine the influence of the D-distribution on the transient behavior of the hydraulic head gradients, three systems with homogeneous K but different S_s between layers such that the same overall D-distributions as the systems in Table 5.6 were examined (Scenarios 42a through 44b in Table 5.7). The times to quasi-steady-state for these scenarios were compared to scenarios (i.e., Scenarios 22a through 24b, which have identical system configurations including the same layer-D values as 42a through 44b but with non-homogeneous K values). The times to quasi-steady-state for Scenarios 42a through 44b are, on average, 40% that of the non-homogeneous K systems. Thus, while these results again confirm that time to quasi-steady-state is a function of D, it appears that homogeneous K systems are a special case.

Lastly, systems were analyzed with variable K and S_s, but having D homogeneous throughout the system (Table 5.8). Setting systems up such that D is constant over the thickness of the system results in nearly instantaneous times to quasi-steady-state: less than one second for Scenarios 45 through 47. These results again confirm the findings from Ruud and Kabala [1994, 1996] that it is the ratio of D between layers (rather than

the *K* ratio between layers) that determines the transient behavior of the hydraulic head gradients.

Table 5.6 Summary of Homogeneous S_s Scenarios.

Scenario	b (m)	K_1 (m/d)	K_2 (m/d)	K_3 (m/d)	S_{s1} (1/m)	S_{s2} (1/m)	S_{s3} (1/m)	D_1 (m^2/d)	D_2 (m^2/d)	D_3 (m^2/d)	Q_p (L/min)	5% RPD t_{QSS} (s)
22a	7.2	1	0.01	0.2	3.5E-04	3.5E-04	3.5E-04	3.E+03	3.E+01	6.E+02	1	32,365
23a	7.2	1	0.01	0.2	6.0E-05	6.0E-05	6.0E-05	2.E+04	2.E+02	3.E+03	1	5,640
24a	7.2	1	0.01	0.2	1.0E-03	1.0E-03	1.0E-03	1.E+03	1.E+01	2.E+02	1	93,060
22b	7.2	10	0.1	2	3.5E-03	3.5E-03	3.5E-03	3.E+03	3.E+01	6.E+02	1	32,615
23b	7.2	10	0.1	2	6.0E-04	6.0E-04	6.0E-04	2.E+04	2.E+02	3.E+03	1	5,640
24b	7.2	10	0.1	2	1.0E-02	1.0E-02	1.0E-02	1.E+03	1.E+01	2.E+02	1	94,418

Notes:
Highlighted cells indicate the t_{QSS} is greater than 30 minutes.

Table 5.7 Summary of Homogeneous K Scenarios.

Scenario	b (m)	K_1 (m/d)	K_2 (m/d)	K_3 (m/d)	S_{s1} (1/m)	S_{s2} (1/m)	S_{s3} (1/m)	D_1 (m^2/d)	D_2 (m^2/d)	D_3 (m^2/d)	Q_p (L/min)	5% RPD t_{QSS} (s)
42a	7.2	1	1	1	3.3E-04	3.3E-02	1.7E-03	3.E+03	3.E+01	6.E+02	1	12,420
43a	7.2	1	1	1	6.0E-05	6.0E-03	3.0E-04	2.E+04	2.E+02	3.E+03	1	2,346
44a	7.2	1	1	1	1.0E-03	1.0E-01	5.0E-03	1.E+03	1.E+01	2.E+02	1	36,780
42b	7.2	10	10	10	3.3E-03	3.3E-01	1.7E-02	3.E+03	3.E+01	6.E+02	1	12,420
43b	7.2	10	10	10	6.0E-04	6.0E-02	3.0E-03	2.E+04	2.E+02	3.E+03	1	2,346
44b	7.2	10	10	10	1.0E-02	1.0E+00	5.0E-02	1.E+03	1.E+01	2.E+02	1	36,780

Notes:

Table 5.8 Summary of Homogeneous *D* Scenarios.

Scenario	b (m)	K_1 (m/d)	K_2 (m/d)	K_3 (m/d)	S_{s1} (1/m)	S_{s2} (1/m)	S_{s3} (1/m)	D_1 (m^2/d)	D_2 (m^2/d)	D_3 (m^2/d)	Q_p (L/min)	5% RPD t_{QSS} (s)
45	7.2	1	0.01	0.2	1.0E-03	1.0E-05	2.0E-04	1.E+03	1.E+03	1.E+03	1	0.063
46	7.2	1	0.01	0.2	2.0E-04	2.0E-06	4.0E-05	5.E+03	5.E+03	5.E+03	1	0.007
47	7.2	1	0.01	0.2	2.0E-03	2.0E-05	4.0E-04	5.E+02	5.E+02	5.E+02	1	0.255

Notes:
Highlighted cells indicate the t_{QSS} is greater than 30 minutes.

The effect of varying S_s across layers versus varying K across layers can be seen in Figures 5.20 and 5.21. In Figure 5.20, K is variable and S_s is constant. As can be seen, the flows from the high-K layer are initially smaller than their quasi-steady-state values and conversely, the flows from the lower-K layers are initially greater than their quasi-steady-state values.

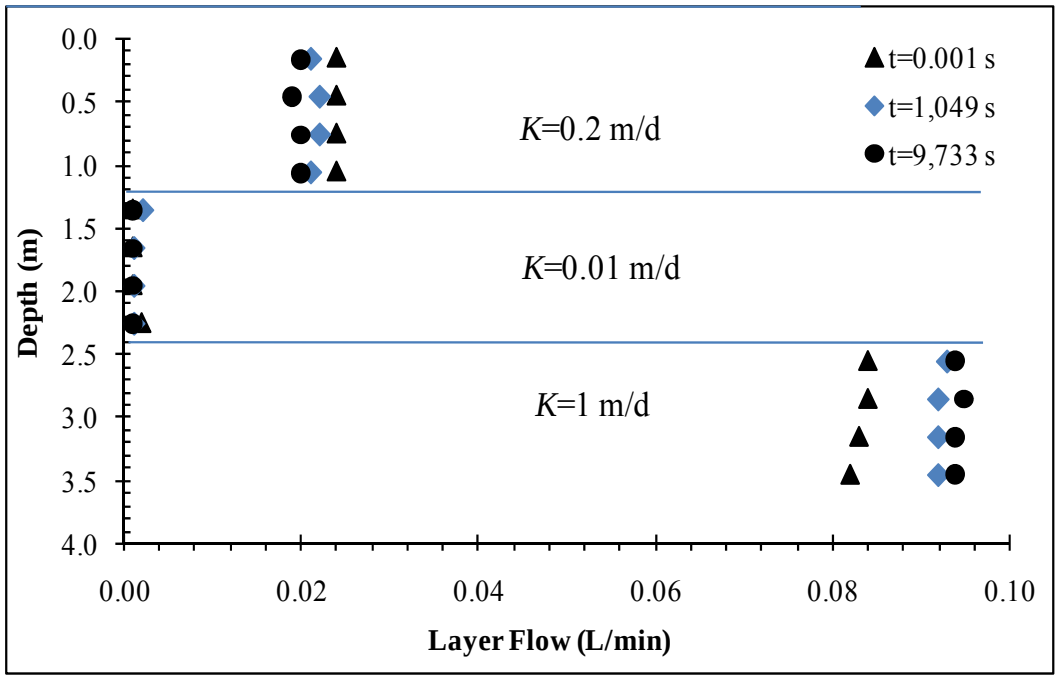

Figure 5.20 Layer flow by depth for Scenario 15.

In Figure 5.21, S_s is variable and K is constant. Here, the flows from the high-D layers are initially smaller than their quasi-steady-state values and conversely, the flow from the low-D layer is initially greater than their quasi-steady-state values. These layer flows are initially discrete values and behave more like a continuous function as they approach steady-state. As expected, the flows for the homogeneous K scenario

equilibrate to the same value, with early time differences in behavior driven by differences in D or S_s.

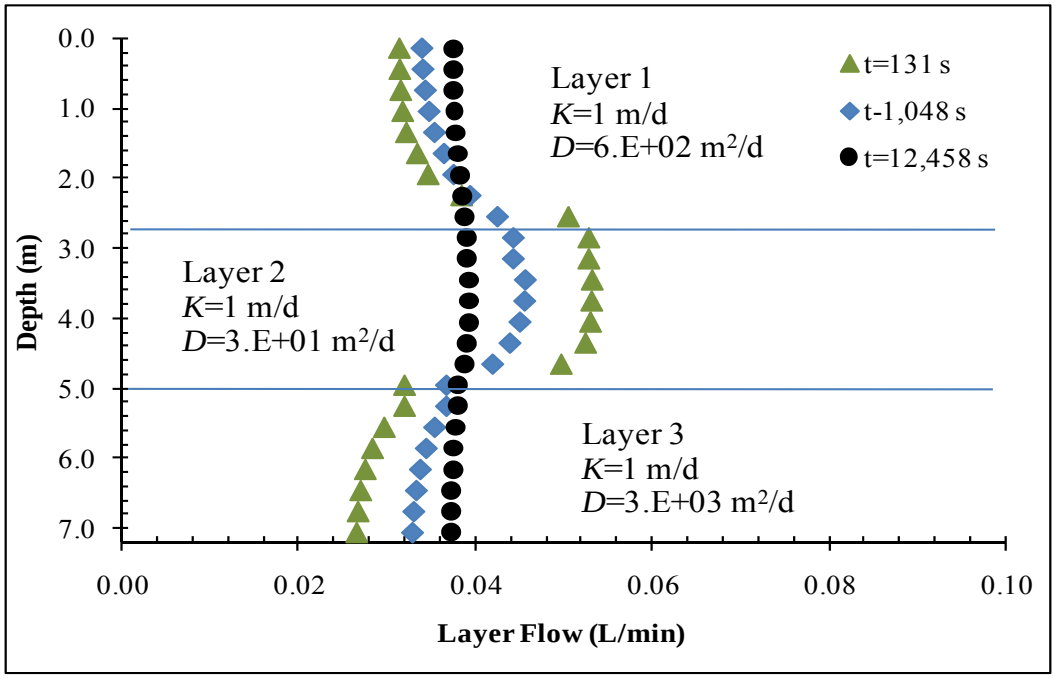

Figure 5.21 Layer flow by depth for Scenario 42a.

Anisotropy Effects

It is common for aquifers to exhibit directional differences in K, or anisotropy. To determine the effects of anisotropy on the time for hydraulic gradients at the well to attain quasi-steady-state, the system described by Scenario 27 was analyzed for anisotropy ratios (K_z/K_r) ranging from 0.1 to 1.5 (Scenarios 27 and 48 through 52). These scenarios and their results are summarized in Table 5.9 and Figure 5.22.

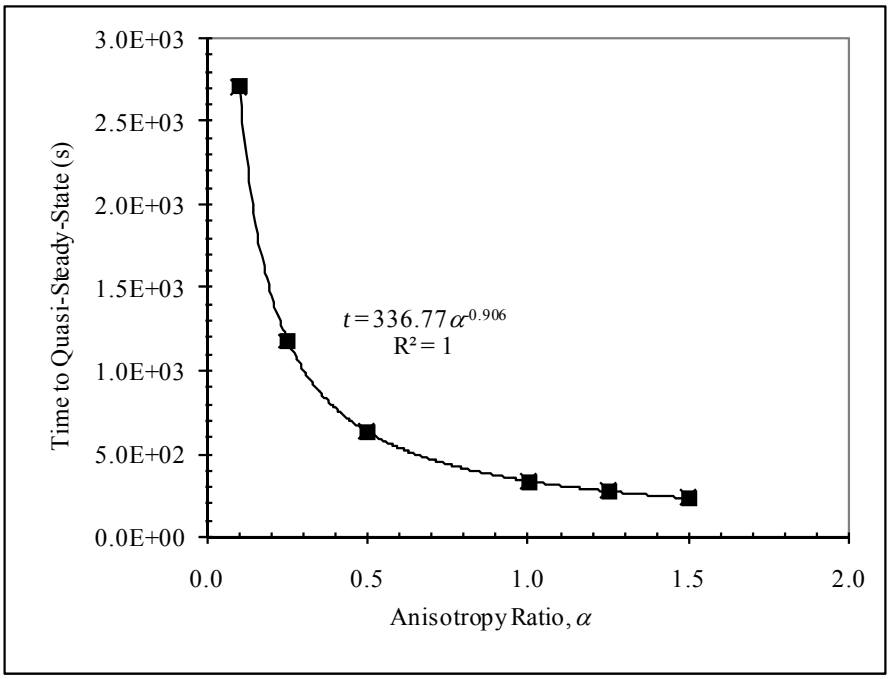

Figure 5.22 Time to attain quasi-steady-state as a function of anisotropy ratio for Scenario 27 and Scenarios 48-52.

The results of the anisotropy analysis imply that as the vertical K of the layers is increased, the amount of crossflow at early times increases, resulting in a smaller time to quasi-steady-state. This behavior is analogous to that described by Katz and Tek [1962] who found that the upper limit for crossflow occurs when the vertical hydraulic conductivity (K_z) approaches infinity compared to the horizontal hydraulic conductivity (K_r). In other words, as the vertical hydraulic conductivity (K_z) increases relative to the horizontal hydraulic conductivity (K_r), resistance to crossflow decreases and the time over which vertical flow significantly affects the overall system behavior decreases.

Table 5.9 Summary of Anisotropy Scenarios.

Scenario	b (m)	a	K_1 (m/d)	K_2 (m/d)	K_3 (m/d)	S_{s1} (1/m)	S_{s2} (1/m)	S_{s3} (1/m)	D_1 (m^2/d)	D_2 (m^2/d)	D_3 (m^2/d)	Q_p (L/min)	5% RPD t_{QSS} (s)
48	7.2	1.5	100	1	20	3.5E-04	3.5E-04	3.5E-04	3.E+05	3.E+03	6.E+04	5	234
29	7.2	1.25	100	1	20	3.5E-04	3.5E-04	3.5E-04	3.E+05	3.E+03	6.E+04	5	274
27	7.2	1	100	1	20	3.5E-04	3.5E-04	3.5E-04	3.E+05	3.E+03	6.E+04	5	334
50	7.2	0.5	100	1	20	3.5E-04	3.5E-04	3.5E-04	3.E+05	3.E+03	6.E+04	5	637
51	7.2	0.25	100	1	20	3.5E-04	3.5E-04	3.5E-04	3.E+05	3.E+03	6.E+04	5	1,179
52	7.2	0.1	100	1	20	3.5E-04	3.5E-04	3.5E-04	3.E+05	3.E+03	6.E+04	5	2,712

Notes:

Highlighted cells indicate the t_{QSS} is greater than 30 minutes.

CHAPTER 6

INTERPRETATION OF RESULTS

Having examined the influence of key parameters on the hydraulic gradient response (including layer hydraulic conductivity, layer specific storage, layer arrangement, layer thickness, and overall system thickness), the effects of these factors on the determination of layer *K* from flowmeter tests will now be examined. In addition, the data from the simulations performed during this study will be evaluated to determine whether the standard pumping duration of 30 minutes is sufficient for attaining meaningful results from EBF testing and whether a dimensionless time may be defined such that it may be applied to different systems and function as a predictive tool for the time to quasi-steady-state (i.e., provide a guideline for the pumping duration required prior to taking flowmeter readings). The times to quasi-steady-state for the scenarios discussed in Chapter 5 are summarized in Table 6.1.

Application of Model Results to EBF Analysis

The general practice when performing flowmeter tests has been to pump the well for 30 minutes at a low flow rate selected based on professional judgment and the results of previous studies performed in the vicinity or on similar sediments. Earlier, a maximum RPD between the gradients at the well of 5% was set forth as a viable definition of quasi-steady-state. By this definition, many of the scenarios modeled in this study would not achieve quasi-steady-state in 30 minutes or less; this is the case in 29 of the 85 scenarios presented in Table 6.1. Knowing this, the next step in assessing early-

Table 6.1 Summary of Time to Quasi-Steady-State for Study Scenarios.

Scenario	b (m)	a	K_1 (m/d)	K_2 (m/d)	K_3 (m/d)	S_{s1} (1/m)	S_{s2} (1/m)	S_{s3} (1/m)	Q_p (L/min)	Δz (m)	5% RPD t_{QSS} (s)
Q1	0.9	1	1	0.01	0.2	3.5E-04	3.5E-04	3.5E-04	0.300	0.30	933
Q2	0.9	1	100	0.01	0.2	3.5E-04	3.5E-04	3.5E-04	0.208	0.30	1,623
Q3a	0.9	1	0.01	0.0001	0.002	3.5E-04	3.5E-04	3.5E-04	0.00300	0.30	93,600
Q3b	1.8	1	0.01	0.0001	0.002	3.5E-04	3.5E-04	3.5E-04	0.00600	0.30	337,232
Q3c	3.6	1	0.01	0.0001	0.002	3.5E-04	3.5E-04	3.5E-04	0.01200	0.30	927,600
Q3d	7.2	1	0.01	0.0001	0.002	3.5E-04	3.5E-04	3.5E-04	0.0240	0.30	3,222,700
Q3e	14.4	1	0.01	0.0001	0.002	3.5E-04	3.5E-04	3.5E-04	0.0480	0.60	11,133,700
Q3f	28.8	1	0.01	0.0001	0.002	3.5E-04	3.5E-04	3.5E-04	0.0960	1.20	39,898,200
Q4a	0.9	1	1	0.01	0.2	3.5E-04	3.5E-04	3.5E-04	0.300	0.30	933
Q4b	1.8	1	1	0.01	0.2	3.5E-04	3.5E-04	3.5E-04	0.600	0.30	2,886
Q4c	3.6	1	1	0.01	0.2	3.5E-04	3.5E-04	3.5E-04	1.20	0.30	9,716
Q4d	7.2	1	1	0.01	0.2	3.5E-04	3.5E-04	3.5E-04	2.40	0.30	32,219
Q4e	14.4	1	1	0.01	0.2	3.5E-04	3.5E-04	3.5E-04	4.80	0.60	113,308
Q4f	28.8	1	1	0.01	0.2	3.5E-04	3.5E-04	3.5E-04	9.60	1.20	398,857
Q5a	0.9	1	100	1	20	3.5E-04	3.5E-04	3.5E-04	30.0	0.30	10
Q5b	1.8	1	100	1	20	3.5E-04	3.5E-04	3.5E-04	60.0	0.30	29
Q5c	3.6	1	100	1	20	3.5E-04	3.5E-04	3.5E-04	120	0.30	98
Q5d	7.2	1	100	1	20	3.5E-04	3.5E-04	3.5E-04	240	0.30	322
Q5e	14.4	1	100	1	20	3.5E-04	3.5E-04	3.5E-04	480	0.60	1,115
Q5f	28.8	1	100	1	20	3.5E-04	3.5E-04	3.5E-04	960	1.20	3,990
Q6a	0.9	1	10,000	100	2,000	3.5E-04	3.5E-04	3.5E-04	2,999	0.30	0.13
Q6b	1.8	1	10,000	100	2,000	3.5E-04	3.5E-04	3.5E-04	5,999	0.30	0.38
Q6c	3.6	1	10,000	100	2,000	3.5E-04	3.5E-04	3.5E-04	11,997	0.30	0.96
Q6d	7.2	1	10,000	100	2,000	3.5E-04	3.5E-04	3.5E-04	23,994	0.30	3.2
Q6e	14.4	1	10,000	100	2,000	3.5E-04	3.5E-04	3.5E-04	47,989	0.60	11
Q6f	28.8	1	10,000	100	2,000	3.5E-04	3.5E-04	3.5E-04	95,977	1.20	40

Table 6.1 Summary of Time to Quasi-Steady-State for Study Scenarios, continued.

Scenario	b (m)	a	K_1 (m/d)	K_2 (m/d)	K_3 (m/d)	S_{s1} (1/m)	S_{s2} (1/m)	S_{s3} (1/m)	Q_p (L/min)	Δz (m)	5% RPD t_{QSS} (s)
Q7a	0.9	1	1	0.2	0.01	3.5E-04	3.5E-04	3.5E-04	0.300	0.30	993
Q7b	0.9	1	0.2	1	0.01	3.5E-04	3.5E-04	3.5E-04	0.300	0.30	903
Q7c	28.8	1	1	0.2	0.01	3.5E-04	3.5E-04	3.5E-04	9.60	1.20	434,094
Q7d	28.8	1	0.2	1	0.01	3.5E-04	3.5E-04	3.5E-04	9.60	1.20	433,965
1	0.9	1	1	0.01	0.2	3.5E-04	3.5E-04	3.5E-04	0.1	0.3	916
2	0.9	1	1	0.01	0.2	6.0E-05	6.0E-05	6.0E-05	0.1	0.3	157
3	0.9	1	1	0.01	0.2	1.0E-03	1.0E-03	1.0E-03	0.1	0.3	2,613
4	0.9	1	1	0.01	0.2	3.5E-04	3.5E-04	3.5E-04	0.6	0.3	916
5	0.9	1	100	1	20	3.5E-04	3.5E-04	3.5E-04	5	0.3	9.09
6	0.9	1	10,000	100	2,000	3.5E-04	3.5E-04	3.5E-04	5	0.3	0.127
7	1.8	1	1	0.01	0.2	3.5E-04	3.5E-04	3.5E-04	0.3	0.3	2,836
7a	1.8	1	1	0.01	0.2	3.5E-04	3.5E-04	3.5E-04	0.3	0.3	1,473
8	1.8	1	1	0.01	0.2	6.0E-05	6.0E-05	6.0E-05	0.3	0.3	513
9	1.8	1	1	0.01	0.2	1.0E-03	1.0E-03	1.0E-03	0.3	0.3	8,220
10	1.8	1	1	0.01	0.2	3.5E-04	3.5E-04	3.5E-04	5	0.3	2,853
11	1.8	1	100	1	20	3.5E-04	3.5E-04	3.5E-04	0.5	0.3	36.4
12	1.8	1	100	1	20	3.5E-04	3.5E-04	3.5E-04	5	0.3	33.9
13	1.8	1	100	1	20	3.5E-04	3.5E-04	3.5E-04	40	0.3	36.4
14	1.8	1	10,000	100	2,000	3.5E-04	3.5E-04	3.5E-04	5	0.3	0.351
15	3.6	1	1	0.01	0.2	3.5E-04	3.5E-04	3.5E-04	0.5	0.3	9,733
16	3.6	1	1	0.01	0.2	6.0E-05	6.0E-05	6.0E-05	0.5	0.3	1,623
17	3.6	1	1	0.01	0.2	1.0E-03	1.0E-03	1.0E-03	0.5	0.3	27,330
18	3.6	1	1	0.01	0.2	3.5E-04	3.5E-04	3.5E-04	5	0.3	9,278
18a	3.6	1	1	0.01	0.2	3.5E-04	3.5E-04	3.5E-04	5	0.3	2,206
19	3.6	1	1	0.01	0.2	3.5E-04	3.5E-04	3.5E-04	10	0.3	9,300
20	3.6	1	100	1	20	3.5E-04	3.5E-04	3.5E-04	5	0.3	98.3

Table 6.1 Summary of Time to Quasi-Steady-State for Study Scenarios, continued.

Scenario	b (m)	a	K_1 (m/d)	K_2 (m/d)	K_3 (m/d)	S_{s1} (1/m)	S_{s2} (1/m)	S_{s3} (1/m)	Q_p (L/min)	Δz (m)	5% RPD t_{QSS} (s)
21	3.6	1	10,000	100	2,000	3.5E-04	3.5E-04	3.5E-04	5	0.3	1.31
22a	7.2	1	1	0.01	0.2	3.5E-04	3.5E-04	3.5E-04	1	0.3	32,365
23a	7.2	1	1	0.01	0.2	6.0E-05	6.0E-05	6.0E-05	1	0.3	5,640
24a	7.2	1	1	0.01	0.2	1.0E-03	1.0E-03	1.0E-03	1	0.3	93,060
22b	7.2	1	10	0.1	2	3.3E-03	3.3E-03	3.3E-03	1	0.3	32,615
23b	7.2	1	10	0.1	2	6.0E-04	6.0E-04	6.0E-04	1	0.3	5,640
24b	7.2	1	10	0.1	2	1.0E-02	1.0E-02	1.0E-02	1	0.3	94,418
25	7.2	1	1	0.01	0.2	3.5E-04	3.5E-04	3.5E-04	5	0.3	32,106
25a	7.2	1	1	0.01	0.2	3.5E-04	3.5E-04	3.5E-04	5	0.3	16,478
25b	7.2	1	1	0.01	0.2	3.5E-04	3.5E-04	3.5E-04	5	0.3	7,827
25c	7.2	1	1	0.01	0.2	3.5E-04	3.5E-04	3.5E-04	5	0.3	3,161
26	7.2	1	1	0.01	0.2	3.5E-04	3.5E-04	3.5E-04	10	0.3	32,468
27	7.2	1	100	1	20	3.5E-04	3.5E-04	3.5E-04	5	0.3	334
28	7.2	1	10,000	100	2,000	3.5E-04	3.5E-04	3.5E-04	5	0.3	5.38
29	14.4	1	1	0.01	0.2	3.5E-04	3.5E-04	3.5E-04	5	0.6	111,549
30	14.4	1	1	0.01	0.2	6.0E-05	6.0E-05	6.0E-05	5	0.6	19,518
31	14.4	1	1	0.01	0.2	1.0E-03	1.0E-03	1.0E-03	5	0.6	322,034
32	14.4	1	100	1	20	3.5E-04	3.5E-04	3.5E-04	5	0.6	1,306
33	14.4	1	10,000	100	2,000	3.5E-04	3.5E-04	3.5E-04	5	0.6	24.3
34	28.8	1	1	0.01	0.2	6.0E-05	6.0E-05	6.0E-05	5	1.2	75,737
35	28.8	1	1	0.01	0.2	1.0E-03	1.0E-03	1.0E-03	5	1.2	1,256,220
36	28.8	1	1	0.01	0.2	3.5E-04	3.5E-04	3.5E-04	5	1.2	398,507
37	28.8	1	1	0.01	0.2	3.5E-04	3.5E-04	3.5E-04	40	1.2	397,241
38	28.8	1	100	1	20	3.5E-04	3.5E-04	3.5E-04	5	1.2	5,803
39	28.8	1	100	1	20	3.5E-04	3.5E-04	3.5E-04	40	1.2	4,419
40	28.8	1	10,000	100	2,000	3.5E-04	3.5E-04	3.5E-04	5	1.2	111

Table 6.1 Summary of Time to Quasi-Steady-State for Study Scenarios, continued.

Scenario	b (m)	a	K_1 (m/d)	K_2 (m/d)	K_3 (m/d)	S_{s1} (1/m)	S_{s2} (1/m)	S_{s3} (1/m)	Q_p (L/min)	Δz (m)	5% RPD t_{QSS} (s)
41	28.8	1	10,000	100	2,000	3.5E-04	3.5E-04	3.5E-04	40	1.2	88.1
42a	7.2	1	1	1	1	3.3E-04	3.3E-02	1.7E-03	1	0.3	12,420
43a	7.2	1	1	1	1	6.0E-05	6.0E-03	3.0E-04	1	0.3	2,346
44a	7.2	1	1	1	1	1.0E-03	1.0E-01	5.0E-03	1	0.3	36,780
42b	7.2	1	10	10	10	3.3E-03	3.3E-01	1.7E-02	1	0.3	12,420
43b	7.2	1	10	10	10	6.0E-04	6.0E-02	3.0E-03	1	0.3	2,346
44b	7.2	1	10	10	10	1.0E-02	1.0E+00	5.0E-02	1	0.3	36,780

Notes:

Highlighted cells indicate the t_{QSS} is greater than 30 minutes.

time flow behavior toward a well under pumping conditions is determining the impact on the calculated *K* values of taking flowmeter measurements prior to the time when the maximum RPD between the gradients at the well is 5% or less. To evaluate this effect, Eqn. 2-3 may be modified such that the ambient flow is removed from the equation to obtain:

$$\frac{K_i}{< K >} = \frac{\Delta Q_i / \Delta z_i}{Q_P / b} \tag{6-1}$$

Using this equation in conjunction with the EBF range of measurement of 40 mL/min (0.05 m^3/d) to 40 L/min (57.6 m^3/d) as well as the device readout truncation, it is possible to calculate the *K* for each model layer at each time step. The model directly outputs the differential flow for each layer into the well (ΔQ_j). The cumulative flow at each successive Δz is calculated based on the raw interval flow contributions. The truncation from the readout device is then applied to the cumulative flow at each interval. The cumulative flow at each interval is then compared to the upper and lower measurement limits of the EBF. It is at this point that the flowmeter analysis is applied, using Eqn. 6-1 to determine the layer-*K* values.

Flowmeter tests using the EBF are conducted by measuring the cumulative flow into or out of the well as the device is raised along the well-face. This implies that if layers or measurement intervals have flow contributions below the device detection limit or the display capabilities, these flows will be incorporated into the next interval measurement where the flow is large enough to be detected. By definition, this will result in a layer with a flow contribution below the detection limit having the same device

reading as the previous interval, whereas the measurement for the interval next reflecting an increase in the cumulative flow will be greater than the true contribution for that interval. In evaluating the scenarios used in the evaluation of flowmeter analysis, the cumulative flow at each interval was compared to the device range of measurements, with values below the lower detection limit set to zero. Additionally, the flow readings from the EBF are truncated to two significant figures after the decimal to reflect the readout capacities of the device.

The *K* values obtained using Eqn. 6-1 can then be compared to the input layer *K* values to determine subjectively when the system has equilibrated sufficiently to yield calculated results representative of the input values, even though these calculated values may not be equal to the input *K* values. This process is, as noted, partly subjective rather than fully quantitative, but in general the times were selected such that when rounded, the *K* values equaled the input values. As an example, the calculated *K* values for the subjective time to quasi-steady-state from Scenario 15 are included in Table 6.2. In this example, the calculated *K* values differ slightly from the input *K* values; however, the difference is slight and is unlikely to result in any qualitative differences in assessment of the aquifer behavior.

Table 6.2 Summary of Input and Calculated *K* values at the Subjective Quasi-Steady-State for Scenario 15

Layer	Layer *K* (m/d)	Depth, *z* (m)	Input *K* (m/d)	Calculated *K* (m/d)	Average Calculated *K* (m/d)
1	1	3.45	1.00	0.97	0.97
		3.15	1.00	0.97	
		2.85	1.00	0.97	
		2.55	1.00	0.98	
2	0.01	2.25	0.01	0.010	0.013
		1.95	0.01	0.010	
		1.65	0.01	0.010	
		1.35	0.01	0.021	
3	0.2	1.05	0.20	0.22	0.23
		0.75	0.20	0.23	
		0.45	0.20	0.23	
		0.15	0.20	0.22	

The subjective times to quasi-steady-state for Scenarios Q1-Q7 and 1-44 are included in Table 6.3. As can be seen in Table 6.3, the subjective times to quasi-steady-state are smaller, often significantly, than those for when the RPD between the gradients at the well is approximately 5%. Corresponding to these shorter times, the RPD between the gradients at the well at the subjective times to quasi-steady-state are significantly larger than 5%, ranging from 8% to 158% with an average of 64% (Table 6.3). This is an important finding because it demonstrates that it is possible to obtain representative *K* values for an aquifer during the period when flow into the well (which is directly proportional to the gradient at the well) is still transient. Using the subjective time to quasi-steady-state, 65 of the 68 scenarios summarized in Table 6.3 attained quasi-steady-state prior to 30 minutes pumping duration.

The calculated *K* values for the three scenarios not considered to have subjectively attained quasi-steady-state before 30 minutes (Scenarios Q4e, 29, and 31) were examined at the output time closest to and less than 30 minutes (Table 6.4). As can be seen, although the output was not subjectively considered to have attained quasi-steady-state at the times nearest 30 minutes (t=1,049 s for Scenarios Q4e and 29, and t=1,704 s for Scenario 31) as not all layer calculated *K*'s rounded to the corresponding input value, assessment of these results show that the individual grid-layer *K* results as well as the average *K* results over each layer are consistent with the input values. Furthermore, the differences seen at these times between the calculated and input *K*-values are not considered significant and would likely not adversely affect any further efforts based on this dataset.

Table 6.3 Summary of Subjective Times to Quasi-Steady-State.

Scenario	b (m)	K_1 (m/d)	K_2 (m/d)	K_3 (m/d)	S_{s1} (1/m)	S_{s2} (1/m)	S_{s3} (1/m)	Q_p (L/min)	5% RPD t_{QSS} (s)	Subjective t_{QSS} (s)	RPD at Subjective t_{QSS}
Q1	0.9	1	0.01	0.2	3.5E-04	3.5E-04	3.5E-04	0.300	933	18	79%
Q2	0.9	100	0.01	0.2	3.5E-04	3.5E-04	3.5E-04	0.208	1,623	8.2	134%
Q3a	0.9	0.01	0.0001	0.002	3.5E-04	3.5E-04	3.5E-04	0.00300	93,600	NA	NA
Q3b	1.8	0.01	0.0001	0.002	3.5E-04	3.5E-04	3.5E-04	0.00600	337,232	NA	NA
Q3c	3.6	0.01	0.0001	0.002	3.5E-04	3.5E-04	3.5E-04	0.01200	927,600	NA	NA
Q3d	7.2	0.01	0.0001	0.002	3.5E-04	3.5E-04	3.5E-04	0.0240	3,222,700	NA	NA
Q3e	14.4	0.01	0.0001	0.002	3.5E-04	3.5E-04	3.5E-04	0.0480	11,133,700	NA	NA
Q3f	28.8	0.01	0.0001	0.002	3.5E-04	3.5E-04	3.5E-04	0.0960	39,898,200	NA	NA
Q4a	0.9	1	0.01	0.2	3.5E-04	3.5E-04	3.5E-04	0.300	933	18	79%
Q4b	1.8	1	0.01	0.2	3.5E-04	3.5E-04	3.5E-04	0.600	2,886	246	38%
Q4c	3.6	1	0.01	0.2	3.5E-04	3.5E-04	3.5E-04	1.20	9,716	1,049	30%
Q4d	7.2	1	0.01	0.2	3.5E-04	3.5E-04	3.5E-04	2.40	32,219	1,180	46%
Q4e	14.4	1	0.01	0.2	3.5E-04	3.5E-04	3.5E-04	4.80	113,308	3,600	43%
Q4f	28.8	1	0.01	0.2	3.5E-04	3.5E-04	3.5E-04	9.60	398,857	262	66%
Q5a	0.9	100	1	20	3.5E-04	3.5E-04	3.5E-04	30.0	10	6.0	8%
Q5b	1.8	100	1	20	3.5E-04	3.5E-04	3.5E-04	60.0	29	NA	NA
Q5c	3.6	100	1	20	3.5E-04	3.5E-04	3.5E-04	120	98	NA	NA
Q5d	7.2	100	1	20	3.5E-04	3.5E-04	3.5E-04	240	322	NA	NA
Q5e	14.4	100	1	20	3.5E-04	3.5E-04	3.5E-04	480	1,115	NA	NA
Q5f	28.8	100	1	20	3.5E-04	3.5E-04	3.5E-04	960	3,990	NA	NA
Q6a	0.9	10,000	100	2,000	3.5E-04	3.5E-04	3.5E-04	2,999	0.13	NA	NA
Q6b	1.8	10,000	100	2,000	3.5E-04	3.5E-04	3.5E-04	5,999	0.38	NA	NA
Q6c	3.6	10,000	100	2,000	3.5E-04	3.5E-04	3.5E-04	11,997	0.96	NA	NA
Q6d	7.2	10,000	100	2,000	3.5E-04	3.5E-04	3.5E-04	23,994	3.2	NA	NA
Q6e	14.4	10,000	100	2,000	3.5E-04	3.5E-04	3.5E-04	47,989	11	NA	NA
Q6f	28.8	10,000	100	2,000	3.5E-04	3.5E-04	3.5E-04	95,977	40	NA	NA

Table 6.3 Summary of Subjective Times to Quasi-Steady-State, continued.

Scenario	b (m)	K_1 (m/d)	K_2 (m/d)	K_3 (m/d)	S_{s1} (1/m)	S_{s2} (1/m)	S_{s3} (1/m)	Q_p (L/min)	5% RPD t_{QSS} (s)	Subjective t_{QSS} (s)	RPD at Subjective t_{QSS}
Q7a	0.9	1	0.2	0.01	3.5E-04	3.5E-04	3.5E-04	0.300	993	63	64%
Q7b	0.9	0.2	1	0.01	3.5E-04	3.5E-04	3.5E-04	0.300	903	33	75%
Q7c	28.8	1	0.2	0.01	3.5E-04	3.5E-04	3.5E-04	9.60	434,094	262	67%
Q7d	28.8	0.2	1	0.01	3.5E-04	3.5E-04	3.5E-04	9.60	433,965	262	66%
1	0.9	1	0.01	0.2	3.5E-04	3.5E-04	3.5E-04	0.1	916	16	83%
2	0.9	1	0.01	0.2	6.0E-05	6.0E-05	6.0E-05	0.1	157	6.0	62%
3	0.9	1	0.01	0.2	1.0E-03	1.0E-03	1.0E-03	0.1	2,613	123	57%
4	0.9	1	0.01	0.2	3.5E-04	3.5E-04	3.5E-04	0.6	916	31	67%
5	0.9	100	1	20	3.5E-04	3.5E-04	3.5E-04	5	9.09	0.54	48%
6	0.9	10,000	100	2,000	3.5E-04	3.5E-04	3.5E-04	5	0.127	0.015	33%
7	1.8	1	0.01	0.2	3.5E-04	3.5E-04	3.5E-04	0.3	2,836	63	68%
7a	1.8	1	0.01	0.2	3.5E-04	3.5E-04	3.5E-04	0.3	1,473	13	91%
8	1.8	1	0.01	0.2	6.0E-05	6.0E-05	6.0E-05	0.3	513	63	31%
9	1.8	1	0.01	0.2	1.0E-03	1.0E-03	1.0E-03	0.3	8,220	273	58%
10	1.8	1	0.01	0.2	3.5E-04	3.5E-04	3.5E-04	5	2,853	153	48%
11	1.8	100	1	20	3.5E-04	3.5E-04	3.5E-04	0.5	36.4	2.0	46%
12	1.8	100	1	20	3.5E-04	3.5E-04	3.5E-04	5	33.9	2.0	44%
13	1.8	100	1	20	3.5E-04	3.5E-04	3.5E-04	40	36.4	2.0	43%
14	1.8	10,000	100	2,000	3.5E-04	3.5E-04	3.5E-04	5	0.351	0.13	19%
15	3.6	1	0.01	0.2	3.5E-04	3.5E-04	3.5E-04	0.5	9,733	1,049	30%
16	3.6	1	0.01	0.2	6.0E-05	6.0E-05	6.0E-05	0.5	1,623	63	51%
17	3.6	1	0.01	0.2	1.0E-03	1.0E-03	1.0E-03	0.5	27,330	1,049	51%
18	3.6	1	0.01	0.2	3.5E-04	3.5E-04	3.5E-04	5	9,278	262	57%
18a	3.6	1	0.01	0.2	3.5E-04	3.5E-04	3.5E-04	5	2,206	8.2	100%
19	3.6	1	0.01	0.2	3.5E-04	3.5E-04	3.5E-04	10	9,300	186	62%
20	3.6	100	1	20	3.5E-04	3.5E-04	3.5E-04	5	98.3	8.2	36%

Table 6.3 Summary of Subjective Times to Quasi-Steady-State, continued.

Scenario	b (m)	K_1 (m/d)	K_2 (m/d)	K_3 (m/d)	S_{s1} (1/m)	S_{s2} (1/m)	S_{s3} (1/m)	Q_p (L/min)	5% RPD t_{QSS} (s)	Subjective t_{QSS} (s)	RPD at Subjective t_{QSS}
21	3.6	10,000	100	2,000	3.5E-04	3.5E-04	3.5E-04	5	1.31	0.61	23%
22a	7.2	1	0.01	0.2	3.5E-04	3.5E-04	3.5E-04	1	32,365	66	55%
23a	7.2	1	0.01	0.2	6.0E-05	6.0E-05	6.0E-05	1	5,640	16	75%
24a	7.2	1	0.01	0.2	1.0E-03	1.0E-03	1.0E-03	1	93,060	246	75%
22b	7.2	10	0.1	2	3.3E-03	3.3E-03	3.3E-03	1	32,615	213	68%
23b	7.2	10	0.1	2	6.0E-04	6.0E-04	6.0E-04	1	5,640	33	70%
24b	7.2	10	0.1	2	1.0E-02	1.0E-02	1.0E-02	1	94,418	328	74%
25	7.2	1	0.01	0.2	3.5E-04	3.5E-04	3.5E-04	5	32,106	33	87%
25a	7.2	1	0.01	0.2	3.5E-04	3.5E-04	3.5E-04	5	16,478	33	75%
25b	7.2	1	0.01	0.2	3.5E-04	3.5E-04	3.5E-04	5	7,827	4.1	114%
25c	7.2	1	0.01	0.2	3.5E-04	3.5E-04	3.5E-04	5	3,161	16	96%
26	7.2	1	0.01	0.2	3.5E-04	3.5E-04	3.5E-04	10	32,468	33	87%
27	7.2	100	1	20	3.5E-04	3.5E-04	3.5E-04	5	334	10	51%
28	7.2	10,000	100	2,000	3.5E-04	3.5E-04	3.5E-04	5	5.38	3.19	24%
29	14.4	1	0.01	0.2	3.5E-04	3.5E-04	3.5E-04	5	111,549	3,600	42%
30	14.4	1	0.01	0.2	6.0E-05	6.0E-05	6.0E-05	5	19,518	524	45%
31	14.4	1	0.01	0.2	1.00E-03	1.00E-03	1.00E-03	5	322,034	5,216	50%
32	14.4	100	1	20	3.5E-04	3.5E-04	3.5E-04	5	1,306	241	21%
33	14.4	10,000	100	2,000	3.5E-04	3.5E-04	3.5E-04	5	24.3	18	18%
34	28.8	1	0.01	0.2	6.0E-05	6.0E-05	6.0E-05	5	75,737	524	50%
35	28.8	1	0.01	0.2	1.0E-03	1.0E-03	1.0E-03	5	1,256,220	131	84%
36	28.8	1	0.01	0.2	3.5E-04	3.5E-04	3.5E-04	5	398,507	131	81%
37	28.8	1	0.01	0.2	3.5E-04	3.5E-04	3.5E-04	40	397,241	33	87%
38	28.8	100	1	20	3.5E-04	3.5E-04	3.5E-04	5	5,803	1,580	28%
39	28.8	100	1	20	3.5E-04	3.5E-04	3.5E-04	40	4,419	34	53%
40	28.8	10,000	100	2,000	3.5E-04	3.5E-04	3.5E-04	5	111	82	27%

Table 6.3 Summary of Subjective Times to Quasi-Steady-State, continued.

Scenario	b (m)	K_1 (m/d)	K_2 (m/d)	K_3 (m/d)	S_{s1} (1/m)	S_{s2} (1/m)	S_{s3} (1/m)	Q_p (L/min)	5% RPD t_{QSS} (s)	Subjective t_{QSS} (s)	RPD at Subjective t_{QSS}
41	28.8	10,000	100	2,000	3.5E-04	3.5E-04	3.5E-04	40	88.1	55	23%
42a	7.2	1	1	1	3.3E-04	3.3E-02	1.7E-03	1	12,420	1.0	132%
43a	7.2	1	1	1	6.0E-05	6.0E-03	3.0E-04	1	2,346	2.1	136%
44a	7.2	1	1	1	1.0E-03	1.0E-01	5.0E-03	1	36,780	4.1	94%
42b	7.2	10	10	10	3.3E-03	3.3E-01	1.7E-02	1	12,420	1.0	158%
43b	7.2	10	10	10	6.0E-04	6.0E-02	3.0E-03	1	2,346	2.1	117%
44b	7.2	10	10	10	1.0E-02	1.0E+00	5.0E-02	1	36,780	4.1	153%

Notes:

Highlighted cells indicate the t_{QSS} is greater than 30 minutes.

NA - The Q_P used for the scenario was not consistent with flowmeter analysis and therefore, the subjective t_{QSS} was not determined

Table 6.4 Summary of Input and Calculated *K* values at the Subjective Quasi-Steady-State for Scenarios Q4e, 29, and 31.

				Scenario Q4e (*t*=1,049 s)		**Scenario 29 (*t*=1,049 s)**		**Scenario 31 (*t*=1,704 s)**	
Layer	**Layer *K* (m/d)**	**Depth, *z* (m)**	**Input *K* (m/d)**	**Calculated *K* (m/d)**	**Average Calculated *K* (m/d)**	**Calculated *K* (m/d)**	**Average Calculated *K* (m/d)**	**Calculated *K* (m/d)**	**Average Calculated *K* (m/d)**
1	1	14.1	1	0.96	0.97	0.96	0.97	0.96	0.96
		13.5	1	0.97		0.97		0.96	
		12.9	1	0.96		0.96		0.96	
		12.3	1	0.97		0.97		0.96	
		11.7	1	0.968		0.97		0.96	
		11.1	1	0.968		0.97		0.96	
		10.5	1	0.975		0.97		0.97	
		9.9	1	0.975		0.97		0.97	
2	0.01	9.3	0.01	0.013	0.016	0.013	0.016	0.015	0.017
		8.7	0.01	0.015		0.015		0.017	
		8.1	0.01	0.017		0.017		0.017	
		7.5	0.01	0.017		0.017		0.017	
		6.9	0.01	0.017		0.017		0.017	
		6.3	0.01	0.015		0.015		0.019	
		5.7	0.01	0.017		0.017		0.017	
		5.1	0.01	0.013		0.013		0.015	
3	0.2	4.5	0.2	0.23	0.23	0.23	0.23	0.24	0.23
		3.9	0.2	0.23		0.23		0.23	
		3.3	0.2	0.23		0.23		0.23	
		2.7	0.2	0.22		0.22		0.23	
		2.1	0.2	0.22		0.22		0.23	
		1.5	0.2	0.22		0.22		0.23	
		0.9	0.2	0.22		0.22		0.23	
		0.3	0.2	0.22		0.22		0.23	

The finding that it is possible to obtain representative *K* values for an aquifer during the period when flow into the well is still transient is, on the surface, contradictory to the findings of Ruud and Kabala [1996], who concluded that systems may be persistently transient for individual layer flows. This study has found results analogous to those of Ruud and Kabala [1996] in that the layer flows in many systems in this study required longer than the t_D of 1,000 defined by Javandel and Witherspoon [1969] for individual layer flows to equilibrate. As will be demonstrated in the next discussion topic, the use of this particular dimensionless time for the prediction of quasi-steady-state is questionable; however, it is possible to evaluate the Ruud and Kabala [1996] results with respect to the flowmeter methodology described above.

Figure 6.1 and Table 6.5 includes the input *K* values and individual layer flow values from the Ruud and Kabala [1996] figure (Figure 6.1) as well as calculated *K* values using the flowmeter methodology described earlier in this Chapter for the different times shown in the figure. As can be seen from the calculated *K* values in Table 6.5, the calculated flow rates for the lower-*K* layer are approximately an order of magnitude different from the input value; however, by *t*=720 s, the calculated *K* value for this same layer is now just a factor of two greater than the input value. For the purposes of most applications, the real-world difference between 0.073 m/d (calculated value at *t*=720 s) and 0.035 m/d (input value) is not significant. Furthermore, the calculated *K* of 3.4 m/d for the dominant layer in the system (i.e., the high-*K* layer, with respect to transport or productivity) is consistent with the input value (3.5 m/d) for even the earliest time included (90 s).

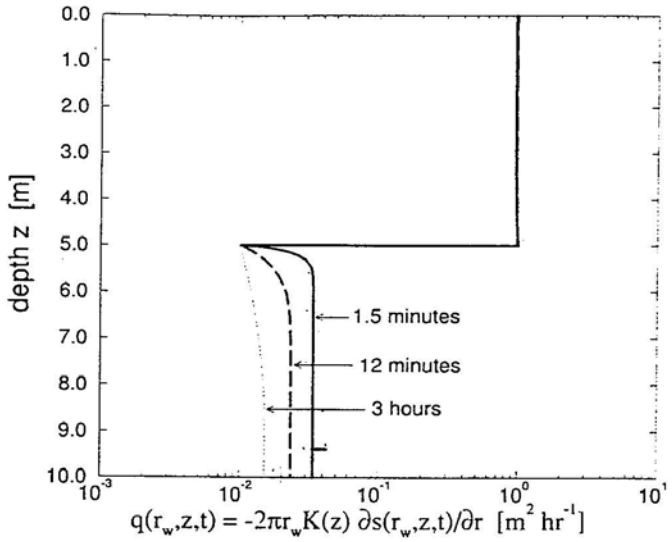

Figure 5. Transient and nonuniform well face flux in a two-layer confined aquifer pumped at a constant rate of $Q = 5$ m^3/h and characterized by $K_1 = 4 \times 10^{-5}$ m/s, $K_2 = 4 \times 10^{-7}$ m/s, $S_{s1} = 10^{-5}$ m^{-1}, and $S_{s2} = 10^{-3}$ m^{-1}. The well face flux is plotted at three different times: $t_1 = 1.5$ min (solid line), $t_2 = 12$ min (dashed line), and $t_3 = 3$ hours (dotted line).

Figure 6.1 Figure 5 from Ruud and Kabala [1996].

Table 6.5 Summary of Input and Calculated *K* values for the Results from Ruud and Kabala [1996] Figure 5

				***t*=90 s**			***t*=720 s**			***t*=10,800 s**		
Layer	**Layer *K* (m/d)**	**Depth, *z* (m)**	**Input *K* (m/d)**	**ΔQ (m^3/d)**	**Calculated *K* (m/d)**	**Average Calculated *K* (m/d)**	**ΔQ (m^3/d)**	**Calculated *K* (m/d)**	**Average Calculated *K* (m/d)**	**ΔQ (m^3/d)**	**Calculated *K* (m/d)**	**Average Calculated *K* (m/d)**
1	4	0.5	3.5	23	3.4	3.4	23	3.4	3.4	23	3.4	3.4
		1.5	3.5	23	3.4		23	3.4		23	3.4	
		2.5	3.5	23	3.4		23	3.4		23	3.4	
		3.5	3.5	23	3.4		23	3.4		23	3.4	
		4.5	3.5	23	3.4		23	3.4		23	3.4	
2	0.035	5.5	0.035	0.74	0.1	0.11	0.50	0.07	0.073	0.36	0.05	0.052
		6.5	0.035	0.74	0.1		0.50	0.07		0.36	0.05	
		7.5	0.035	0.74	0.1		0.50	0.07		0.36	0.05	
		8.5	0.035	0.74	0.1		0.50	0.07		0.36	0.05	
		9.5	0.035	0.74	0.1		0.50	0.07		0.36	0.05	

Flowmeter Analysis Performance

The ability of the flowmeter test and data analysis to resolve high-*K* layers at early times is an important feature of this analysis. As has been shown throughout this study, the hydraulic gradients at the well associated with high-*K* layers resort rapidly to their steady-state values, with the lower-*K* layers requiring more time and in many cases, the lowest-*K* layer may not resolve fully during a flowmeter test. More importantly, the flowmeter test is able to reliably and reasonably predict layer *K* values far earlier than quasi-steady-state as defined by hydraulic gradients or layer flows approaching their steady-state values.

To understand why the flowmeter analysis (Eqn. 6-1) is able to obtain representative *K* values prior to the hydraulic gradients or the layer flows are in quasi-steady-state, it is important to understand the derivation of the equation. Javandel and Witherspoon [1969] showed that flow at the wellbore rapidly becomes horizontal even for large permeability contrasts between layers. Once the flows into the well are horizontal, layer flow into the well is proportional to the transmissivity of the layer such that (ignoring ambient flow):

$$\Delta Q_i = \alpha \Delta z_i K_i \tag{6-2}$$

where α is a constant determined by summing ΔQ_i over the aquifer thickness, b:

$$\sum_{i=1}^{n} \left(Q_i \right) = Q_p = \alpha \sum_{i=1}^{n} \Delta z_i K_i \tag{6-3}$$

Solving Eqn. 6-3 for α yields:

$$\alpha = \frac{Q_p}{b\langle K \rangle} \tag{6-4}$$

Substituting Eqn. 6-4 into Eqn. 6-2 and rearranging yields Eqn. 6-1. The incorporation of the aquifer average K ($<K>$) is what lends the flowmeter application its flexibility and robustness in terms of changing layer flows or hydraulic gradients at the wellbore. The combined use of a proportion ($\Delta Q_i / \Delta Q_p$) and the average K serves to smooth out small variations in layer flows (ΔQ_i) occurring prior to the 5% RPD quasi-steady-state. Additionally, the system arithmetic average K is determined independently from the flowmeter test (i.e., via pumping tests), further smoothing out small variations in the layer flows. These features of the analysis explain why the methodology is able to accurately calculate K values for high-K layers at very short times as it has been demonstrated through this and other studies that the highest-K layers in a system deviate less from the Theis solution for the aquifer and rapidly attain quasi-steady-state within the layer itself.

Definition of Dimensionless Time

In analyzing these results of the modeling performed for this study, it is helpful to non-dimensionalize the time to quasi-steady-state using a transformation comprised of the key parameters that govern flow behaviors in aquifers. Javandel and Witherspoon [1969] employed the following dimensionless time in assessing their results for flow to a well from multi-layer systems:

$$t_D = \frac{t}{r^2} \frac{\sum_{i=1}^{n} K_i b_i}{\sum_{i=1}^{n} S_{Si} b_i} \tag{6-2}$$

The use of the well radius (r_w) in Eqn. 6-2 was important for the presentation of data throughout the radial domain. By converting time in this manner and examining drawdown throughout the aquifer (also in dimensionless terms), Javandel and Witherspoon concluded that deviations in drawdown from the Theis solution in different layers was an early-time phenomenon and that by t_D=1,000, these deviations were negligible. This then became their definition for the time at which a system may be considered to be at quasi-steady-state. However, they did not test this definition rigorously.

For a dimensionless number to be useful as a predictive tool, the results of the non-dimensionalization should collapse to a single number or a relatively small range of numbers. If a large range of dimensionless numbers is achieved for a set of model results, it should be concluded that the non-dimensionalization does not fully capture the critical parameters governing system behavior. To further evaluate the use of Eqn. 6-2 as a predictive tool of when a system may be expected to attain quasi-steady-state, Eqn. 6-2 was applied to the results from each of the systems modeled during this study. For the purposes of this stage of the assessment, the time to quasi-steady-state defined by the time where the hydraulic gradients are approximately 5% RPD was employed as this is a more rigorous (i.e., mathematical) definition than the subjective time to quasi-steady-state. Once the dimensionless time is well understood for the 5% RPD case, the

dimensionless time will be applied to the subjective time to quasi-steady-state. As shown in Table 6.6 and Figure 6.2, rather than producing a relatively focused set of t_D results, this non-dimensionalization resulted in a large range of t_D's: 4.6E+03 to 5.7E+06. As such, this non-dimensionalization by itself is a poor tool for predicting the time to quasi-steady-state. Summary statistics included at the bottom of Table 6.6 also indicate that this is a poor relationship for predictive purposes, given the large variance (1.1E+12) and standard deviation (1.0E+06).

Table 6.6 Summary of Time to Quasi-Steady-State and Corresponding Dimensionless Times Calculated using Eqn. 6-2.

Scenario	5% RPD t_{QSS} (s)	t_D *(Eqn. 6-2)*
Q1	933	4,781
Q2	1,623	688,701
Q3a	93,600	4,796
Q3b	337,232	17,281
Q3c	927,600	47,535
Q3d	3,222,700	165,146
Q3e	11,133,700	570,542
Q3f	39,898,200	2,044,568
Q4a	933	4,781
Q4b	2,886	14,787
Q4c	9,716	49,789
Q4d	32,219	165,106
Q4e	113,308	580,642
Q4f	398,857	2,043,927
Q5a	10	5,136
Q5b	29	14,873
Q5c	98	50,375
Q5d	322	164,769
Q5e	1,115	571,444
Q5f	3,990	2,044,460
Q6a	0.13	6,508
Q6b	0.38	19,627
Q6c	0.96	49,144
Q6d	3.2	164,751
Q6e	11	584,547
Q6f	40	2,044,404
Q7a	993	5,087
Q7b	903	4,626
Q7c	434,094	2,224,498
Q7d	433,965	2,223,837
1	916	4,696
2	157	4,734
3	2,613	4,726
4	916	4,696
5	9.09	4,657
6	0.127	6,508

Table 6.6 Summary of Time to Quasi-Steady-State and Corresponding Dimensionless Times Calculated using Eqn. 6-2, continued.

Scenario	5% RPD t_{QSS} (s)	t_D *(Eqn. 6-2)*
7	2,836	14,533
7a	1,473	7,549
8	513	15,459
9	8,220	14,869
10	2,853	14,619
11	36.4	18,644
12	33.9	17,363
13	36.4	18,644
14	0.351	17,987
15	9,733	49,875
16	1,623	48,925
17	27,330	49,438
18	9,278	47,547
18a	2,206	11,307
19	9,300	47,657
20	98.3	50,375
21	1.31	67,182
22a	32,365	165,853
23a	5,640	170,040
24a	93,060	168,339
22b	32,615	176,995
23b	5,640	170,040
24b	94,418	170,796
25	32,106	164,524
25a	16,478	84,439
25b	7,827	40,108
25c	3,161	16,198
26	32,468	166,378
27	334	171,066
28	5.38	275,542
29	111,549	571,629
30	19,518	588,434
31	322,034	582,539
32	1,306	669,050
33	24.3	1,246,295
34	75,737	2,283,382

Table 6.6 Summary of Time to Quasi-Steady-State and Corresponding Dimensionless Times Calculated using Eqn. 6-2, continued.

Scenario	5% RPD t_{QSS} (s)	t_D *(Eqn. 6-2)*
35	1,256,220	2,272,420
36	398,507	2,042,134
37	397,241	2,035,646
38	5,803	2,973,771
39	4,419	2,264,269
40	111	5,703,270
41	88.1	4,516,034
42a	12,420	4,730
43a	2,346	4,962
44a	36,780	4,669
42b	12,420	4,730
43b	2,346	4,962
44b	36,780	4,669
Summary Statistics		
No. of Data Points	85	85
Minimum	0.1	4.6E+03
Average	7.1E+05	5.5E+05
Maximum	4.0E+07	5.7E+06
Range	4.0E+07	5.7E+06
Variance	2.0E+13	1.1E+12
Standard Deviation	4.5E+06	1.0E+06
Coefficient of Variation	6.3	1.9
95% UCL	7.5E+06	1.7E+06

Notes:
Highlighted cells indicate the t_{QSS} is greater than 30 minutes.

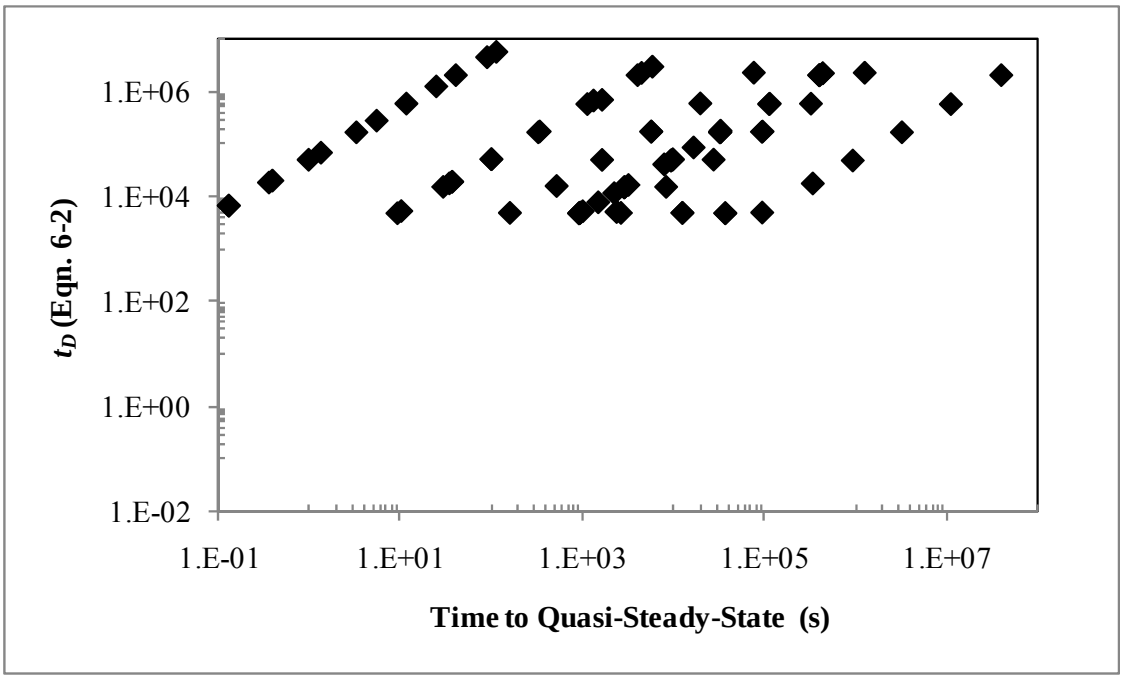

Figure 6.2 Relationship between t_D as defined by Eqn. 6-2 and time to quasi-steady-state.

The visual representation of the relationship between t_D and time to quasi-steady-state provided in Figure 6.2 indicates that the aquifer thickness, *b*, is an important factor in the time to quasi-steady-state (as evidenced by the clustering of results).

Careful examination of the results shown in Table 6.6 indicates a correlation between the overall aquifer thickness (*b*) and time to quasi-steady-state as well as between hydraulic conductivity (*K*) and time to quasi-steady-state, and possibly between hydraulic diffusivity (*D*) and time to quasi-steady-state. Based on this observation, three new non-dimensionalizations for time were considered:

$$t_D = \frac{t}{b^2} \frac{\sum_{i=1}^{n} K_i b_i}{\sum_{i=1}^{n} S_{Si} b_i} \tag{6-3}$$

$$t_D = \frac{t}{b^2} \frac{\sum_{i=1}^{n} \frac{b_i}{S_{Si}}}{\sum_{i=1}^{n} \frac{b_i}{K_i}} \tag{6-4}$$

$$t_D = \frac{t}{b^2} D_{\min} \tag{6-5}$$

The first of these non-dimensionalizations (Eqn. 6-3), is similar to Eqn. 6-2, with *b* substituted for *r,* since it appears from observation of the results in Table 6.1 and Figure 6.2 that the time to quasi-steady-state is at least partially a function of *b*. The second non-dimensionalization (Eqn. 6-4) is based on a harmonic average of the hydraulic conductivities (*K*) for a given system; the harmonic average is often used to determine equivalent *K* values for systems where flow is perpendicular to the system layers (e.g. as with crossflow). The last non-dimensionalization (Eqn. 6-5) employs the minimum hydraulic diffusivity (D_{min}). The results of these non-dimensionalizations are included in Table 6.7. The summary statistics for the non-dimensionalizations are also included in Table 6.7.

The non-dimensionalization employing D_{min} (Eqn. 6-5) exhibits the smallest range of results (0.20 to 0.66), the smallest variance across the dataset (0.013), the smallest standard deviation (0.12), and the smallest coefficient of variation (0.47), indicating that of the non-dimensionalizations employed, this is the best mathematically for the purposes of predicting time to quasi-steady-state. Looking at the dataset as a whole for the D_{min} non-dimensionalization (Eqn. 6-5), the average t_D is 0.25. The 95% upper confidence

limit (UCL)[1] for this dataset is t_D=0.30. In theory, this value for t_D defined by Eqn. 6-5 should reasonably serve as a predictive tool (in the absence of site-specific information) for the time to quasi-steady-state (defined by the time where the hydraulic gradients are approximately 5% RPD) in 95% of cases.

[1] The UCL values were determined using the United States Environmental Protection Agency (USEPA) software ProUCL 4.0 (USEPA, 2008).

Table 6.7 Summary of Time to Quasi-Steady-State and Corresponding Dimensionless Times Calculated using Eqns. 6-3 through 6-5.

Scenario	**5% RPD t_{QSS} (s)**	***t_D (Eqn. 6-2)***	***t_D (Eqn. 6-3)***	***t_D (Eqn. 6-4)***	***t_D (Eqn. 6-5)***
Q1	933	4,781	15	1.1	0.38
Q2	1,623	688,701	2,194	1.9	0.66
Q3a	93,600	4,796	15	1.1	0.38
Q3b	337,232	17,281	14	0.97	0.34
Q3c	927,600	47,535	9.5	0.66	0.23
Q3d	3,222,700	165,146	8.2	0.58	0.20
Q3e	11,133,700	570,542	7.1	0.50	0.18
Q3f	39,898,200	2,044,568	6.4	0.45	0.16
Q4a	933	4,781	15	1.1	0.38
Q4b	2,886	14,787	12	0.83	0.29
Q4c	9,716	49,789	10	0.70	0.25
Q4d	32,219	165,106	8.2	0.58	0.20
Q4e	113,308	580,642	7.2	0.51	0.18
Q4f	398,857	2,043,927	6.4	0.45	0.16
Q5a	10	5,136	16	1.1	0.41
Q5b	29	14,873	12	0.83	0.29
Q5c	98	50,375	10	0.70	0.25
Q5d	322	164,769	8.2	0.58	0.20
Q5e	1,115	571,444	7.1	0.50	0.18
Q5f	3,990	2,044,460	6.4	0.45	0.16
Q6a	0.13	6,508	21	1.5	0.51
Q6b	0.38	19,627	16	1.1	0.39
Q6c	0.96	49,144	10	0.69	0.24
Q6d	3.2	164,751	8.2	0.58	0.20
Q6e	11	584,547	7.3	0.51	0.18
Q6f	40	2,044,404	6.4	0.45	0.16
Q7a	993	5,087	16	1.1	0.40
Q7b	903	4,626	15	1.0	0.37
Q7c	434,094	2,224,498	6.9	0.49	0.17
Q7d	433,965	2,223,837	6.9	0.49	0.17
1	916	4,696	15	1.0	0.37
2	157	4,734	15	1.1	0.37
3	2,613	4,726	15	1.1	0.37
4	916	4,696	15	1.0	0.37
5	9.09	4,657	15	1.0	0.37
6	0.127	6,508	21	1.5	0.51

Table 6.7 Summary of Time to Quasi-Steady-State and Corresponding Dimensionless Times Calculated using Eqns. 6-3 through 6-5, continued.

Scenario	**5% RPD t_{QSS} (s)**	***t_D (Eqn. 6-2)***	***t_D (Eqn. 6-3)***	***t_D (Eqn. 6-4)***	***t_D (Eqn. 6-5)***
7	2,836	14,533	12	0.81	0.29
7a	1,473	7,549	6.0	0.42	0.15
8	513	15,459	12	0.86	0.31
9	8,220	14,869	12	0.83	0.29
10	2,853	14,619	12	0.82	0.29
11	36.4	18,644	15	1.0	0.37
12	33.9	17,363	14	0.97	0.34
13	36.4	18,644	15	1.0	0.37
14	0.351	17,987	14	1.0	0.36
15	9,733	49,875	10	0.70	0.25
16	1,623	48,925	10	0.68	0.24
17	27,330	49,438	10	0.69	0.24
18	9,278	47,547	9.5	0.66	0.23
18a	2,206	11,307	2.3	0.16	0.056
19	9,300	47,657	9.5	0.67	0.24
20	98.3	50,375	10	0.70	0.25
21	1.31	67,182	13	0.94	0.33
22a	32,365	165,853	8.3	0.58	0.20
23a	5,640	170,040	8.5	0.59	0.21
24a	93,060	168,339	8.4	0.59	0.21
22b	32,615	176,995	8.8	0.6	0.22
23b	5,640	170,040	8.5	0.6	0.21
24b	94,418	170,796	8.5	0.6	0.21
25	32,106	164,524	8.2	0.57	0.20
25a	16,478	84,439	4.2	0.29	0.10
25b	7,827	40,108	2.0	0.14	0.050
25c	3,161	16,198	0.81	0.057	0.020
26	32,468	166,378	8.3	0.58	0.21
27	334	171,066	8.5	0.60	0.21
28	5.38	275,542	14	0.96	0.34
29	111,549	571,629	7.1	0.50	0.18
30	19,518	588,434	7.3	0.51	0.18
31	322,034	582,539	7.2	0.51	0.18
32	1,306	669,050	8.3	0.58	0.21
33	24.3	1,246,295	16	1.1	0.38
34	75,737	2,283,382	7.1	0.50	0.18

Table 6.7 Summary of Time to Quasi-Steady-State and Corresponding Dimensionless Times Calculated using Eqns. 6-3 through 6-5, continued.

Scenario	5% RPD t_{QSS} (s)	t_D *(Eqn. 6-2)*	t_D *(Eqn. 6-3)*	t_D *(Eqn. 6-4)*	t_D *(Eqn. 6-5)*
35	1,256,220	2,272,420	7.1	0.50	0.18
36	398,507	2,042,134	6.4	0.45	0.16
37	397,241	2,035,646	6.3	0.44	0.16
38	5,803	2,973,771	9.3	0.65	0.23
39	4,419	2,264,269	7.0	0.49	0.17
40	111	5,703,270	18	1.2	0.44
41	88.1	4,516,034	14	0.99	0.35
42a	12,420	4,730	0.24	3.4	0.08
43a	2,346	4,962	0.25	3.5	0.09
44a	36,780	4,669	0.23	3.3	0.08
42b	12,420	4,730	0.24	3.4	0.08
43b	2,346	4,962	0.25	3.5	0.09
44b	36,780	4,669	0.23	3.3	0.08
Summary Statistics					
No. of Data Points	85	85	85	85	85
Minimum	0.1	4.6E+03	0.23	0.057	0.020
Average	7.1E+05	5.5E+05	35	0.93	0.25
Maximum	4.0E+07	5.7E+06	2.2E+03	3.5	0.66
Range	4.0E+07	5.7E+06	2.2E+03	3.5	0.64
Variance	2.0E+13	1.1E+12	5.6E+04	0.56	0.013
Standard Deviation	4.5E+06	1.0E+06	237	0.75	0.12
Coefficient of Variation	6.3	1.9	6.7	0.81	0.47
95% UCL	7.5E+06	1.7E+06	196	1.3	0.30

Notes:

Highlighted cells indicate the t_{QSS} is greater than 30 minutes.

Figures 6.3, 6.4, and 6.5 illustrate the relationship between the dimensionless times defined by Eqns. 6-3, 6-4, and 6-5, respectively, and the time to quasi-steady-state. As can be seen in the figures, the dimensionless times defined by Eqns. 6-4 and 6-5 (Figures 6.4 and 6.5), exhibit tighter relationships than the dimensionless times defined by Eqns. 6-2 and 6-3 (Figures 6.2 and 6.3), with the tightest visual correlation evidenced by Eqn. 6-5 (Figure 6.5). The visual conclusions match the statistical evaluation discussed above which found that the dimensionless time defined using D_{min} should reasonably serve as a predictive tool. This non-dimensionalization has a range of results from 0.02 to 0.66, with a variance across the dataset of 0.013, a standard deviation of 0.12, and a coefficient of variation of 0.47. The average t_D for Eqn. 6-5 is 0.25. The 95% UCL for this dataset is t_D=0.30.

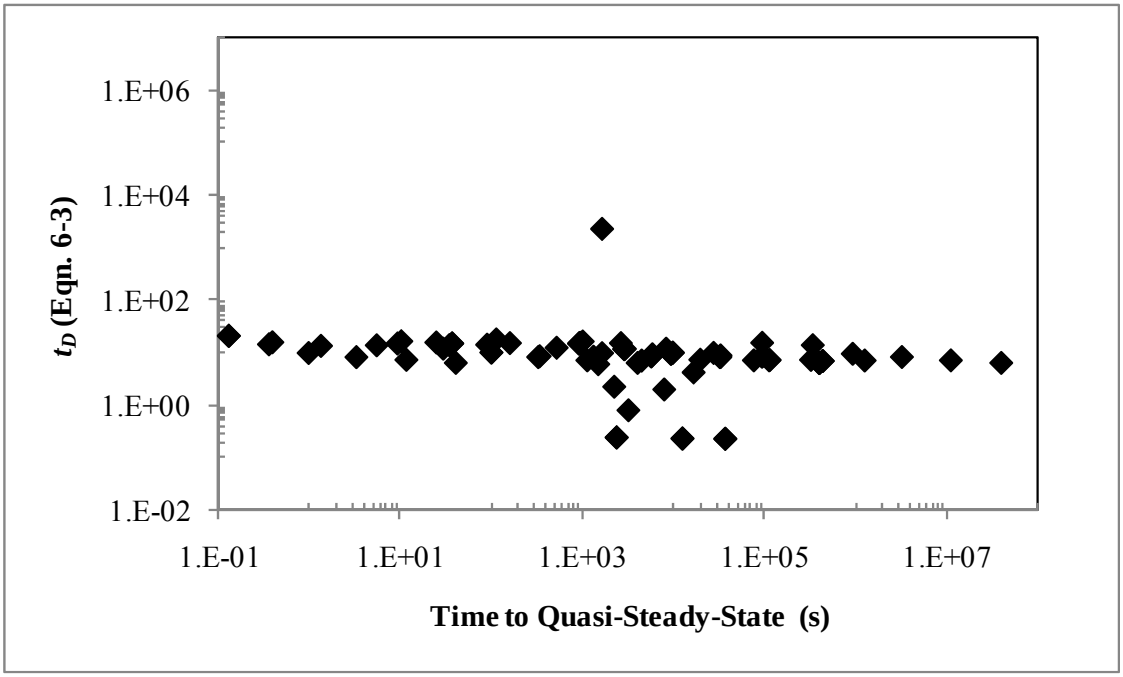

Figure 6.3 Relationship between t_D as defined by Eqn. 6-3 and time to quasi-steady-state.

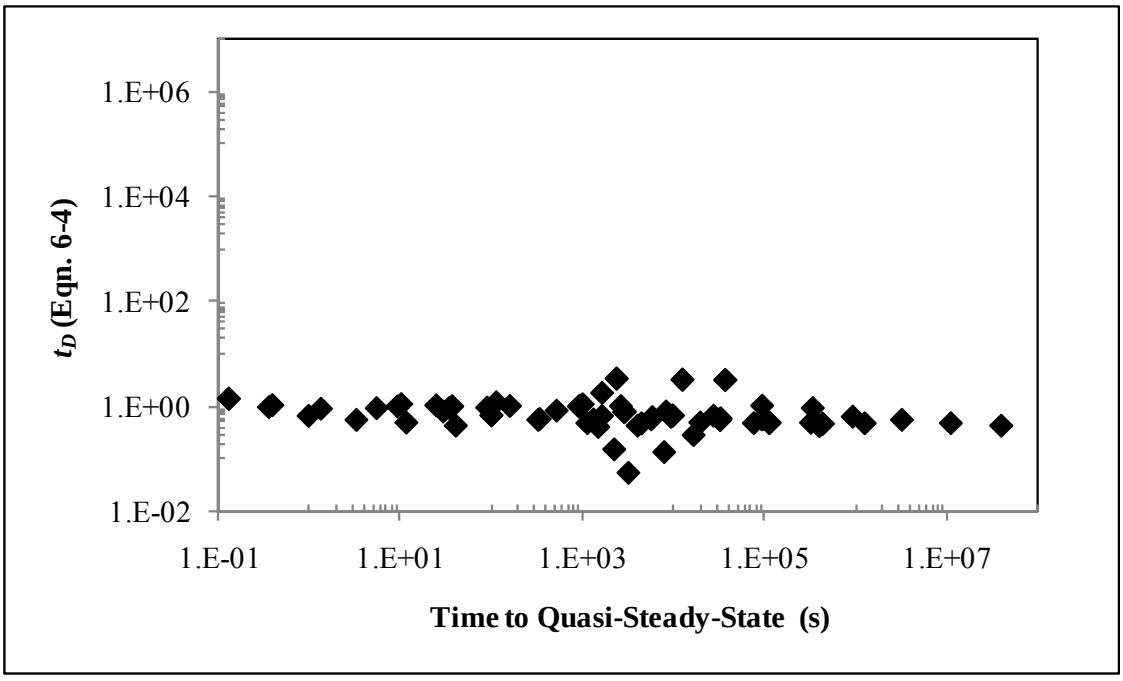

Figure 6.4 Relationship between t_D as defined by Eqn. 6-4 and time to quasi-steady-state.

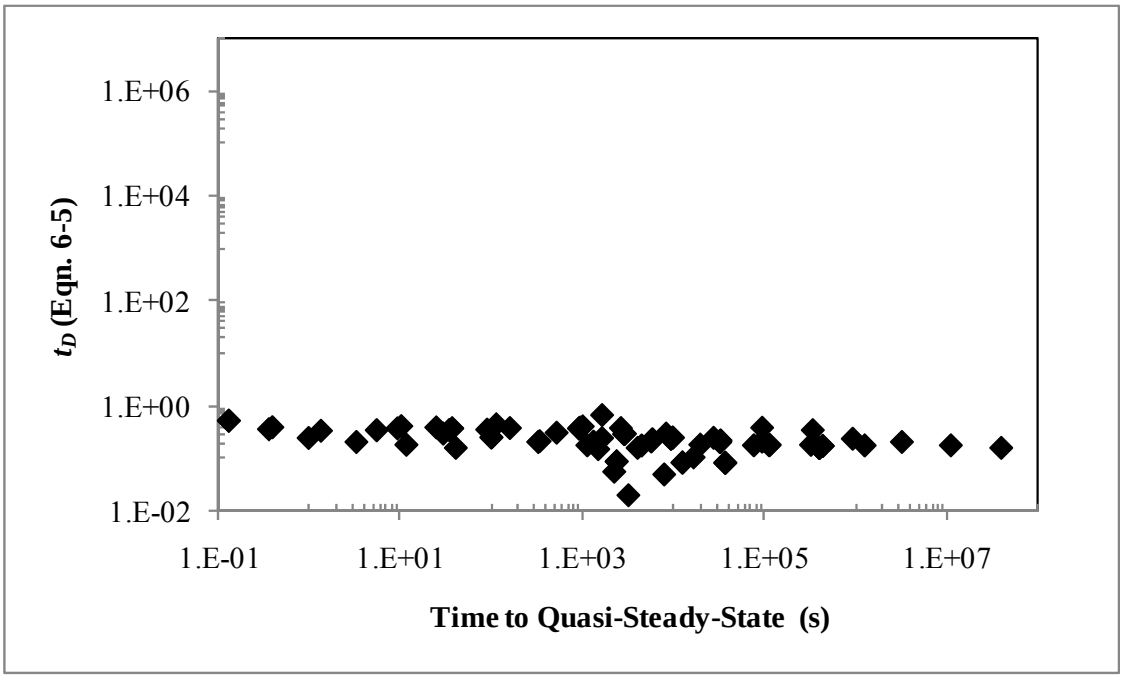

Figure 6.5 Relationship between t_D as defined by Eqn. 6-5 and time to quasi-steady-state.

Now that a non-dimensionalization has been selected for time to quasi-steady-state defined by the time where the hydraulic gradients are approximately 5% RPD, this non-dimensionalization may be applied to the subjective time to quasi-steady-state (Table 6.8). The 95% UCL for this non-dimensionalized dataset is 0.11. As with the times at 5% RPD, this value should reasonably serve as a predictive tool for the subjective time to quasi-steady-state in 95% of cases. It is important to note; however, that because this is a UCL, this value may overshoot the actual pumping duration required to attain meaningful flowmeter readings.

Table 6.8 Summary of Subjective Time to Quasi-Steady-State and Corresponding Dimensionless Times Calculated using Eqn. 6-5.

Scenario	**Subjective t_{QSS} (s)**	***t_D (Eqn. 6-5)***
Q1	18	0.0074
Q2	8.2	0.0033
Q3a	NA	NA
Q3b	NA	NA
Q3c	NA	NA
Q3d	NA	NA
Q3e	NA	NA
Q3f	NA	NA
Q4a	18	0.0074
Q4b	246	0.025
Q4c	1,049	0.027
Q4d	1,180	0.0075
Q4e	3,600	0.0057
Q4f	262	0.00010
Q5a	6.0	0.24
Q5b	NA	NA
Q5c	NA	NA
Q5d	NA	NA
Q5e	NA	NA
Q5f	NA	NA
Q6a	NA	NA
Q6b	NA	NA
Q6c	NA	NA
Q6d	NA	NA
Q6e	NA	NA
Q6f	NA	NA
Q7a	63	0.025
Q7b	33	0.013
Q7c	262	0.00010
Q7d	262	0.00010
1	16	0.0066
2	6.0	0.014
3	123	0.018
4	31	0.013
5	0.54	0.022
6	0.015	0.061

Table 6.8 Summary of Subjective Time to Quasi-Steady-State and Corresponding Dimensionless Times Calculated using Eqn. 6-5, continued.

Scenario	Subjective t_{QSS} (s)	t_D *(Eqn. 6-5)*
7	63	0.0064
7a	13	0.0013
8	63	0.037
9	273	0.0097
10	153	0.015
11	2.0	0.021
12	2.0	0.021
13	2.0	0.021
14	0.13	0.13
15	1,049	0.027
16	63	0.0093
17	1,049	0.0094
18	262	0.0066
18a	8.2	0.0002
19	186	0.0047
20	8.2	0.021
21	0.61	0.15
22a	66	0.00041
23a	16	0.001
24a	246	0.0005
22b	213	0.0014266
23b	33	0.0012193
24b	328	0.0007316
25	33	0.00021
25a	33	0.00021
25b	4.1	0.00003
25c	16	0.00010
26	33	0.00021
27	10	0.0065
28	3.19	0.20
29	3,600	0.0057
30	524	0.0049
31	5,216	0.0029
32	241	0.038
33	18	0.29
34	524	0.0012

Table 6.8 Summary of Subjective Time to Quasi-Steady-State and Corresponding Dimensionless Times Calculated using Eqn. 6-5, continued.

Scenario	Subjective t_{QSS} (s)	t_D *(Eqn. 6-5)*
35	131	0.000018
36	131	0.000052
37	33	0.000013
38	1,580	0.062
39	34	0.0013
40	82	0.33
41	55	0.22
42a	1.0	0.0000069
43a	2.1	0.0000763
44a	4.1	0.0000091
42b	1.0	0.0000068
43b	2.1	0.0000763
44b	4.1	0.0000092
Summary Statistics		
No. of Data Points	68	68
Minimum	0.015	0.0000068
Average	3.5E+02	0.032
Maximum	5.2E+03	0.33
Range	5.2E+03	0.33
Variance	8.0E+05	0.0048
Standard Deviation	8.9E+02	0.070
Coefficient of Variation	2.6	2.2
95% UCL	3.0E+03	0.11

Notes:
Highlighted cells indicate the t_{QSS} is greater than 30 minutes.

CHAPTER 7

CONCLUSIONS

Resolution of Literature Findings

Through a comparison of the published models [Katz and Tek 1962; Javandel and Witherspoon 1969; Ruud and Kabala 1996; Hemker 1999a, 1999b; Kabala and El-Sayegh 2002] and the use of an independent model capable of accurately and reliably reproducing the primary results of the published models while addressing the smaller inconsistencies between them, meaningful and conclusive data regarding the hydraulic gradient behavior for layered systems was obtained. Single-domain, multi-layer confined aquifers with homogeneous and isotropic or anisotropic layers were evaluated for a variety of aquifer parameters during this study.

To better understand the factors influencing hydraulic gradient behavior in multi-layer, confined aquifers, the numerical model TMVOC was employed in this study. This model makes no simplifying assumptions other than boundary condition assumptions and successfully reproduced or resolved the primary results published by other researchers on related topics. Whereas none of the four published studies discussed throughout this report [Katz and Tek 1962; Javandel and Witherspoon 1969; Ruud and Kabala 1996, 1997; Hemker 1999a, 199b; Kabala and El-Sayegh 2002] focused solely on hydraulic gradient behavior, qualitative statements were made regarding the effects of aquifer properties on crossflow and other factors influencing the time required for a system to reach quasi-steady-state.

The difference between the Ruud and Kabala [1997] and Javandel and Witherspoon [1969] conclusions is the most significant theoretical difference between the models examined in this study. The other differences in conclusions between the published models involve small-scale boundary effects (Ruud and Kabala [1996, 1997] and Hemker [1999a, 1999b]) and increases in error with increases in hydraulic diffusivity [Kabala and El-Sayegh 2002]. Based on the comparison of the models and the results obtained here, it is likely, given the small magnitude of these differences, that differences in the approximation of the layer interfaces and grid formation are responsible. The primary difference in implementation between the four published models is the solution of the system at the layer interface. The differences in grid formulation can be disregarded as insignificant compared to the solution at the layer interface, as each of the models was analyzed for errors and a sufficiently dense grid was used to satisfy error criteria.

The solution of the crossflow components has been handled implicitly [Javandel and Witherspoon 1969], approximately using increases in grid density and employing averages in K [Ruud and Kabala 1996, 1997; Hemker 1999a, 1999b], and by assuming crossflow to be in pseudo-steady-state [Kabala and El-Sayegh 2000]. Only by using the continuity equation at the layer interface or by implicitly solving the system using an integral finite difference grid, can the crossflow component be solved exactly. These approaches in-turn minimize the overall numerical error of the model by solving the term directly. The scenarios assessed during this study were each modeled using TMVOC, an integral finite difference model.

Ruud and Kabala [1996] and Javandel and Witherspoon [1969]

The results of Ruud and Kabala's modeling efforts suggest that, contrary to the Theis [1935] model and the results of Javandel and Witherspoon [1969] model, the flux along the wellbore for some layers may be persistently transient or non-uniform. The Theis [1935] model assumes that flows toward a well in layered aquifers are uniform and quickly become horizontal, which is what the Javandel and Witherspoon [1969] model confirms. The Ruud and Kabala [1996] model findings therefore deviate from the Javandel and Witherspoon [1969] model findings and are inconsistent with the Theis [1935] solution. Based on these findings, Ruud and Kabala [1996] conclude that the Theis [1935] model may be inadequate and too simplistic in nature to accurately describe the hydraulic behavior of layered aquifers. Another key finding of the Ruud and Kabala [1996] study was the confirmation of the Kabala [1994] results indicating that the hydraulic diffusivity contrast between adjacent layers, rather than the magnitude of the corresponding K ratio, is the dominant factor for accurately estimating parameters in the flowmeter analyses.

The seemingly conflicting statements of the time required for quasi-steady-state from Javandel and Witherspoon [1969] (i.e., short times to quasi-steady-state) and Ruud and Kabala [1997] (i.e., persistently transient conditions for some situation) have been resolved here. This study has found results analogous to those of Ruud and Kabala [1996] in that the layer flows in many systems in this study required longer than the dimensionless time of 1,000 defined by Javandel and Witherspoon [1996] for individual layer flows to equilibrate. As was demonstrated in the Section 6, the use of this particular

dimensionless time for the prediction of quasi-steady-state is not appropriate and a non-dimensional time based on the aquifer D_{min} was defined.

Additionally, data included in Figure 5 from Ruud and Kabala [1996] was analyzed using the flowmeter methodology and equations. The finding of this analysis was that, for the purposes of most applications, the real-world difference between the calculated-*K* and input-*K* values was not significant. Furthermore, the calculated-*K* for the dominant layer in the system (i.e., the high-*K* layer, with respect to transport or productivity) is consistent with the input value for even the earliest time included in the figure.

Ruud and Kabala's [1996] assertion that the Theis solution was overly simplistic was based in part on their findings that the layer flows into the well are persistently transient. It has been demonstrated that while this is true mathematically, the transient nature of the flows is not an issue except at very early times. This is based on the finding of this study that representative *K* values may be obtained from the flowmeter test as early in the pumping as when the hydraulic head gradients are within 64% RPD on average.

Application of Findings to EBF Testing

The ability of the flowmeter test and data analysis to rapidly resolve high-*K* layers is an important feature of the analysis. As has been shown throughout this study, the hydraulic gradients at the well associated with high-K layers resolve rapidly to their steady-state values, with the lower-*K* layers requiring more time and in many cases, the lowest-*K* layer may not resolve during a flowmeter test. More importantly, the flowmeter

test is able to reliably and reasonably predict layer *K* values far earlier than quasi-steady-state as defined by hydraulic gradients or layer flows resolving to their steady-state values. As was observed in Section 6 (Table 6.3), it is possible to get order of magnitude calculated K values within seconds or minutes.

Flowmeter testing is often not performed, with many practitioners preferring to perform pumping tests. The pumping test is a valuable test, and is essential to the flowmeter test, by providing the aquifer average *K*. The limitation of the pumping test is that it provides only information averaged over the thickness of the aquifer. The importance of performing both tests can be seen when examining an aquifer comprised of predominantly low to mid-*K* layers but with a single high-*K* layer. An example of such a system is as follows in Table 7.1 (assume all layers are of the same thickness).

Table 7.1 Summary of Layer-*K* values for a Hypothetical Aquifer.

Layer	***K*** **(m/d)**
10	1
9	2
8	4
7	5
6	100
5	15
4	40
3	5
2	2
1	10

Here, the arithmetic average *K* for the system that would be obtained from the pumping test would be 18 m/d. However, note the presence of the *K*=100 m/d layer at mid-depth in the aquifer. In terms of transport properties, this layer will dominate the

system behavior, but is not reflected properly in the pumping test. In fact, the pumping test could underestimate transport velocities by more than a factor of 5. Now, imagine that this highest-*K* layer is thinner than the lower-*K* layers. The transport velocity potential of the highest-*K* layer would be the same, but the average *K* obtained from the pumping test would be biased even lower than the 18 m/d obtained for the all layers of equal thickness scenario. This simple example illustrates the importance of performing flowmeter tests in addition to pumping tests.

Summary of Findings

To summarize, the various influences of system parameters on hydraulic gradient behavior in multi-layer confined aquifers in response to a pumping influence are:

1. Aquifer Thickness: The time to attain quasi-steady-state is a function of the ratio of the hydraulic diffusivities (*D*) between the layers as well as the overall aquifer thickness (*b*). As *b* is increased, the time to quasi-steady-state increases according to a power relationship. The relationship is a power relationship, indicating that the increase in the time required to attain quasi-steady-state is small at smaller thicknesses and becomes larger between successive increases in aquifer thickness. However, the results of the scenarios modeled during this study show that representative *K* values may be obtained far earlier (at 64% RPD) than the quasi-steady-state defined by the time when the hydraulic gradients are within 5% RPD of each other.

2. Layer Thickness: As the layer thickness is decreased, the time to quasi-steady-state decreases in a linear fashion. However the times remain greater than that for the minimum scenario (Scenario Q1, b=0.9 m) even when the layers are the same thickness and arrangement as employed in Scenario Q1. This reinforces the conclusions from the aquifer thickness analysis that as the overall aquifer thickness is increased, the time to quasi-steady-state increases.
3. Pumping Rate: In general, increasing the Q_P resulted in small differences in the time required to attain quasi-steady-state. Therefore, pumping rate is not considered to be a significant factor in the time needed to attain quasi-steady-state, and the pumping rate should be selected based on the study limitations (i.e., time, purge water disposal costs/options, etc.).
4. Layer Arrangement: The arrangement of layers in a system, all other parameters being equal, does not significantly affect the time to subjective quasi-steady-state for the thin systems analyzed. However, the thick systems did experience differences in times to quasi-steady-state, where the scenarios with largest times to quasi-steady-state are those where the lower-K layers are adjacent to one another with the lowest-K layer located adjacent to a boundary condition (Scenarios Q7a and Q7c). In both thicknesses, the subjective times to quasi-steady-state were identical for the three layer arrangements, however, indicating that the layer arrangement will not influence the flowmeter results.

5. Hydraulic Diffusivity, Part 1: The time to quasi-steady-state as a function of S_s is linear. All other parameters being equal, systems with larger S_s take longer to reach quasi-steady-state than those with smaller S_s. This is due to an increase in available water volume for release from storage and the longer time period over which this release occurs.
6. Hydraulic Diffusivity, Part 2: Systems where D is constant over the thickness of the system results in nearly instantaneous times to quasi-steady-state. These results confirm in part the findings from Ruud and Kabala [1994, 1996] that the ratio of D between layers (rather than the K ratio between layers) is important in determining the transient behavior of the hydraulic head gradients.
7. Hydraulic Diffusivity, Part 3: The times to quasi-steady-state for systems with homogeneous K and variable S_s are, on average, half that of the non-homogeneous K and constant S_s systems. Two conclusions may be draw from these results:
    a. Holding K uniform throughout the system results in no crossflow between the three layers due to hydraulic head differences resulting from K; the hydraulic head differences in these situations must therefore be a function of a system's D distribution. Again, this supports in part the findings from Ruud and Kabala [1996].
    b. The case of a homogeneous K appears to be a special case. Based on this finding, it is not possible to say that D is the sole driving

force behind the time required to attain quasi-steady-state. Were that the case, systems of the same configuration and with the same D distribution should attain quasi-steady-state at the same time. The results from this study show this to not be the case; rather, both the S_s and K-distributions play a role. Crossflow influences related to hydraulic head differences as a function of S_s play a smaller role in the transient behavior of the hydraulic head gradients than differences in K.

8. Hydraulic Diffusivity, Part 4: The sum of these conclusions is that although D is important, it is not the sole parameter determining the behavior of hydraulic gradients under pumping conditions. Aquifer thickness and layer thickness also both play an important role in the gradient behavior.
9. Anisotropy: As the vertical K of the layers is increased, the amount of crossflow at early times increases, resulting in a smaller time to quasi-steady-state. This behavior confirms the findings of Katz and Tek [1962] who found that the upper limit for crossflow occurs when the vertical hydraulic conductivity (K_z) approaches infinity compared to the horizontal hydraulic conductivity (K_r). In other words, as the vertical hydraulic conductivity (K_z) increases relative to the horizontal hydraulic conductivity (K_r), resistance to crossflow decreases and the time over

which crossflow significantly affects the overall system behavior decreases.

10. RPD: The initial hypothesis that systems should be considered to be in quasi-steady-state when the maximum difference between hydraulic gradients at the well were approximately 5% is found to be too stringent. Given the large times to quasi-steady-state reflected by the 5% RPD criteria, the data were evaluated to determine at what time did the flowmeter analysis yield calculated *K* values representative of the input values. These subjective times to quasi-steady-state yielded representative *K* values as early in the pumping as when the hydraulic head gradients are within 64% RPD on average and in many cases at larger RPDs. This is an important finding because it demonstrates that it is possible to obtain representative *K* values for an aquifer during the period when flow into the well (which is directly proportional to the gradient at the well) is still transient.
11. The non-dimensionalization of time developed by Javandel and Witherspoon [1969] and employed by Ruud and Kabala [1996] was found to be a poor tool for predicting time to quasi-steady-state. Rather, a relationship incorporating D_{min} and the aquifer thickness was found to be a good predictor of subjective time to quasi-steady-state (Eqn 6-5):

$$t_D = \frac{t}{b^2} D_{\min} \tag{7-1}$$

The 95% UCL for the non-dimensionalization of the subjective time to quasi-steady-state was determined to be t_D=0.11. This value should reasonably serve as a predictive tool for the subjective time to quasi-steady-state in 95% of cases.

REFERENCES

Anderson, M. P. and Woessner, W. W. 1992. Applied Groundwater Modeling. Academic Press, San Diego, California.

Arnold, K. B. and Molz, F. J. 2000. In-well hydraulics of the electromagnetic borehole flowmeter: further studies. Ground Water Monitoring & Remediation. Winter:52-55.

Batu, V. 1998. Aquifer Hydraulics A Comprehensive Guide to Hydrogeologic Data Analysis. John Wiley & Sons, Hoboken, New Jersey.

Boggs, J. M.; Young, S. C.; Beard, L. M.; Gelhar, L. W.; Rehfeldt, K. R.; and Adams, E. E. 1990. Field study of dispersion in a heterogeneous aquifer 1: Overview and site description. Water Resources Research. 28:3281-3291.

Boman, G. K.; Molz, F. J.; and Boone, K. D. 1997. Borehole flowmeter application in fluvial sediments: methodology, results, and assessment. Ground Water. 35(3):443-450.

Cooley, R. L. 1971. A finite difference method for unsteady flow in a variably saturated porous media: application to a single pumping well. Water Resources Research. 7(6): 1607-1625.

Cooper, Jr., H. H. and Jacob, C. E. 1946. A generalized graphical method for evaluations of formation constants and summarizing well-field history. Transactions of the American Geophysical Union. 27:526-534.

Crisman, S. A.; Molz, F. J.; Dunn, D. L.; and Sappington, F. C. 2001. Application for the Electromagnetic Borehole Flowmeter in Shallow Unconfined Aquifers. Groundwater Monitoring & Remediation. Fall:96-100.

De Hoog, F. R., Knight, J. H., and Stokes, A. N. 1982. An improved method for numerical inversion of Laplace transforms. SIAM Journal on Scientific and Statistical Computing. 3:357-366.

Dinwiddie, C. L.; Foley, N. A.; and Molz, F. J. 1999. In-well hydraulics of the electromagnetic borehole flowmeter. Ground Water. 37(2):305-315.

Elci, A., Molz, F.J., and Waldrop, W. R. 2001. Implications of Observed and Simulated Ambient Flow in Monitoring Wells. Ground Water, v. 36, no. 6, pp. 853-862.

Finsterle, S.; Kowalsky, M.; Rutqvist, J.; and Xu, T. 2006. IAEA Technical Co-operation Project C7-INT 9.173.009 Numerical Simulation of Subsurface Processes; TOUGH Training Course. August 14-17, 2006. Report No. LBNL-60134. Lawrence Berkely Laboratory. Berkeley, California.

Flach, G. P., Sappington, F. C., Johnson, W. P., and Hiergesell, R. A. 2000. Electromagnetic Borehole Flowmeter (EBF) Testing in R-area (U). Westinghouse Savannah River Company, Report WSRC-2000-00170.

Hantush, M. S. 1964. Hydraulics of Wells. Advances in Hydroscience. Academic Press, New York, pp. 281-442.

Hemker, C. J. 1985. Transient well flow in leaky multiple-aquifer systems. Journal of Hydrology. 81:111-126.

Hemker, C. J. 1999a. Transient well flow in vertically heterogeneous aquifers. Journal of Hydrology. 225:1-18.

Hemker, C. J. 1999b. Transient well flow in layered aquifer systems: the uniform well-face drawdown solution. Journal of Hydrology. 225:19-44.

Hemker, C. J. and Maas, C. 1987. Unsteady flow to wells in layered and fissured aquifer systems. Journal of Hydrology. 90:231-249.

Hunt, B. 1985. Flow to a well in a multilayer aquifer. Water Resources Research. 21(11):1637-1641.

Jaquard, P. 1960. Etude mathematique du drainage d'un reservoir heterogene. Rev. Inst. Frr. Petrole Ann. Combust. Liquides. 15(10):1384.

Javandel, I. and Witherspoon, P. A. 1980. A semianalytical solution for partial penetration in two-layer aquifers. Water Resources Research. 16(6):1099-1106.

Javandel, I. and Witherspoon, P. A. 1983. Analytical solution of a partially penetrating well in a two-layer aquifer. Water Resources Research. 19(2):567-578.

Javandel, I. and Witherspoon, P. A. 1969. A method of analyzing transient fluid flow in multilayered aquifers. Water Resources Research. 5:856-869.

Kabala, Z. J. 1994. Measuring distributions of hydraulic conductivity and specific storativity by the double flowmeter test. Water Resources Research. 30(3):685-690.

Kabala, Z. J. and El-Sayegh, H. K. 2002. Transient flowmeter test: semi-analytic crossflow model. Advances in Water Resources. 25:103-121.

Katz, M. L. and Tek, M. R. 1962. A theoretical study of pressure distribution and fluid flux in bounded stratified porous systems with crossflow. Society of Petroleum Engineers Journal. 2(1):68-82.

Lee, T. C. 1998. Applied Mathematics in Hydrogeology. CRC Press.

Maas, C. 1987. Groundwater flow to a well in a layered porous medium 2. Nonsteady multiple-aquifer flow. Water Resources Research. 23(8):1683-1688.

Maidment, D.R. 1993. Handbook of Hydrology. McGraw-Hill Professional.

Molz, F. J.; Guven, O.; Melville, J. G.; and Cardone, C. 1989. Hydraulic conductivity measurement at different scales and contaminant transport modeling. Cushman, J. H., ed. Dynamics of fluids in hierarchal porous media. New York: Academic Press; pp. 35-79.

Molz, F. J. and Young, S. C. 1993. Development and application of borehole flowmeters for environmental assessment. The Log Analyst. 3:13-23.

Moridis, G.J., and Pruess, K. 1995. Flow and Transport Simulations UsingT2CG1, A Package of Preconditioned Conjugate Gradient Solvers for the TOUGH2 Family of Codes, LBL Report No. 36235. Lawrence Berkely Laboratory. Berkeley, California.

Neuman, S. P. and Witherspoon, P. A. 1969. Theory of flow in a confined two aquifer system. Water Resources Research. 5(4):803-816.

Pruess, K. and Battistelli, A. 2002. TMVOC, A Numerical Simulator for Three-Phase Non-isothermal Flows of Multicomponent Hydrocarbon Mixtures in Saturated-Unsaturated Heterogeneous Media. Report No. LBNL-49375. Lawrence Berkely Laboratory. Berkeley, California.

Pruess, K., Oldenburg, C. and Moridis, G. 1999. TOUGH2 User's Guide, Version 2. Report No. LBNL-43134. Lawrence Berkely Laboratory. Berkeley, California.

Pruess, K., Simmons, A., Wu, Y. S. and Moridis, G. 1996. TOUGH2 Software Qualification. Report No. LBNL-38383. Lawrence Berkely Laboratory. Berkeley, California.

Press, W. H.; Teukolsky, S. A.; Vetterling, W. T.; and Flannery, B. P. 1992, Numerical Recipes in Fortran: The Art of Scientific Computing. Cambridge University Press; pp. 346-347.

Rehfeldt, K. R.; Hufschmied, P.; Gelhar, L. W.; and Schaefer, M. E. 1989. The borehole flowmeter techniques for measuring hydraulic conductivity variability: Electric Power Research Institute, Interim Report EM-6511, Palo Alto, California.

Russell, D. G. and Prats, M. 1962. Performance of layered reservoirs with crossflow - single-compressible-fluid case. Society of Petroleum Engineers Journal. 2(1):53-67.

Ruud, N. C. and Kabala, Z. J. 1996. Numerical evaluation of flowmeter test interpretation methodologies. Water Resources Research. 32(4):845-852.

Ruud, N. C. and Kabala, Z. J. 1997. Numerical evaluation of the flowmeter test in a layered aquifer with skin zone. Journal of Hydrology. 203:101-108.

Ruud, N. C.; Kabala, Z. J.; and Molz, F. J. 1999. Evaluation of flowmeter-head loss effects in the flowmeter test. Journal of Hydrology. 224:55-63.

Sen, Z. 1989. Radial flow in vertically graded hydraulic conductivity aquifers. Journal of Hydraulic Engineering. 115(12):1667-1682.

Szekely, F. 1995. Estimation of unsteady, three-dimensional drawdown in single, vertically heterogeneous aquifers. Ground Water. 33(4):669-674.

Theis, C. V. 1935. The relation between the lowering of the piezometric surface and the rate and duration of discharge of a well using ground-water storage. EOS Trans. AGU. 16:519-524.

Thiem, G. 1906. Hydrologishe Methoden (in German), J. M. Gebhardt, Leipzig, Germany.

United States Environmental Protection Agency (USEPA) 2008. ProUCL Version 4.0, a Statistical Software, National Exposure Research Lab, EPA, Las Vegas Nevada. ProUCL 4.0 can be freely downloaded from the USEPA website: http://epa.gov/esd/tsc/TSC_form.htm

Waldrop, W. R. 1995. A summary of hydrogeologic studies with the Electromagnetic Borehole Flowmeter. Report QEC T-102, Quantum Engineering Corporation, 112 Tigitsi Lane, Loudon, Tennessee, 37774, 615-458-0506.

Wolfram, S. 1999. The Mathematica Book, 4th Edition. Wolfram Media and Cambridge University Press, Champaign, Illinois.